Safety and therapeutic efficacy of adoptive p53-specific T cell antigen receptor (TCR) gene transfer

Dissertation

for the award of the degree

"Doctor rerum naturalium" (Dr. rer. nat.)

Faculty of Biology

of the Johannes Gutenberg-University Mainz

Jutta Petschenka

Born on January 12, 1984

in Hanau

Mainz, April 2014

Dean:

1st correspondent:

2nd correspondent:

Day of oral exam: June 4th, 2014

“There are more things in heaven and earth, Horatio,
than are dreamt of in our philosophy”

[Shakespeare, Hamlet 1,5]

Affidavit

Summary

Immunotherapy with T cells genetically modified by retroviral transfer of tumor-associated antigen (TAA)-specific T cell receptors (TCR) is a promising approach in targeting cancer. Therefore, using a universal TAA to target different tumor entities by only one therapeutic approach was the main criteria for our TAA-specific TCR. Here, an optimized (opt) αβ-chain $p53_{(264-272)}$-specific and an opt single chain (sc) $p53_{(264-272)}$-specific TCR were designed, to reduce mispairing reactions of endogenous and introduced TCR α and TCR β-chains, which might lead to off-target autoimmune reactions, similar to Graft-versus-host disease (GvHD).
In this study we evaluated the safety issues, which rise by the risk of p53TCR gene transfer-associated on/off-target toxicities as well as the anti-tumor response *in vivo* in a syngeneic HLA-A*0201 transgenic mouse model. We could successfully demonstrate that opt sc p53-specific TCR-redirected T cells prevent TCR mispairing-mediated lethal off-target autoimmunity in contrast to the parental opt αβ-chain p53-specific TCR. Since the sc p53-specific TCR proofed to be safe, all further studies were performed using sc p53-specific TCR redirected T cells only. Infusion of p53-specific TCR-redirected T cells in Human p53 knock-in (Hupki) mice after lymphodepletion-preconditioning regimen with either sublethal body irradiation (5Gy) or chemotherapy (fludarabine and cyclophosphamide) in combination with vaccination (anti-CD40, CpG1668 and $p53_{(257-282)}$ peptide) did not result in a depletion of hematopoietic cells. Moreover, adoptive transfer of high numbers of p53-specific TCR-redirected T cells in combination with Interleukin 2 (IL-2) also did not lead to toxic on-target reactions. The absence of host tissue damage was confirmed by histology and flow cytometry analysis. Furthermore, p53-specific TCR-redirected T cells were able to lyse $p53^{+}A2.1^{+}$ tumor cells *in vitro*. However, *in vivo* studies revealed the potent suppressive effect of the tumor microenvironment (TME) mediated by tumor-infiltrating myeloid-derived suppressor cells (MDSC). Accordingly, we could improve an insufficient anti-tumor response *in vivo* after injection of the sc p53-specific TCR-redirected T cells by additional depletion of immunosuppressive cells of the myeloid lineage.

Together, these data suggest that the optimized sc $p53_{(264-272)}$-specific TCR may represent a safe and efficient approach for TCR-based gene therapy. However, combinations of immunotherapeutic strategies are needed to enhance the efficacy of adoptive cell therapy (ACT)-mediated anti-tumor responses.

Zusammenfassung

Immuntherapien mit T-Zellen, welche durch retroviralen T-Zell Rezeptor (TZR) Gentransfer modifiziert wurden, sind ein vielversprechender Ansatz für die Krebstherapie. Hauptkriterium unseres therapeutischen Ansatzes ist das Verwenden von TZR, die spezifisch für universelle Tumor-assoziierte Antigene (TAA) sind, um so verschiedene Tumorentitäten anzusprechen. Hierzu wurde ein optimierter (opt) αβ-Ketten $p53_{(264-272)}$-spezifischer TZR und ein opt einzelketten $p53_{(264-272)}$-spezifischer TZR entwickelt, um gezielt die Fehlpaarung von endogenen und retroviral eingeführten TZR-Ketten zu verhindern. Fehlpaarungen können zu sogenannter ‚off-target' Toxizität führen, die in ihrer Art einer 'Graft-versus-host' Reaktion (GvHD) ähnelt und somit ein wichtiges Kriterium in Bezug auf die Sicherheit des adoptiven TZR-Gentransfers darstellt.

In dieser Studie wurde sowohl der Sicherheitsaspekt des adoptiven p53-spezifischen TZR-Gentransfers, als auch die anti-tumorale Antwort *in vivo* mittels eines syngenen HLA-A*0201 transgenen Mausmodells untersucht.

Wir konnten erfolgreich zeigen, dass T-Zellen, die mit dem opt einzelketten p53-spezifischen TZR – im Gegensatz zu dem opt αβ-Ketten p53-spezifischen TZR – transduziert wurden, eine durch Fehlpaarung induzierte lethale GvHD verhindern. Auch das Einbringen des einzelketten p53-spezifischen TZR in T-Zellen von Mäusen, die ein humanes p53 'knock-in' Gen besitzen (HupKi Mäuse), zeigt nach Lymphodepletion durch Bestrahlung (5Gy) oder Chemotherapie (Fludarabin und Cyclophosphamid) in Kombination mit Vakzinierung (anti-CD40, CpG1668 und $p53_{(257-282)}$ Peptid) oder Interleukin-2 (IL-2) keine ‚on-target' Toxitizät oder Depletion von hämatopoietischen Wirtszellen. Das Ausbleiben von Gewebsschäden konnte durch histologische und durchflusszytometrische Analysen bestätigt werden. Wir konnten zeigen, dass der einzelketten p53-spezifische-TZR eine Lyse von $p53^{+}A2.1^{+}$ Tumorzellen *in vitro* bewirkt. Jedoch offenbarten weitere *in vivo* Untersuchungen, dass das Tumormikromilieu maßgeblich durch die Infiltration von 'myeloid-derived suppressor cells' (MDSC) einen starken immuninhibitorischen Effekt ausübt. Erst durch die kombinierte Infusion von p53-spezifischen TZR T-Zellen und zusätzlicher Depletion der MDSCs konnte eine zuvor unzureichende anti-tumorale Antwort *in vivo* gesteigert werden.

Zusammenfassend zeigte sich, dass der einzelketten p53-spezifische TZR einen sicheren und effizienten Therapieansatz für eine TZR-basierte Gentherapie darstellt. Die Kombination verschiedener immuntherapeutischer Strategien kann dabei die Effizienz der durch TZR-Gentransfer vermittelten anti-tumoralen Antwort steigern.

Table of Content

List of Figures

List of Tables

Abbreviations

^{51}Cr	Radioactive Sodium Chromate chromium 51 isotope
A2	HLA-A2.1
$A2K^b$	$A2/K^b$ chimeric MHC I molecule (human α1/α2 A2 domain and mouse α3 $H\text{-}2K^b$ domain)
ACT	Adoptive cell transfer
APC	Antigen presenting cell
APC	Allophycocyanine
aq^{dest}	Bidestilled water
BM	Bone marrow
bp	Base pair
BSA	Bovine serum albumin
C57BL6/J	C57 Black 6/ Jackson Laboratories
CD	Cluster of differentiation
CDR	Complementary-determining regions
CFSE	5-(and 6)-Carboxyfluorescein diacetate succinimidyl esterl
Con A	Concanavalin A
DAB substrate	3,3-diaminobenzidine tetrahydrochloride
DAPI	4’,6-diamidino-2-phenylindole
DC	Dendritic cell
DMEM	Dulbecco’s Modified Eagle Medium
DMSO	Dimethylsulfoxide
ELB	Erythrocyte Lysis Buffer
FACS	Fluorescent activated cell sorting
FCS	Fetal calf serum

FITC	Fluorescein isothiocyanate
FluM1	Influenza virus matrix protein M1
GvHD	Graft versus host disease
h	Hour
HCl	Hydrochloric acid
HEPES	4-(2-hydroxyethyl)-1-piperazineethanesulfonic acid
i.p.	Intraperitoneal
i.v.	Intravenous
IFN	Interferon
IL	Interleukin
IRES	Internal ribosomal entry site
IU	International unit
kb	Kilo base
LB(-medium/-plates)	Luria-Bertani (-medium/-plates)
LPS	Lipopolysaccharide
LTR	Long terminal repeats
mAb	Monoclonal antibody
MACS	Magnetic activated cell sorting
MDSC	Myeloid derived suppressor cell
MHC	Major histocompatibility complex
min	Minute
NaCl	Sodium chloride
NEAA	Non-essential amino acids
NO	Nitric oxide
O/N	Over night
OD	Optical density
PBS	Phosphate-buffered saline

PCR	Polymerase chain reaction
PE	Phycoerythrin
ROS	Reactive oxygen species
RPMI1640	Cell culture medium for normal and neoplastic Leucocytes, developed at the Roswell Park Memorial Institute
s.c.	Subcutaneous
sc.	Single chain
sec	Second
SOB-medium	Super optimal broth-medium
TBS	Tris-buffered saline
TCGF	T cell growth factor
TCR	T cell receptor
Tet	Tetracycline
Tg	Transgenic
TGF	Transforming growth factor
T_H	Helper T cell
TNF	Tumor necrosis factor
U	Unit
VEGF	Vascular endothelial growth factor
WT	Wild type
β2M	Beta-2 microglobulin

1 Introduction

1.1 The different types of cancer immunotherapy

The history of cancer immunotherapy of solid tumors started a long time ago. William Coley made the first immunotherapeutic approaches by intratumoral injection of *Streptococcus pyogenes* and *Serratia marcescens* in 1891. The sarcoma of his patients regressed after several rounds of injection (1). However, due to severe risks for the patients and lack of reproducibility, oncologists continued to use surgery instead and started to apply new promising methods, such as radiation therapy and later on chemotherapy to treat cancer patients. Today, Coley's idea is applied to patients with superficial bladder cancer, who receive an intravesicular injection of live bacillus Calmette-Guérin after surgical tumor removal (2). An older clinical trial with a ten years follow-up period showed that the combination of surgery and bacillus Calmette-Guérin therapy led to 61.9% progression-free survival compared to 37% in patients who received surgery only (3).

Meanwhile, there are more options to treat cancer patients besides the most common approaches of radiation and chemotherapy. It happened to be just by chance, that the hematopoietic cell transplantation was developed, by trying to rescue patients after high dose of myeloablative chemoradiotherapy, which was administered to increase tumor cell killing after refractory leukemia (4). During the last five years the field of immunotherapy expanded dramatically and is in general divided into two approaches, active and passive immunotherapy. Monoclonal antibody therapy (5) and cellular therapy, e.g. donor lymphocyte infusion (6), or adoptive T cell transfer (ACT) (7) belong to the group of passive immunotherapies and are characterized by their passive transfer, without stimulation of the patient's immune system. In contrast, active immunotherapy such as vaccination with dendritic cells (8) or with peptides and adjuvants (9), application of immunomodulators like OX40 (10) or recombinant cytokines, such as interleukin 2 (IL-2) or interferon alpha (IFN-α) (11) stimulate the patient's immune system to generate an active immune response against existing cancer cells.

Focusing on adoptive T cell therapy Steven A. Rosenberg was one of the first scientists who used this approach in melanoma patients (12). He treated metastatic melanoma patients after preconditioning with cyclophosphamide by adoptive transfer of *in vitro* expanded tumor-infiltrating lymphocytes (TILs) together with IL-2.

Preconditioning proofed to be beneficial prior to ACT by (i) generating cytokine sinks, (ii) make space for the infused T cells to proliferate, as well as (iii) depleting T regulatory cells (T_{regs}), which inhibit the anti-tumor T cell response by their immunosuppressive features. In his study, Rosenberg observed cancer regression in 55% of the patients. Regression lasted between 2 and more than 13 months and *in vitro* expanded TILs were shown to lyse specifically autologous tumor cells, but not allogenic tumor cells or autologous normal cells. Moreover, in a recently published readout from three sequential clinical trials Rosenberg showed that 93 patients with measurable metastatic melanoma, who were treated after a lymphodepleting regimen with adoptive transfer of autologous TILs together with IL-2 showed in 22% a complete tumor regression and the 3- and 5-year survival rates for all patients were around 36% and 29%, respectively (13). As a founder of the TIL infusion, he not only developed a new method for extraction, *in vitro* expansion and reinfusion of TILs to cure melanoma patients (12), but also set up a starting-point for other researchers to find new strategies to overcome the limitations of TIL therapy. Drawbacks of TIL therapy are for example less immunogenic tumors, which do not show sufficient infiltrating T cells compared to melanoma. Furthermore, the period of extraction, *in vitro* expansion and testing of TILs can be shortened by using specific T cells, which can be generated by retroviral transduction of patients blood lymphocytes. For that, the knowledge of the composition of T cell receptors is of main importance.

1.1.1 The Biology of T cell receptors

T cells are a major component of the adaptive immune system and as such are indispensible for cell-mediated immune responses. T cell progenitors derive from pluripotent hematopoietic stem cells in the bone marrow and migrate to the thymus for maturation and selection. Each T cell has about 30.000 identical antigen-receptors on its surface and after selection there is a large repertoire of specific T cells with receptors, which are highly diverse in their antigen-binding sites and recognize pathogen-derived proteins and peptides, which are presented by major histocompatibility complex (MHC) molecules on antigen-presenting cells (APCs) (14). T cell receptors (TCR) simply deliver the message ‘bound to specific antigen’ to the cell; all other subsequent immunological effects depend on the actions of the T cell itself. There are two types of TCRs, the α/β and γ/δ TCRs. The function of γ/δ T cells

is less well known than that of α/β T cells. γ/δ TCRs are encoded by rearranging genes (as α/β-TCRs) and show the highest diversity in the δ-chain. γ/δ T cells are accounting for less than 5% of total T cells in the peripheral blood and are mainly located in the mucosal and epithelial tissue. It is thought that γ/δ T cells play important roles in anti-infection, antitumor and autoimmune responses, therefore having important functions in both innate and adaptive immune responses. However, the precise function and role of this cell subset is not entirely clear yet (15).

An α/β-TCR consists of two different polypeptide chains, the TCRα and the TCRβ chain. Each TCR chain has an amino-terminal variable domain (Vα and Vβ) and a constant region (Cα and Cβ) with a short segment, which contains a cysteine residue that forms the interchain disulfide bond to link both constant TCR chains. A hydrophobic transmembrane domain, which ends in a short cytoplasmic tail anchors the constant regions of each TCR chain in the cell membrane.

Besides the TCRα and the TCRβ chain the CD3 complex is required for the TCR to be expressed on the cell surface. Here, TCR the α:β heterodimer is associated with a complex of four signaling protein chains (γ-, δ-, and two ε-chains). The complex is called CD3 and is required for the cell-surface expression of the TCR and its downstream signaling. Together with the association of a homodimer of ζ chains with the cell-surface receptor complex, activation signaling is initiated. Therefore, each CD3 chain contains one immunoreceptor tyrosine-based activation motif (ITAM), whereas the ζ chains have each three copies of ITAMs, which gives the TCR complex a total of 10 ITAMs. It is thought that interaction takes place by the positive charge of the TCRα chain, which interacts with the negatively charged CD3 δ:ε dimer, and the positively charged TCRβ chain, which interacts with the negatively charged CD3 γ:ε dimer. The negatively charged CD3 ζ homodimer thus interacts with the remaining positive charges of the TCRα chain.

The whole α:β heterodimer is similar in its structure to the Fab fragment of a immunoglobulin molecule and has one antigen-binding site defined by the Vα and Vβ regions. Three complementary-determining regions (CDR1, 2, 3) from each of the heavy and light chains build together six hypervariable loops which determine the antigen specificity and are assembled by somatic recombination. The highest diversity is in the CDR3 loops, which bind to the central amino acids of the presented peptide. The CDR3 loops at the center of the antigen-binding site are flanked by the CDR1 and CDR2 loops. Here the TCR Vα and Vβ regions of the CDR1 and CDR2

loops interact with the helices of the peptide:MHC complex at the site of the amino and carboxy terminus of the bound peptide, respectively. Due to the variability within the CDRs, TCRs show a high diversity. Upon encounter of a specific antigen presented on the surface of an APC, which expresses the co-stimulatory molecules of the B7 family (CD80/B7.1 and CD86/B7.2), naïve T cells produce IL-2 to drive proliferation and differentiation into effector cells. Therefore, antigens are presented by APCs via MHC molecules. MHC molecules are able to bind peptides with high affinity but also have the ability to bind a wide variety of different peptides, in doing so the MHC complex is stabilized on the cell surface. MHC I presents peptides of 8-10 amino acids (AA) length, whereas MHC II presents peptides of 13-18 AA length.

In general there are two types of T cells to distinguish, which either bind to MHC II or MHC I molecules by the expression of their co-receptors CD4 and CD8, respectively. The CD4 co-receptor is a single-chain molecule made up of four immunoglobulin-like domains: D1 and D2, which are connected via a flexible hinge to D3 and D4. The CD4 co-receptor binds mainly via the D1 domain to the β2 domain of a MHC II molecule. In contrast, the CD8 co-receptor is either a disulfide-linked dimer of one α- and one β-immunoglobulin-like domain or a homodimer of two α-immunoglobulin-like domains, which are connected to the membrane by a glycosylated segment of extended polypeptide chains. The CD8 α:β hererodimer or the CD8 α homodimer interact with the α3 domain of a MHC I molecule. In general, the CD4 and CD8 co-receptors bind their respective MHC molecules nearest to the membrane and distant from the peptide-binding cleft and by this stabilize the TCR:MHC interaction. In addition, both co-receptors strongly interact in the intracellular compartment with the cytoplasmic tyrosine kinase Lck, thereby bringing it in close proximity to the signaling components of the TCR complex, which subsequently results in an enhancement of the signal that is generated after TCR binding to its peptide antigen.

Prior to antigen encounter in the periphery, T cells undergo thymic education processes to prevent harming the host by recognizing self-antigen. In brief, the very basic mechanism of this central tolerance is the following: T cells undergo maturation and selection in the thymus, where interaction with the thymic stroma also determines their lineage (α/β-, γ/δ- or NK T cells). In the thymus T cells undergo two selection processes, positive and negative selection. During positive selection the $CD4^+CD8^+$ double-positive bone marrow derived progenitor T cells are tested for their recognition of peptide:self-MHC complexes expressed on thymic cortical

epithelial cells. Depending on their recognition of either MHC II or I molecules cells are positively selected and become mature single-positive ($CD4^+$ or $CD8^+$) T cells. Afterwards, T cells undergo negative selection, where self-antigens are presented in context of self-MHC molecules by bone marrow derived APCs. In case the already selected T cells show a too strong reaction with self-antigens, those T cells will be deleted to avoid self-reacting T cells in the repertoire. Finally, the negatively selected T cells egress to the peripheral lymphoid organs (lymph nodes and spleen).

CD4 T cells bind to antigens presented via the MHC II molecules and become specialized effectors that promote inflammatory (TH1), humoral or allergenic (TH2), or acute (TH17) immune responses by secretion of specific cytokines. CD8 T cells are cytotoxic cells, which store preformed cytotoxins in cytotoxic granules. The content of the cytotoxic granules (granzymes, perforin, granulysin) is released upon encounter of the specific antigen presented via MHC I molecules, which causes the death of the target cell. In addition, CD8 effector T cells also secrete the cytokine IFN-γ, which activates macrophages to engulf cell debris, upregulates MHC molecules on target cells and express Fas ligand (CD95L or CD178), which induces apoptosis upon ligation with its receptor Fas (CD95 or apoptosis antigen 1, APO-1). Upon antigen encounter the number of effector T cells increases dramatically (= expansion) and decreases again (= contraction) to a level of 100-1000-fold above the initial frequency for the rest of the live of the organism. Persisting cells are termed memory T cells, which are long-lived and in addition are equipped with a particular set of cell-surface molecules and receptors. CD8 memory cells are more sensitive to restimulation by antigen and more quickly and vigorously in producing cytokines such as IFN-γ as compared to naïve CD8 cells. CD4 memory cells require additional restimulation, compared to CD8 memory cells, before they can act on target cells. In general, memory cells divide more frequently and a balance between proliferation and cell death tightly controls their expansion. There are two types of memory cells: effector memory and central memory cells. Effector memory T cells are able to mature more rapidly into effector T cells and secrete large amounts of cytokines (IFN-γ, IL-4 and IL-5) directly after restimulation with antigen. In contrast central memory T cells take longer than effector memory cells to differentiate into effector T cells and do not secrete high levels of cytokines early after restimulation.

According to the biology of TCRs T cells equipped with their specific receptors play a major role in fighting infection and disease. Therefore, in order to target solid tumors or cancer in general it is necessary to identify accurate antigens, which are preferably expressed only or in excessive amount by the neoplastic cell, to distinguish tumors from healthy host tissue.

1.1.2 Classification of tumor-associated antigens

Neoplastic cells can be discriminated from healthy cells by their antigen expression pattern. In general there are two categories of tumor antigens: (i) tumor-specific antigens and (ii) tumor-associated antigens. Chromosomal rearrangement, splice variants, point mutations or oncogenes (introduced into the cell by viruses), lead to the expression of tumor-specific antigens (TSAs). Such antigens are exclusively expressed by cancer cells. Accordingly, an immune response can theoretically be elicited since T cells directed against TSAs do not undergo negative selection in the thymus. However, TSAs are expressed only to very small amounts on the cell surface of tumors, which impede a TSA-directed immune response. In contrast tumor-associated antigens (TAAs) are ubiquitous protein, which are expressed by tumor and healthy cells. Although TAAs are usually overexpressed due to frequent mutations of proto-oncogenes or tumor suppressors, they do not, or only in rare events, elicit an immune response. Nevertheless, TAAs can be targeted by immunotherapeutic approaches such as adoptive TCR gene transfer. Thus, in comparison to TSAs, which are highly cancer-specific and can differ in-between different patients and cancer entities, TAAs are universal and therefore represent an overlapping approach to target different cancer entities and a wide range of patients. TAAs can be divided into different groups according to their phenotype (16).

- Oncofetal tumor antigens are only expressed in cancerous somatic cells and fetal tissue, such as tumor-associated glycoprotein-72 (TAG-72) in prostate carcinoma (17).
- Oncoviral tumor antigens are encoded by tumorigenic transforming viruses, such as Epstein-Barr virus (EBV) in nasopharyngeal carcinoma (18) or human papillomavirus (HPV) in cervix carcinoma (19).

- Cancer-testis antigens are expressed besides cancer cells in adult reproductive tissues such as testis and placenta, which lack MHC molecules. An example is NY-ESO-1 in non-small cell lung carcinoma (NSCLC) (20).
- Lineage-restricted or differentiation antigens are only expressed by the cell type, which is the origin of the tumor and by the tumor itself, such as Melan-A/MART-1 or Tyrosinase (Tyr) in melanoma (21, 22).
- Posttranslationally altered antigens show for example alterations in glycosylation pattern, such as Mucin 1 antigen (MUC-1) in breast cancer (23).
- Idiotypic cancer antigens evolve in lymphoproliferative disorders (B cell or T cell lymphoma/leukemia) and express a specific 'clonotype', resulting from clonal abberancies, such as TCRs in T cell lymphomas (24).
- Mutated antigens result from genetic mutations or alterations in transcription, such as p53 (TP53) (25) or Ras in cancer cells (26).
- Overexpressed or accumulated antigens are expressed by normal and tumor cells, although in the latter with highly elevated expression levels, such as the tumor-suppressor protein p53 (TP53) (25), survivin (27) or mouse double minute 2 (MDM2) in chronic lymphocytic leukemia (CLL) (28).

TAAs are processed by the proteasome like many other endogenous proteins to 8-10 AA long peptides and presented via MHC I on the cell surface of neoplastic cells. Nevertheless, most TAAs, although presented on the cell surface, cannot be targeted by the immune system, since most of the TAAs are also expressed by healthy cells (self-antigens) and in case of recognition would lead to autoimmune reactions. Therefore, to efficiently target TAAs self-tolerance has to be overcome, to enable T cells to target tumors.

p53, the tumor-suppressor protein, is a nuclear phosphoprotein, which functions as DNA damage-inducible sequence specific transcription factor and is phosphorylated in response to stress. A G1-arrest is mediated by p53 in presence of low doses of DNA damage, heat shock, hyperoxia, hypoxia and other forms of cellular stress, through targeting cyclin-dependent kinase inhibitors like $p21^{WAF-1}$ or 14-3-3. This arrest provides a sufficient break to allow damaged DNA to be repaired. In contrast, in case of severe DNA damage or extreme stress p53 triggers the activation of genes implicated in the apoptotic cascade such as NOXA, PUMA, Fas/APO-1. However, MDM2, an E3 ubiquitin ligase, acts as antagonist to p53 by limiting the growth-suppressive function in healthy cells through transfer of monoubiquitin tags onto

lysine residues mainly in the COOH terminus of p53 (29). Therefore, in unstressed cells p53 is unstable with a short half-life of 5-30min and is present only at low intracellular levels due to continuous degradation induced by MDM2 (30, 31). This auto-regulatory negative feedback loop of MDM2 and p53 is blocked in case of DNA damage, which promotes phosphorylation of p53 and MDM2, thus inhibiting their interaction, therefore stabilizing p53. Still, the precise mechanisms of p53 activation are not fully understood. It is thought that they include posttranslational modifications (ubiquitination, acetylation, phosphorylation, sumoylation, neddylation, methylation, glycosylation) of the p53 polypeptide.

In this study we focused on p53 as a universal TAA, since missense mutations at one of several defined hotspots in the p53 gene (*TP53*) lead to inactivation or loss of function (32) as well as stabilization of p53 protein and overexpression on the cell surface of tumor cells (33) (Table 1.1).

Table 1.1 Somatic mutations of p53 – TP53 mutation prevalence by tumor site (n=26.325).
IARC TP53 Database, R17, November 2013; http://p53.iarc.fr/SelectedStatistics.aspx

Cancer type	Mutational prevalence [%]
Colorectum	43.28%
Head and Neck	42.51%
Esophagus	41.21%
Female genital organs	38.57%
Pancreas	34.67%
Skin	34.73%
Stomach	32.38%
Liver	31.19%
Urinary tract	26.87%
Nervous system	25.95%
Breast	22.8%
Soft tissue	21.36%
Lymph nodes	19.34%
Male genital organs	16.38%
Endocrine glands	15.88%
Bones	14.43%

1.1.3 Advantages of TCR gene therapy

As already shown by Rosenberg, T cell therapy with TILs shows high response rates in melanoma patients (12), but nevertheless also comes with some disadvantages like graft-versus-host disease (GvHD, see also section 1.1.4) or graft rejection after allogenic stem cell transplantation in HLA-mismatched immunodeficient patients. TIL therapy is also a time consuming and costly process, since it is difficult to extract, screen and cultivate TILs within a limited timeframe before reinjection into the patient. Moreover, it is difficult to reach persistence of high numbers of TILs in patients after infusion, same as it is challenging to isolate high-affinity TILs in a reproducible manner. Therefore, at the same time alternative methods were established. In 1986 it

was demonstrated that by transfer of TCR genes into primary T cells a strategy was found to circumvent all limitations that go along with adoptive T cell therapy. With this method it was possible to transfer T cell immunity in a passive manner. In this context Dembić and others showed that the TCR specificity of one cytotoxic T cell could be transferred to another by transfection of the host cells with TCR α- and β-chain genes from the donor cell (34). Roughly 15 years later the transfer of TCR specificity of MART-1 (35) and HIV (36) to mature peripheral T cells could be demonstrated *in vitro*. Simultaneously, other groups showed the feasibility of TCR gene transfer *in vivo* by transferring redirected Epstein-Barr virus-specific T cells to mice infected with an EBV lymphoma (37). Those promising results paved the way for the first clinical trials. One of them published by Rosenberg and colleagues showed tumor regression in almost 12% of all lymphodepleted patients with metastatic melanoma after infusion of *in vitro* expanded autologous polyclonal T cells transduced with a MART-1-specific TCR (38). Finally, it was shown that in TCR gene therapy there is no reactivity of the endogenous TCR repertoire against the introduced T cells also when transduced T cells show a self-antigen reactivity and the capacity to induce a strong antigen-specific T cell responsiveness in partially MHC-mismatched hosts (39).
Meanwhile, concerns arose about the use of γ-retroviral vectors, which can cause adverse events in patients due to insertional mutagenesis. However, this issue is controversially discussed and so far there is no clear evidence that this process takes place in mature T cells (40).

In conclusion, TCR gene therapy is a strategy to instantly generate a defined T cell immunity by introducing TCRs with high affinity, which is not naturally present thereby overcoming the limitations of the host immune system. In contrast to the limitations of TIL therapy, α and β chains of TCRs can be transduced into large numbers of patient T cells, which then can be expanded to even larger numbers within short time in order to reach therapeutic quantities of antigen-specific T cells. In addition it was shown that the injection of a bulk population of redirected $CD8^+$ and $CD4^+$ cells is important to maintain a functional $CD8^+$ T-cell memory (41). Moreover, also redirected $CD4^+$ cells with T helper (T_H) phenotype could control tumor outgrowth (42).

1.1.4 Challenges and pitfalls of TCR gene therapy

Despite the observed clinical success, TCR gene therapy also showed some drawbacks during its development. In the study described in 1.1.3, Rosenberg and colleagues used a MART-1-specific TCR to transduce autologous polyclonal T cells. However, later analysis showed that the introduced TCR chains were only poorly expressed, as demonstrated by only 17% bound MART-1 tetramer at the time of injection. Moreover, one month after injection the retroviral transgene could be detected in only 26% of the patients' peripheral T cells and less than 1% of these T cells bound MART-1 tetramer (38). There are two explanations for the partial failure of the trial: (i) earlier results of other groups already showed that retroviral vectors can be silenced *in vivo* due to methylation of the long terminal repeats (LTR), which stably integrate the virus DNA into the host cell genome (43). By downregulation of the introduced TCR in transduced cells they fail to lyse their targets. By choosing a strong constitutive promoter this drawback can be circumvented (36). (ii) MART-1 specificity can also be lost because of mispairing of endogenous (native) TCR α or β chains with exogenous (introduced) TCR α or β chains, respectively (44, 45). Here, the introduction of exogenous TCRs with another specificity in mature T cells, which already have a natural TCR repertoire, can lead to mixed dimer formation between exogenous and endogenous TCR chains. The newly formed TCRs with unknown specificity can potentially harm by recognizing host antigens, which can lead to autoimmunity (Figure 1.1). In an autoimmune reaction caused by newly formed mispaired TCRs, T cells attack non-hematopoietic tissues such as endothelia, liver, skin, kidney, spleen and intestine (46). These processes or mispairing events are called 'off-target' reactions and can be prevented by using single chain TCRs instead of αβ TCRs.

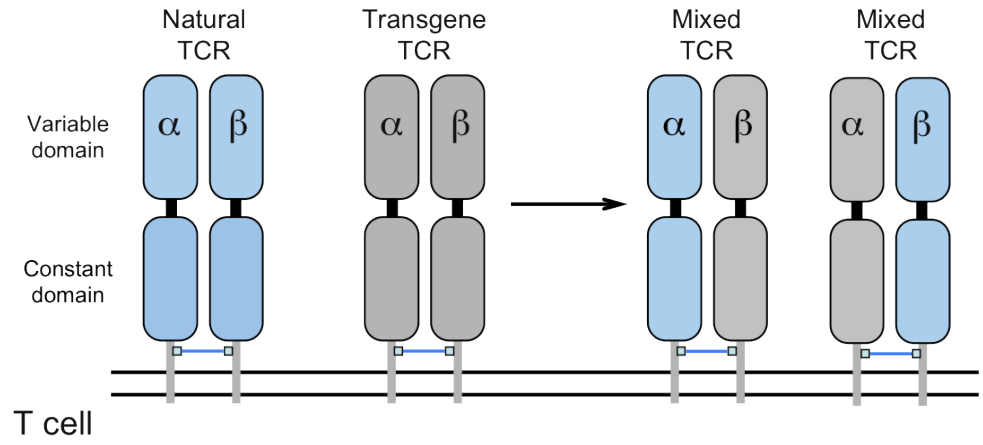

Figure 1.1 Formation of mixed heterodimers after transduction of mature T cells.
After retroviral transduction of a transgenic TCR (grey) into a mature T cell with natural occurring TCRs (blue), mixed TCR dimers can emerge by pairing of natural and transgenic TCR chains during assembling of the TCR in the endoplasmatic reticulum. In case of presentation on the cell surface, they might harm the host tissue due to their unknown specificity.

Adverse effects can also occur in patients as a reaction to immunogenic retroviral vectors (47), by an overwhelming immune response of the host against the modified T cell population (48) or by an excessive TCR signaling after infusion of redirected T cells upon recognition of low amounts of presented antigens (49). In the first study Morgan and colleagues observed that the secretion of inflammatory cytokines (cytokine storm) in addition to the infiltration and proliferation of T cells redirected with a chimeric antigen receptor (CAR) in the lung was much stronger than expected and led to the death of the patient within five days after infusion of T cells. Such host responses might be controlled or prevented by immediate immunosuppression, for example by application of steroids. At the same time Melief and colleagues were able to show GvHD reactions induced by continuous peptide vaccination after transfer of redirected T cells in a mouse model (50).

Although immunotherapy with transgenic TCRs has been revised after the severe outcomes of earlier studies, there are still pitfalls to give way. Just recently two clinical trials were published using HLA-A*01 and HLA-A*02 anti-MAGE-A3 TCRs, which showed off-target/off-tumor (51) and on-target/off-tumor toxicity (52), respectively. In the latter on-target toxicity could be demonstrated by proving that the anti-MAGE-A3 TCR was also able to target MAGE-A2/ A6/ A9 and A12, due to sequence similarities and site-directed mutagenesis in the CDR3 region to further increase the avidity. Targeting additionally MAGE-A12, which is expressed in a subset of neuronal cells in the brain, resulted in death of 2 out of 9 patients as well as severe neurological side effects in 2 other patients of the trial. A proof for off-target

toxicity was made by Linette and colleagues, who showed that another MAGE-A3 tg TCR recognized the protein titin, which is neither related structurally nor functionally to MAGE-A3 and is expressed in actively beating cardiac myocytes. The first two patients developed a cardiogenic shock one week after TCR infusion and died within 10 days, consequently leading to an immediate stop of the trial. To circumvent side effects and disadvantages of αβ TCR transfer, several strategies have been established and are described in section 1.1.5.

1.1.5 Circumventing self-tolerance to p53 and optimizing p53-specific TCRs

To be able to target different tumor entities with only one therapeutic approach requires finding a universal TAA. The disadvantage of such TAAs is that they are usually also expressed on healthy host tissue. Targeting universal TAAs, such as p53 or MDM2, with a TCR gene therapy therefore can lead to on-target toxicity, which manifests in autoimmune reactions similar to GvHD. This severe reaction plays a major role during bone marrow transplantation and is characterized by the recognition of host (recipient) tissue by donor T cells, which recognize the host as 'foreign'. HLA mismatches between donor and recipient are major cause for this disease, which occurs to some extent with a pronounced morbidity and mortality, depending on the organ of clinical manifestation, and can require permanent immunosuppression and intense follow up treatment. For mouse studies the clinical index of GvHD is determined by a grading from 0-2 for five given criteria. These criteria include the percentage of body weight change, posture (hunching), activity, fur texture and skin integrity (53). Hence, thinking of isolating high affinity p53-specific CTLs or transferring p53TCR-modified T cells raises doubt due to the self-tolerance mechanism. However, it could be shown that TCR modified T cells, which recognize a potent self-antigen, are indeed able to induce a TCR response towards that self-antigen (39), whereas – due to tolerance – no reactivity by the endogenous T cell compartment was observed (54, 55). Already in 1995 Theobald and colleagues could induce a CTL response towards human p53 peptides $p53_{(264-272)}$ and $p53_{(149-157)}$, which were non-homologous to mouse p53 sequences, after immunization of A2.1/K^b-Transgenic (Tg) or A2.1-Tg mice (56). Because of the inability of the mouse CD8 co-receptor to interact with the α3 domain of the human A2.1 molecule, CTLs were co-receptor-independent in their recognition of target cells and showed

increased affinity towards cells of the A2.1-Tg mice. Moreover, by testing normal cells, recognition of presented A2.1-bound p53 peptide failed because of insufficient levels of presented peptide compared to p53 overexpressing tumor cells. These results underlined previous reports, which demonstrated that the amount of antigen required for negative selection is less than that required for recognition by effector T cells (57) and that high-affinity TCRs recognizing self-MHC survive negative selection due to the lack of co-receptor signaling (58). Optimizations of TCR constructs such as murinisation of the TCR constant domains (59, 60) or by removing defined N-glycosylation sites in the TCR constant domain (61) as well as introduction of additional disulfide bonds between the constant TCR domains (62) further helped to support a preferential pairing of the introduced TCR chains and to avoid mispairing reactions (see 1.1.4). In addition to enable an effective TCR expression optimized retroviral vector systems, which are usually less sensitive to silencing, are used. A stabilized vector expression supports nuclear uptake of the TCR genes and subsequent chromosomal integration.

The isolated $p53_{(264-272)}$ TCR used in this thesis was optimized to reach a more efficient expression and functionality for an increased clinical relevance in terms of safety of adoptive TCR gene transfer. In brief, codon optimization of the TCR gene leads to a more efficient transduction efficacy, an additional disulfide bond was added between the TCR constant domains and the whole TCR was cloned in one retroviral construct. Here, the TCR α chain was connected to the TCR β chain via a 2A element (63) to achieve equimolar levels of TCR transcripts. As an additional approach for increased safety of the TCR construct a single-chain $p53_{(264-272)}$-specific TCR was generated, in which the variable α chain of the TCR is connected via a glycine/serine-rich SL7 linker peptide to the variable β chain of the TCR β chain (64) (Figure 1.2).

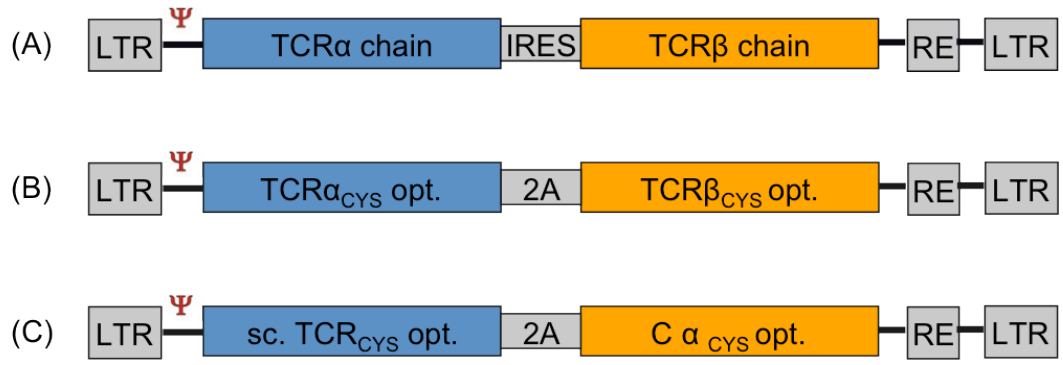

Figure 1.2 Retroviral vector constructs for the p53$_{(264-272)}$A2.1-specific TCR
All retroviral constructs are cloned into pGMP vectors and genes are flanked by long terminal repeat (LTR) sequences. (A) In the wt. p53TCR construct the full TCR α-chain gene is connected via an internal ribosomal entry site (IRES) to the TCR β-chain gene. (B) The αβ- or double chain p53-specific TCR construct was codon optimized (opt.) and an additional disulfide bond was added between the constant domains (C) of the TCR α- and β-chain (CYS). Both transgenes are linked via a 2A element (2A). (C) In single chain (sc.) p53-specific TCR the sequences are similar to the αβ-chain TCR opt. and the constant domains (C) show an additional disulfide bond (CYS). Here, the sc. transgene is connected via a 2A element to the Cα transgene. The single chain consists of a variable α-chain connected via a SL-2 linker to the full β-chain transgene (see also Figure 4.1).

In this dissertation, the different p53-specific TCR constructs were tested for safety and efficacy *in vitro* and *in vivo*.

1.2 Tumor immune escape mechanisms – the role of the tumor microenvironment

According to the 'hallmarks of cancer', a paper published first in 2000 (65) and last revised in 2011, all cancers share 10 common features or principles, that cause the transformation of normal to malignant cells. In 2011, attributes such as avoiding immune destruction, tumor-promoting inflammation, deregulation of cellular energetics, genome instability and mutation were included. All together, these hallmarks allow cancer cells to survive, proliferate and disseminate in the multistep process of tumorigenesis (66). Still, many scientists tried to shed more light on the process of tumor evolvement especially in the mechanism of tumor immune escape to improve current therapeutic approaches. Simultaneously to the revised 'hallmarks', Schreiber and colleagues published a highly controversial theory of tumor immune escape, where they described two roles of the immune system, either host-protective or tumor promoting. Moreover, they split the process of tumor escape in three crucial steps: elimination, equilibrium and escape (67). In the latter step, under constant immune selection and pressure, tumor cell variants emerge that (i) are no longer recognized by the immune system due to antigen loss or defects in the antigen processing machinery (68), (ii) become insensitive to immune effector mechanisms (69) or (iii) induce an immunosuppressive tumor microenvironment (TME) by

recruiting immunosuppressive cells, expression of inhibitory ligands or by immunosuppressive cytokines (70, 71). Therefore, detailed analysis of the TME with the aim to remove or suppress the 'key players' in the TME are indispensable as basis for new therapeutic approaches, since it will enhance tumor recognition and regression.

The TME is characterized by hypoxic conditions and extracellular adenosine and – besides tumor cells – consists of infiltrating stromal cells, lymphocytes and myeloid cells. Stromal cells have a main impact on how the immune system interacts with the tumor by building a hypoxic environment (72). Infiltrating lymphocytes can be separated in $CD4^+$ and $CD8^+$ T cells (TILs) and regulatory T (T_{reg}) cells, which have a highly immunosuppressive capacity. The presence of T_{reg} cells in tumors is cancer type-specific. In metastatic melanoma T_{reg} cells show highly increased frequencies in the tumor compared to the peripheral blood (73) and although their function in the TME is not completely clear, the presence of those cells correlates with poor clinical outcome (74). Moreover, it could be demonstrated that infiltrating $CD8^+$ T cells expressing vascular endothelial growth factor receptor-1 (VEGFR1) show chemotaxis towards high amounts of vascular endothelial growth factor-A (VEGF-A) (expressed in the TME) and, upon encounter of the ligand, decrease their IFN-γ production and increase IL-10 secretion, thereby favoring an immunosuppressive TME (75). This process also reflects the importance of the TME, which is able to reprogram initially cytotoxic TILs into harmless inactive or anergic cells (76). Among the terminally differentiated myeloid cells three groups are discriminated: dendritic cells (DCs), macrophages and granulocytes, all of which are converted within the TME into potent immunosuppressive cells. Increased accumulation of immature DCs and an impaired functionality of mature DCs could be shown in patients with non-small cell lung cancer (NSCLC) (77). Macrophages, which infiltrate into tumors are called tumor-associated macrophages (TAMs) and show an M2-like phenotype of alternative activation. They are activated by inflammatory cytokines such as IL-4 and IL-13 and secrete high levels of IL-10 and transforming growth factor-β (TGF-β). TAMs support tumor progression by different mechanisms such as the promotion of angiogenesis (78), facilitation of tumor cell metastasis (79) and protection of tumor cells from chemotherapy-induced apoptosis (80). Moreover, it could be shown, that in patients with NSCLC the cc chemokine ligand 2 (CCL2) serum levels were dramatically increased compared to healthy controls (81). CCL2 is important in recruiting

macrophages, therefore, a positive feedback and amplification loop arise in the tumor micro milieu (82).

The most frequent representatives of granulocytes are neutrophils, which usually engulf and destroy bacteria. However, they can also serve as a prognostic marker for poor clinical outcome in hepatocellular carcinoma and other cancer types (83) by shifting from anti-tumor activity to a pro-tumoral phenotype in the presence of TGF-β (84). Besides mature myeloid cells, also immature myeloid cells, called myeloid-derived suppressor cells (MDSCs), infiltrate into the TME. MDSCs are the main source and the most potent cells for immunosuppression, neovascularization and metastasis. Their appearance and mode of suppression is highly dependent on the type of cancer, as shown in a study of Corzo and colleagues, in which they observed a differentiation from MDSCs towards a macrophage phenotype in a hypoxic TME (85). In general, MDSCs can be divided into two subtypes, polymorphonuclear (granulocytic) and monocytic MDSCs. Granulocytic MDSCs are characterized by their high expression of arginase 1 (ARG1), myeloperoxidase and reactive oxygen species (ROS) (86). In contrast monocytic MDSCs are more immunosuppressive, express high levels of iNOS and ARG1 (87). MDSCs exert immunomodulatory functions on T cells by driving them into an anergic state. One major mechanism for this process is the deprivation of nutrients, e.g. L-arginine and L-cysteine in the TME (88, 89). Those amino acids are required for T cell function as their depletion causes the down-regulation of the ζ chain, which leads to proliferation arrest of antigen-specific T cells. Moreover, MDSCs produce ROS and reactive nitrogen species through ARG1, iNOS and NADPH oxidase (90), thus generating oxidative stress, which also leads to the loss of TCR ζ chains and reduced cytokine production (91) as well as loss of IL-2 production and the inability to up-regulate early activation markers (92). Finally, MDSCs are also able to hinder lymphocytes from homing to lymph nodes by expression of ADAM17, thereby hindering them from getting activated (93), or from trafficking to the tumor core by nitration of the chemokine CCL2 (94), leading to trapped antigen-specific T cells in the tumor stroma. MDSCs can also induce T cell tolerance and accumulation of T_{reg} cells by expression of CD40 (95) or by the secretion of cytokines such as IFN-γ, IL-10 or TGF-β (96).

In summary, the TME is characterized by the presence of different non-tumor cell subsets and an inflammatory environment, all of which is indispensible in the neoplastic process by promoting proliferation, migration and survival of tumor cells.

However, MDSCs are key players in maintaining an immunosuppressive and tolerogenic TME in many cancers (97). This heterogeneous population of immature myeloid cells is able to efficiently inhibit an antitumor response and thus limits the efficiency of antitumor immunotherapy.

1.3 Future trends – combined immunotherapy

The TME contributes to tumor initiation and progression and particularly determines the response rate to therapy. However, chemotherapies, which were initially developed through screening for effective compounds that eliminate rapidly dividing cells, are still the treatment of choice for cancer, even though this approach is limited by a narrow therapeutic index, harmful toxicities and frequently acquired resistances.

Today, by being able to distinguish diagnostically defined populations, new therapeutic approaches, such as targeted therapy and cancer immunotherapy, have been established. Targeted therapy comprises agents, which inhibit molecular pathways that are crucial for tumor growth and maintenance. Immunotherapy, as described above, intends to stimulate the host immune response to give rise to long-lived tumor destruction. Although both approaches are very effective in modulating immune responses, still, therapies sometimes fail to control disease burden due to therapy resistance (98). Since combinations of chemotherapeutic drugs are already an important element to treat cancer (99), the next logical approach should be the combination of targeted therapy with cytotoxic agents or immunotherapeutic approaches to improve clinical outcome. An important aspect to think of when combining different treatments should be to match appropriate therapies in a way that they can activate the host's immune system during tumor reduction and remission to obtain a long-term and durable benefit.

It could be shown that a therapy with trastuzumab, a monoclonal antibody targeting human epidermal growth factor receptor 2 (HER2) followed by anti-CD137 antibody treatment significantly reduced tumor growth and increased survival in a mouse model for breast cancer, when compared to treatment with either antibody alone (100). Even more convincing was the study of combining ipilimumab (antibody against cytotoxic T-lymphocyte-associated antigen 4, CTLA-4) and nivolumab (antibody against programmed death 1 (PD-1) receptor) to treat advanced melanoma patients. Both antibodies target inhibitory CD28-related receptors expressed by T

cells, which are normally induced on activated T cells to regulate T cell signaling and prevent their over-activation. Ligands for both receptors are used by tumors as escape strategy to limit the antigen-specific function of TILs. The objective response rate in this study was 40% and it could be shown that a simultaneous treatment with ipilimumab and nivolumab led to controllable side effects and a fast tumor regression in a large number of patients (101). Moreover, combined therapy using gene modified T cells and anti-PD-1 antibody treatment showed enhanced therapeutic efficiency of the injected HER2-specific CAR T cells *in vivo* in a mouse model for breast cancer (102).

Finally, by the discovery of crucial molecular pathways in cancer cells, which are necessary for cancer growth and survival, we are now able to use this knowledge for translation into a more efficient immunotherapy and the development of drugs, which target those molecular pathways in cancer cells. Therefore, to combine targeted agents with immunotherapeutic approaches to reach a therapeutic concurrence leading to prolonged patient survival and tumor regression is more than feasible and an outstanding aim in cancer therapy.

2 Aim of the Study

The mouse CD8-independent sc p53-specific TCR, which recognizes the HLA-A*0201 restricted epitope 264-272 of the human p53, was used in this study to investigate its safety and efficacy in adoptive TCR gene transfer in HLA-A2 transgenic mice. Because earlier studies showed that the transfer of redirected OT-I specific T cells in mice can lead to severe side effects resulting in death (103), our main focus was on the safety issue of adoptive transfer of p53TCR-redirected T cells. Moreover, several studies already gave hints that complex cellular interactions within the tumor stroma support tumor immune escape mechanisms and lead to the failure of immunotherapeutic approaches. Therefore, we used the mouse sc p53TCR in different humanized mouse models for preclinical studies to address the safety, feasibility and efficacy of adoptive p53-specific TCR gene transfer.

The following four specific questions were addressed:

(i) Can we prevent mispairing-induced off-target autoimmunity by using sc p53-specific TCRs as compared to conventional optimized αβ-chain TCRs?

(ii) Does the sc p53TCR discriminate between cancer and healthy p53-expressing tissue in terms of undesirable on-target related toxicity?

(iii) Do we observe any therapeutic potential by means of tumor eradication via the sc p53TCR?

(iv) Can we modulate the immunosuppressive tumor microenvironment to improve adoptive TCR gene therapy?

Tumor-mediated changes in the tumor microenvironment can lead to phenotypical and functional changes of infiltrating immune cells, which might result in failure of tumor recognition by the immune system. Therefore, this work also aimed to find a therapeutic intervention to improve immunotherapy with optimized TCRs.

3 Material and Methods

3.1 Laboratory equipment

Table 3.1 Overview of the laboratory devices

Device	Identification	Manufacturer
Balance	L2200S	Sartorius, Göttingen, Germany
Fluorescent camera	Spot FLEX	Visitron System, Puchheim, Germany
Transmitted light camera	Leica DCF 480	Leica Microsystems, Wetzlar, Germany
Cell irradiation machine	Gammacell 2000	Mølsgaard Medical, Ganløse, Denmark
Centrifuge	5417R	Eppendorf, Hamburg, Germany
Centrifuge	Megafuge 1.0R	Heraeus, Hanau, Germany
Centrifuge	Biofuge fresco	Heraeus, Hanau, Germany
CO_2 Incubator	Heracell	Heraeus, Hanau, Germany
CO_2 Incubator	Function line	Heraeus, Hanau, Germany
Cryostat	Leica CM 1900	Leica Microsystems, Wetzlar, Germany
Electrophoresis power supply	EPS600	Pharmacia Biotech, München, Germany
Flow Cytometer	Calibur	Becton Dickinson, Heidelberg, Germany
Flow Cytometer	Canto II	Becton Dickinson, Heidelberg, Germany
Flow Cytometer	Vantage SE	Becton Dickinson, Heidelberg, Germany
Flow Cytometer	Aria	Becton Dickinson, Heidelberg, Germany
Fluorescent lamp	HB100	Leistungselektronik GmBH Jena (Jena)
Gamma counter	Cobra II	Canberra Packard, Schwadorf,

		Austra
Laminar Flow/ Clean bench	S2020 1.8	Thermo Scientific, Langenselbold, Germany
MACS-Systems	MACS MultiStand and MidiMACS Separator	Miltenyi Biotec (Bergisch Gladbach)
Microscope	Axiostar	Zeiss, Jena, Germany
Microscope	Wilovert	Hund, Wetzlar, Germany
Microscope	Leica DMR	Leica Microsystems, Wetzlar, Germany
Microscope	Axiophot	Zeiss, Jena, Germany
Microscope power adapter	Ebq 100	Leistungselektronik Jena, Jena, Germany
Mouse irradiation machine	OB58-BA	Buchler, Braunschweig, Germany
PCR Cycler	MasterCycler Gradient	Eppendorf, Hamburg, Germany
pH meter	Knick pH-Meter 766	Calimatic, Zweibrücken, Germany
Photometer	Ultraspec 1000	Pharmacia Biotech, München, Germany
Photometer	Gene Quant II	Pharmacia Biotech, München, Germany
Shaker	Aerotron	Infors AG, Bottmingen, Switzerland
UV documentation	Transilluminator	Biostep GmbH, Jahnsdorf, Germany
Water bath	1003	Gesellschaft für Labortechnik, Burgwedel, Germany
Water bath	F12	Julabo Labortechnik GmbH, Seelbach, Germany

3.2 Chemicals and reagents

Unless otherwise noted, all chemicals were purchased from Merck (Darmstadt, Germany), Roth (Karlsruhe, Germany) or Sigma Aldrich (Deishofen, Germany).

All buffers were prepared with Millipore bidestilled water and if necessary sterile filtered with Steritop^{TM} Filter Units (Merck Millipore, Darmstadt, Germany).

Table 3.2 Important chemicals and reagents for cell culture, *in vivo* studies and molecular biology

Reagent	Manufacturer
Cell culture	
Anti-PE microbeads	Miltenyi-Biotec, Bergisch Gladbach, Germany
β2M	Sigma, Deisenhofen, Germany
BSA	Sigma, Deisenhofen, Germany
CD3/CD28 beads	Invitrogen, Darmstadt, Germany
Chromium-51 ($Na_2{}^{51}CrO_4$)	Perkin Elmer, Boston, USA
Concanavalin A	Calbiochem, Darmstadt, Germany
DMSO	Sigma, Deisenhofen, Germany
DMEM	BioWhittaker, Verviers, Belgium
EDTA	Sigma, Deisenhofen, Germany
FCS	PAA, Linz, Austria
Fugene 6	Promega, Madison, USA
Geneticin (G418)	Gibco, Eggensheim, Germany
Gentamicin	BioWhittaker, Verviers, Belgium
HEPES-Buffer	BioWhittaker, Verviers, Belgium
L-glutamine	BioWhittaker, Verviers, Belgium
Na-Penicillin/Streptomycin	Gibco, Eggensheim, Germany
NEAA	BioWhittaker, Verviers, Belgium
1x PBS (sterile)	Gibco, Eggensheim, Germany

Polybrene	Sigma, Deisenhofen, Germany
RPMI1640	BioWhittaker, Verviers, Belgium
Trypsin-EDTA	Gibco, Eggensheim, Germany
Trypan blue	Sigma, Deisenhofen, Germany
***In vivo* studies**	
Aldara	MEDA Pharma, Bad Homburg, Germany
Anti-CD40, mouse mAB (FKG45)	Enzo® Life Sciences, Lörrach, Germany
Dexpanthenol eye ointment	Bayer Vital, Leverkusen, Germany
Human IL-2 (Proleukin® S)	Novartis, Basel, Switzerland
Ketamine	Pfizer, Berlin, Germany
Sulfate latex 4% w/v 5µm	Invitrogen, Darmstadt, Germany
Tissue-Tek® O.C.T.™	Sakura Finetek, Alphen aan den Rijn, Netherlands
Xylazine (Rompun 2%)	Bayer Vital, Leverkusen, Germany
Molecular biology	
Agar	Starlab, Hamburg, Germany
Agarose	Roth, Karlsruhe, Germany
Ampicllin	Sigma, Deisenhofen, Germany
Bactotryptone	Roth, Karlsruhe, Germany
1x BSA	New England Biolabs, Frankfurt/ Main, Germany
DNA ladder 100bp and 1kb	New England Biolabs, Frankfurt/ Main, Germany
Ethidiumbromide	Merck, Darmstadt, Germany
6x Gel Loading Dye	New England Biolabs, Frankfurt/ Main, Germany
JM109 stock solution	New England Biolabs, Frankfurt/ Main, Germany
Restriction endonuclease Bam HI	New England Biolabs, Frankfurt/ Main, Germany
Restriction endonuclease CIP	New England Biolabs, Frankfurt/ Main, Germany
Restriction endonuclease EcoRV	New England Biolabs, Frankfurt/ Main, Germany

Restriction endonuclease Not I	New England Biolabs, Frankfurt/ Main, Germany
Restriction endonuclease SwaI	New England Biolabs, Frankfurt/ Main, Germany
Pfx50 Polymerase	Invitrogen, Darmstadt, Germany
T4 Ligase	New England Biolabs, Frankfurt/ Main, Germany
Tetracyclin	Sigma, Deisenhofen, Germany
XL-1 Blue stock solution	New England Biolabs, Frankfurt/ Main, Germany
Yeast extract	Roth, Karlsruhe, Germany

3.3 Buffer and cell culture media

3.3.1 Buffer for molecular biology

LB-medium
10g NaCl
10g Bactotryptone
5g Yeast extract
adjust to 1l with aq^{dest}, adjust to pH 7.0, autoclave for sterilization.

LB-plates
10g NaCl
10g Bactotryptone
5g Yeast extract
15g Agar
adjust to 1l with aq^{dest}, adjust to pH 7.0, autoclave for sterilization.

For antibiotic selection 100µg/ml amp was added to LB-medium or LB-plates.

SOB-medium
0.5g NaCl
20g Bactotryptone
5g Yeast extract
10ml 250mM KCl
5ml 2M $MgCl_2$

	adjust to 1l with aq^{dest}, adjust to pH 7.0, autoclave for sterilization
50x TAE Buffer	242g Tris base
	100ml 0.5M Na_2EDTA pH8.0
	57.1ml Acetic acid
	adjust to 1l with aq^{dest}.
TfB I Buffer	30mM Cobaltacetat
	50mM MnCl2
	100mM CaCl2
	15% Glycerin
	adjust to pH 5.8 with acetic acid, filter sterile.
TfB II Buffer	10mM Mops-Na pH 7.0
	75mM $CaCl_2$
	10mM KCl
	15% Glycerin
	filter sterile.

3.3.2 Buffer for histology

10x TBS Buffer	0.5M Tris base
	1.5M NaCl
	adjust to 1l with aq^{dest}, adjust pH to 7.5 with HCl
10x PBS Buffer	80g NaCl
	2g KCl
	26.8g Na_2HPO_4-$7H_2O$
	2.4g KH_2PO_4
	adjust to 1l with aq^{dest}, adjust pH to 7.4 with HCl
1x PBS-Tx	1x PBS
	0.1% Triton X-100

3.3.3 Buffer for cell culture

MACS Buffer	0.5% BSA
	2-4mM Na_2EDTA
	dilute in 1x PBS, filter sterile
1-4% PFA	10g/ 40g PFA
	adjust to 1l 1x PBS and dissolve at 60°C in the water bath.
Erythrocyte Lysis Buffer	174mM NH_4Cl
	10mM $KHCO_3$
	0.1mM Na_2EDTA
	adjust to 500ml aq^{dest}, adjust to pH 7.3.

3.3.4 Cell culture media

RPMI1640	10% Heat inactivated FCS
	1% L-glutamine
	100U/µg/ml Penicillin-streptomycin
	adjust to 500ml with RPMI1640, filter sterile
RPMI only	RPMI1640 without supplements
TCGF medium	10% Heat inactivated FCS
	1% L-glutamine
	1% Hepes
	50µg/ml Gentamicin
	2.5 mg/ml Con A
	adjust to 500ml with RPMI1640, filter sterile

DMEM	10% Heat inactivated FCS
	1% L-glutamine
	1% Hepes
	1% NEAA
	100U/µg/ml Penicillin-streptomycin
	adjust to 500ml with DMEM, filter sterile
DMEM only	DMEM without supplements
Freezing media	10% DMSO
	adjust to 30ml with heat inactivated FCS, filter sterile

3.3.5 Peptides

p53 (26-mer):	$p53_{257-282}$	LEDSSGNLLGRNSFEVRVCACPGRDR
p53 (9-mer):	$p53_{264-272}$	LLGRNSFEV
FluM1 (9-mer):	$FluM1_{58-66}$	GILGFVFTL

All peptides were purchased from Biosynthan, Berlin, Germany and dissolved according to their solubility character to 10mg/ml in sterile DMSO or sterile aq^{dest}.

3.4 Methods

3.4.1 Cloning cys. opt. p53TCR α-chain and β-chain

3.4.1.1 Polymerase chain reaction (PCR)

In order to construct a single p53-specific α- and a single p53-specific β- T cell receptor chain a gradient PCR was performed using specific primers to amplify each sequence (Table 7.1). The pGMP89 vector was used (see chapter 7). PCR programs are listed in Table 3.3 and Table 3.4 (section 3.4.1.3)

3.4.1.2 Vectors

Following plasmids were used:

pcDNA3.1, pCL-ECO, pGMP665, pGMP89, pGMP93, pMX-IE-GFP, pMx-Katushka, pMx-Tomato.

All vector maps are listed in the annex (chapter 7).

3.4.1.3 PCR Program

Table 3.3 PCR program to generate the single α-chain construct (1015bp)

Reaction	Temperature	Duration	
Initial denaturation	94°C	2 min	
Denaturation	94°C	45 sec	39 cycles
Hybridization	55-62°C	45 sec	
Elongation	72°C	45 sec	
Terminal Elongation	72°C	5 min	

Table 3.4 PCR program to generate the single β-chain construct (1206bp)

Reaction	Temperature	Duration	
Initial denaturation	94°C	4 min	
Denaturation	94°C	45 sec	39 cycles
Hybridization	55.5, 58.5, 63.5°C	45 sec	
Elongation	72°C	45 sec	
Terminal Elongation	72°C	5 min	

3.4.1.4 Agarose gel electrophoresis

Gel electrophoresis was used to separate DNA according to size. Therefore 1% (w/v) agarose was mixed with 1x TAE buffer and 0.5mg/ml Ethidium bromide, and stored at RT until polymerization. DNA samples were mixed with 1x loading dye and loaded on a gel. In addition 5µl of 1:10 diluted 1kb DNA-ladder was applied as a mix with 1x loading dye. Samples ran for 40-60 min at 100V and were visualized under UV light.

3.4.1.5 Purification of DNA

Purification of DNA fragments of PCR reactions was performed according to the manufacturer protocol (QIAquick Spin Handbook: QIAquick PCR Purification Kit Protocol, QIAGEN, Venlo, The Netherlands). Purified DNA fragments were eluted in 30µl nuclease free sterile filter water.

Extraction and purification of DNA from standard low-melt agarose gels in TAE buffer was performed according to the manufacturer protocol (QIAquick Spin Handbook: QIAquick Gel Extraction Kit Protocol, QIAGEN, Venlo, The Netherlands). Purified DNA was eluted in 30µl nuclease free sterile filter water.

3.4.1.6 Digestion of DNA

Plasmids were incubated with restriction endonucleases for linearization and subsequent gel extraction (3.4.1.5).

2µg pcDNA3.1	1x NEB Buffer 3
	1x BSA
	20U BamHI and 20U EcoRV
	Add to 15µl with aq^{dest}. Incubation for 90min at 37°C
2µg pMX-IE-GFP	1x NEB Buffer 3
	1x BSA
	20U BamHI and 10U NotI
	Add to 15µl with aq^{dest}. Incubation for 90min at 37°C

α- and β-TCR chains were incubated with restriction endonucleases for adjusting the 5’ and 3’ end of the DNA and subsequent purification (3.4.1.5). After purification α- and β-TCR chain were subcloned into pcDNA3.1 vector by ligation followed by plasmid extraction, DNA purification and restriction and final ligation into pMx-IE-GFP plasmid.

30µl purified α-chain:	1x NEB Buffer 3
	1x BSA

20U BamHI and 20U EcoRV

adjust to 40µl with aq^{dest}. Incubation for 90min at 37°C

30µl purified β-chain: 1x NEB Buffer 3

1x BSA

10U SwaI

adjust to 15µl with aq^{dest}. Incubation for 45min at 25°C

Add 20U BamHI

Incubate for 45min at 37°C

After ligation (3.4.1.7) plasmid DNA was checked for insertion of the α-/ β-chain of the p53TCR into pcDNA3.1 or pMx-IE-GFP by digestion with restriction endonucleases. Therefore DNA was incubated according to the following pipetting scheme:

pcDNA3.1 + α-/ β-chain: 1x NEB Buffer 3

1x BSA

BamHI and NotI

Add to 15µl with aq^{dest}. Incubation for 90min at 37°C.

pMx-IE-GFP + α-/ β-chain: 1x NEB Buffer 3

1x BSA

BamHI and NotI

Add to 15µl with aq^{dest}. Incubation for 90min at 37°C.

3.4.1.7 Ligation

Ligation of the purified α-/ β-chain of the p53TCR into pcDNA3.1 was performed using an insert to vector ratio of 3:1. Therefore insert and vector DNA were mixed with 1x T4 Ligation buffer containing ATP and 1µl T4 Ligase. The ligation sample was incubated for 16h at 16°C in the water bath in a total volume of 15µl. As control sample vector DNA was incubated without insert DNA in T4 Ligation buffer with T4 Ligase.

Ligation of the purified α-/ β-chain of the p53TCR after subcloning in pcDNA3.1 into the final vector pMx-IE-GFP was performed using an insert to vector ratio of 3:1. Therefore insert and vector DNA were mixed with 1x T4 Ligation buffer containing ATP and 1µl T4 Ligase. The ligation sample was incubated for 16h at 16°C in the water bath in a total volume of 15µl.

3.4.1.8 Chemocompetent bacteria

Chemocompetent bacteria were generated by O/N culture at 37°C and 250rpm in a rocking incubator. Here, 3ml LB-medium and 5µl competent bacteria stock solution including 100µg/ml tet for the strain XL-1 blue or 100µg/ml amp for the strain JM109. Bacteria were harvested after 16h incubation and stored on ice. OD_{550} was measured and 100ml SOB-medium was inoculated with bacterial culture at a final OD_{550} of 0.05. Cultures were incubated at 37°C in a rocking incubator (250rpm) until OD_{550} reached 0.5. Bacterial cultures were stored on ice, transferred into 50ml tubes and centrifuged for 8min at 4°C and 1200xg. Supernatant was discarded, bacterial cells were resuspended in 15ml TfB I Buffer and stored for 30-60min on ice. Finally, bacterial cells were centrifuged for 6min at 4°C and 823xg. Again, supernatant was discarded and bacterial cells were resuspended in 2ml TfB II Buffer. Chemocompetent cells were stored at -80°C until further use.

3.4.1.9 Transformation

For transformation of plasmid DNA into bacteria either 50µl of chemocompetent XL-1 Blue or JM109 were used. All ligation products were first transformed into XL-1 Blue bacteria. After confirmation of the flawless sequence insertion of the α-/ β-chain into the pMx-IE-GFP target vector, plasmid DNA was transformed into JM109 for higher DNA yield.

Transformation of plasmid DNA into bacteria was carried out by performing a heat shock (60sec at 42°C in the water bath) after bacteria were incubated in presence of plasmid DNA on ice for 30-60min. Immediately after heat shock bacteria were cooled down on ice for 3 min, transferred into 500µl LB-Medium in a rocking incubator at 37°C, 230rpm, 60min. Bacteria were centrifuged (6000rpm, 5min, RT) and resuspended in 80µl of LB-medium prior to plating on LB-amp agar plates. Plates were incubated upside down over night (O/N) at 37°C.

3.4.1.10 Overnight cultures

For plasmid Mini-bacterial cultures one colony from a LB-amp agar plate was picked under sterile conditions and transferred into 5ml LB-amp-medium. Bacteria were incubated for 16h at 37°C and 230rpm in a rocking incubator.

For plasmid Maxi-bacterial culture a single colony was picked and incubated in 2ml LB-amp-medium for 8h at 37°C and 230rpm. After incubation 500µl of the culture was transferred into 100ml LB-amp-medium and incubated for 16h at 37°C and 230rpm.

3.4.1.11 Plasmid DNA preparation

Plasmid DNA purification of 5ml overnight mini-bacterial cultures was performed according to the manufacturer protocol (QIAprep Miniprep Handbook: QIAprep Spin, QIAGEN, Venlo, The Netherlands). Purified DNA was eluted in 30µl nuclease free sterile filter water.

Plasmid DNA purification of 100ml overnight maxi-bacterial cultures was performed according to the manufacturer protocol (EndoFree Plasmid Purification Handbook: EndoFree Plasmid Maxi Kit, QUIAGEN, Venlo, The Netherlands). Purified DNA was eluted in 200µl nuclease free sterile filter water or 1:10 diluted TE buffer.

3.4.1.12 DNA concentration measuring

The concentration of the DNA sample was determined by the absorption at 260nm using an UV spectrometer. A 1:50 dilution of the sample was prepared and the purity grade of the sample was checked by determining the ratio 260/280nm.

3.4.1.13 Sequencing

DNA sequencing was carried out by GENterprise GENOMICS (Gesellschaft für Genanalyse und Biotechnologie mbH, Mainz, Germany) according to the ‘Homerun’ program.

4µl of Miniprep plasmid DNA containing either the α-chain or the β-chain of the

p53TCR was mixed with 2µl of the sequencing primer (Table 7.1) and sent for sequencing.

3.4.2 Animals

All animal procedures were performed according to the German federal and state regulations and approved by the responsible national authority (National Investigation Office Rhineland-Palatinate, Appoval ID: 23 177-07/G10-1-053).

3.4.2.1 Rats

8-10 weeks old female rats were purchased from Charles River Laboratories, Cologne, Germany. Rats were sacrificed using CO_2.

3.4.2.2 Mice

Mice were routinely bred by and obtained from the central animal facility of the Johannes Gutenberg University Mainz, Germany. Strains were housed under normal conditions according to the guidelines for animal care of the Johannes Gutenberg University Mainz. Mice were sacrificed by cervical dislocation.

Used mouse strains:

C57BL6/J	wild-type mice
CyA2K^b	HLA-A2/K^b transgenic mice
HupKi CyA2K^b	HLA-A2/K^b transgenic mice expressing human p53 gene
p53-/-A2K^b	HLA-A2/K^b transgenic mice deficient for p53

All transgenic mice were backcrossed on C537/BL6/J background.

3.4.3 Cell lines

Cells were maintained in RPMI1640 or DMEM.

JA2, T2: The TAP-deficient cell line T2 and the Jurkat-A2 (JA2) cell lines have been described elsewhere (56).

Saos-2, Saos-2/143: The human osteosarcoma either p53-deficient (Saos-2) or transfected with the human *p53* gene harboring the mutation V143A (56, 104).

Phoenix-Ampho: The packaging cells line Phoenix-Ampho was purchased from Nolan Laboratory, Stanford University, USA.

MEFs: Mouse embryonic fibroblasts from p53-/- $A2K^b$ mice transduced with a retroviral vector encoding for wt mouse *p53* gene including specific mutations (mut7: p53 R270C; mut4: p53 R172H), which mimic human p53 hotspot mutations. Additionally cells were transduced with a retroviral construct encoding for the human *p53* gene sequence 264-272 (105). Fibroblasts were immortalized by transduction with a helper plasmid (pCMV.VSV-G) and two retroviral constructs (pBabe-hygro-E1A/ - H-ras). The cells were then selected with Hygromycin B.

3.4.3.1 Generation of primary tumor cell cultures and isolation of splenocytes

For primary tumor cell cultures, ex vivo tumors were dissected out of the flank of tumor bearing mice, homogenized and filtering through 70-100µm nylon-mesh cell strainers. Erythrocytes were lysed (see 3.4.3.2) and cell suspension was plated in 10 cm petri dishes containing 10ml DMEM. DMEM medium was changed on day 1 after tumor plating and as follow up every other day for 1 week. At a confluence of about 80% cells were trypsinized, counted and frozen.

Splenocytes of rats or mice were harvested, homogenized and filtered through 70-100µm nylon-mesh cell strainers. Erythrocytes were lysed (see 3.4.3.2) and cell suspension was either plated or resuspended according to further use (see 3.4.4 to 3.4.6).

3.4.3.2 Erythrocyte lysis of tissue homogenates and blood samples

Right before erythrocyte lysis to remove red blood cells, tissue homogenates or blood samples were pelleted by centrifugation at 470xg, 5min, RT. Cell pellet were resuspended in either 3ml Erythrocyte Lysis Buffer (ELB) per organ and tumor sample or in 2ml ELB per blood sample. Homogenized tissues were incubation for

3min at room temperature (RT); blood samples were incubated for 3min at 37°C (water bath). Addition of 7ml RPMI1640 for tissue homogenates or 2ml PBS for blood samples stopped lysis.

3.4.4 T-cell growth factor (TCGF)

Spleens of female Lewis rats 8-10 weeks old were harvested and homogenized (see 3.4.3.1). Spleen homogenates were incubated with ELB for 2min at 37°C. Cells were washed twice by resuspension in 10ml RPMI1640/ spleen followed by centrifugation at 470xg, 5min, RT and resuspended to $7x10^6$ cells/ml. 50ml cell suspension was plated in a T75 cell culture flask using TCGF medium and incubated for 24h in a humidified atmosphere with 5% CO_2 at 37°C. The supernatant was collected on the next day, centrifuged (10min, 470xg, RT) and sterile filtered using Steritop™ Filter Units. Remaining cells in the T75 flask were resuspended with 15ml TCGF-medium. Pelleted cells were resuspended and transferred back to T75 flask in a total volume of 50ml. Cells were again incubated for 24h in a humidified atmosphere with 5% CO_2 at 37°C. Supernatants of day 1 and day 2 were pooled and 1g/100ml supernatant Methyl α-D-mannopyranoside was added. After dissolving the supernatant was sterile filtered and stored after testing at -20°C.

3.4.5 Retroviral transduction of mouse T cells

Four days before transduction the packaging cell line Phoenix-Ampho was thawed and cultivated in T75 flasks in DMEM. On day one of the transduction the Phoenix-Ampho cells were trypsinized, counted and plated in a density of $1.2x10^6$ cells per 10cm petri dish containing 8ml DMEM. The next day (four hours prior to transfection of the Phoenix-Ampho cell line) medium was changed and replaced by 6ml DMEM. For transfection 800µl DMEM only was provided into a 1.5ml tube. 35µl Fugene 6 were added directly into the medium, mixed and incubated for 5min at RT. Then 7µg of the helper plasmid pCL-ECO and 10µg of the TCR DNA was added into the medium, mixed and incubated for 15min at RT. Finally the solution was slowly dropped on the Phoenix-Ampho cells and incubated in a humidified atmosphere with 5% CO_2 at 37°C. The same day isolated primary splenocytes (see 3.4.3.1) from HupKiCyA2K^b or CyA2K^b mice were pre-activated using 5% TCGF and 2µg/ml Con A

for 48 hours in a humidified atmosphere with 5% CO_2 at 37°C. On day three the medium of the transfected Phoenix-Ampho cells was replaced again by 8ml DMEM. Additionally 24-well plates were coated with 25µg/ml/well Retronectin® (Takara, Clontech) and incubate for 24h at 4°C in the dark. The next day Retronectin® was removed and 24-well plates were blocked with 2% BSA/PBS solution for 30min at RT. Wells were washed with 1x PBS and kept moisten until use. Meanwhile for transduction of the pre-activated splenocytes virus supernatant (SN) was collected from the petri dishes, transferred into 50ml tubes and centrifuged at 836xg for 10min at 32°C to remove cell debris from the SN. For harvesting the splenocytes after 48h cells were intensely resuspended, pooled and counted. The desired volume was transferred and pelleted by centrifugation (470xg, 5min, RT). The pre-activated splenocytes were resuspended to $4x10^6$ cells/ml in virus SN. Polybrene was added in a concentration of 4µg/ml SN and the mixture was plated in the pre-coated 24-well plate to 0.5ml/ well. After centrifugation (90min, 836xg, 32°C, without break) cells were kept for at least 18h in a humidified atmosphere with 5% CO_2 at 37°C. Transduction efficiency was subsequently analyzed by flow cytometry (see 3.4.12).

3.4.6 Stimulation and culture of mouse T cells

Mouse T cells were incubated in 24-well plates for 6-7 days in a humidified atmosphere with 5% CO_2 at 37°C.

For weekly stimulation the JA2 cell line was used for antigen presentation. Cells were irradiated with 20,000Gy, washed once with RPMI1640 only and were loaded with 5µg peptide according to the TCR specificity and 5µg β2M for 35min in a humidified atmosphere with 5% CO_2 at 37°C. Afterwards cells were washed twice with RPMI1640, counted and adjusted to $1x10^6$ cells/ml. Freshly isolated splenocytes (see 3.4.3.1) from C57BL6/J mice were used as feeder cells, harvested and irradiated with 3,000 Gy. After irradiation cells were washed by centrifugation (470xg, 5min, RT) and erythrocyte lysis was performed. Cells were counted and adjusted to $10\text{-}12x10^6$ cells/ml and were kept on ice until further usage. As cytokine providing component TCGF was added in a final dilution of 10% per well. Finally T cells were splitted depending on their density between 1:2 and 1:5 and resuspended in 0.5ml/well in RPMI1640. 0.5ml of all components (feeder cells, loaded JA2 cells, TCGF, mouse T cells) were added and mixed in the well to obtain a final volume of 2ml/well.

3.4.7 Adoptive T cell transfer (ACT) *in vivo*

Mouse splenocytes were transduced as mentioned in 3.4.5. One day after transduction cells were harvested and analyzed by flow cytometry for the expression of the transgene. After calculation of the transduction efficiency, cells were washed with 1x PBS and adjusted to the cell number to inject i.v. in the tail vein in 200µl 1x PBS. One day prior to the adoptive cell transfer mice were irradiated with 5.5Gy. For i.v. injection mice were exposed to red light for 10-15min to dilate the tail blood vessels. Mice were fixed in a restrainer for i.v. injection.

3.4.7.1 Interleukin 2 treatment

IL-2 treatment was applied as an i.p. injection of $7.2x10^5$ IU in 200µl of 1x PBS. 200µl IL-2 was injected 5 times in total (twice daily on day 10 and 11 after ACT and once on day 12 after ACT).

3.4.7.2 Peptide vaccination

One day after tumor injection mice were anesthetized by i.p. injection of 1mg Ketamin and 0.16mg Xylazin per 20g bodyweight. Peptide vaccination (100µg of the $p53_{(257-282)}$ peptide and 40-50µg anti-CD40 antibody) was applied s.c.. Additionally as a third component 62mg of Aldara 5% cream (similar to 3mg imiquimod) was applied on the skin at the site of tumor injection. During the time of anesthesia dexpanthenol eye ointment was applied to the eyes to protect them from drying-out.

3.4.7.3 Blood collection

5-50µl Blood samples were collected on weekly basis by puncture of the vena facialis anterior (facial vein/ cheek puncture). Blood volume was measured with pipettes and erythrocytes were lysed subsequently (see 3.4.3.2). After repeated washing with 1x PBS by centrifugation (600xg, 3min, RT) blood samples were stained, fixed in 200µl 1% PFA and stored at 4°C until analysis by flow cytometry as described in 3.4.12. Prior to analysis 20µl of 1:1000 diluted 4% sulfate latex beads were added to determine the cell count/µl of the blood sample (106) according to the formula below:.

$$\frac{\text{Number of events in the region containing the population of interest}}{\text{Number of events in region containing beads}} \text{ x } \frac{\text{Number of beads per tube}}{\text{Sample volume}} = \text{Absolute count of lymphocyte subset}$$

3.4.8 MACS Separation

To isolate Myeloid derived suppressor cells (MDSC) from spleen or tumor of tumor-bearing mice, tissue was harvested sterile, homogenized, filtered and erythrocytes were lysed using erythrocyte-lysis buffer (see 3.4.3.1 and 3.4.3.2). After counting the cells were resuspended to $1x10^7$ cells/100µl in MACS buffer and stained with 4-6µl of anti-Gr-1-PE antibody for 20min at 4°C in the dark. After staining cells were washed 2x with 10ml MACS buffer (400xg, 5min, 4°C) and resuspended in 80µl MACS buffer per 10^7 cells. Subsequently, the cells were magnetically labeled with 20µl per 10^7 cells anti-PE MicroBeads for 15min at 4°C. After washing with MACS buffer cells were resuspended to $1x10^8$ 500ml MACS buffer. Then the MACS® LS-Column (MACS Miltenyi, Bergisch Gladbach, Germany), which was placed in the magnetic field of a MACS Separator (MACS Miltenyi, Bergisch Gladbach, Germany) was equilibrated with 3ml MACS buffer and cell suspension was loaded on a pre-separation filter on top of the LS column. The magnetically labeled cells were retained in the column while the unlabeled cells ran through. The column was rinsed 3x with 3ml MACS buffer to clear all unlabeled cells. After removal of the column from the magnetic field, the magnetically retained cells could be eluted as the positively selected cell fraction by removing the pre-separation filter, adding 5ml MACS buffer on the column and inserting the plunger to flush the column. Cells were counted again and either used directly in an assay or additionally stained for a following cell sorting (3.4.12.4).

3.4.9 Histology

For histological tissue analysis lung, liver, spleen, skin and colon or tumor of mice were harvested at termination of the experiment, quickly rinsed in 1x PBS and immediately transferred into plastic molds containing Tissue-Tek® O.C.T.™ compound embedding media. Molds were snap frozen on dry ice and stored until further usage at -80°C.

Tissue sections were prepared at -20°C to -16°C using a cryostat. 2-6µm sections were transferred on Superfrost® Plus microscope slides, dried at RT and fixed for 15min in prechilled acetone. After drying slides were stored at -20°C. Prior to staining slides were thawed and rehydrated by washing twice in 1xTBS for 5min.

3.4.9.1 Histochemistry

Rehydrated slides were blocked for 20-30min in a wet chamber to avoid unspecific antibody binding depending on the staining performed (Table 3.5). For tissues with elevated endogenous peroxidase activity such like liver and tumor samples an additional blocking step was applied. Therefore slides were washed 3x for 5min with 1xTBS after the normal blocking step and were incubated afterwards with Avidin/Biotin blocking kit (Vector Laboratories) as noted by the manufacturer. The slides were quickly rinsed in 1xTBS and were now incubated for 60-90 min with the primary antibody (Table 3.6) at RT in a wet chamber. Slides were washed 3x for 5min with 1x TBS and incubated with the secondary antibody for 45-60min at RT in a wet chamber. For detection slides were washed 2x for 5min in 1x TBS and 1-2x for 5min with 1x PBS and incubated for 30-45min with 1:1000 diluted ExtrAvidin® Peroxidase (Sigma Aldrich) at RT in a wet chamber. After incubation slides were washed 3x with 1x PBS for 5min followed by incubated in 0.5% DAB substrate solution (49ml PBS, 20µl 30% H_2O_2, 1ml DAB stock 25mg/ml) for 10-20min. To stop the enzymatic reaction slides were washed 2x in deionized water. Staining slides for 1min in Mayers Hemalum solution (Hemalum solution acid according to Mayer) and blueing for 5min under running tab water carried out counterstaining. Slides were dehydrated in increasing alcohol series and xylene. Finally slides were mounted in Roti®-Histokitt-II.

Table 3.5 Blocking procedures for Immunohistochemistry

Pretreatment	Antibody
Incubate 10min at RT in wet chamber: 70% methanol/ 0.03% H_2O_2/TBS, wash 3x TBS, incubate with FCS 10min at RT in wet chamber	Rat anti-mouse CD4
Incubate 30min at RT in wet chamber: 10%BSA/PBS	Rat anti-mouse CD8

Table 3.6 Overview of antibodies used for Immunohistochemistry

Name	Linking	Clone	Company
Anti-Mouse CD4 monoclonal	no	YTS191.1	LifeSpan BioSciences
Anti-Mouse CD8b purified	no	H35-17.2	eBioscience
Anti-Rat IgG Biotin	Biotin	polyclonal	eBioscience
Streptavidin-Peroxidase Polymer		no	Sigma-Aldrich

3.4.9.2 Hematoxylin/ Eosin (H/E) staining

Rehydrated slides were washed for 5min in deionized water and nuclei were stained for 5min in Mayers Hemalum solution. Slides were blued in running tab water for 10min and rinsed afterwards in deionized water. Afterwards slides were incubated for 3min in 0.5% Eosin Y solution with 0.1% pure acetic acid, rinsed quickly in deionized water and were dehydrated by an increasing alcohol series and xylene. Finally slides were mounted in Roti®-Histokitt-II.

3.4.9.3 Immunofluorescence

For immunofluorescent detection of p53 $0.4x10^6$ cells of different tumor cell lines were plated in 6cm petri dishes containing acetone treated cover slips. Cells were incubated in a humidified atmosphere with 5% CO_2 for 16-24h to attach to the cover slips. The next day cover slips were removed, rinsed with 1x PBS and fixed for 10min in 4%PFA/PBS. The staining procedure took place in a 24-well plate with working volume of 200µl. After washing for 10min at RT with PBS-Triton x100 (PBS-Tx) cover slips were blocked for 30min with 7.5% BSA/PBS-Tx at RT. Slides were stained with the primary antibody (p53 CM5, 1:700 diluted in 0.2% BSA/PBS-Tx) for 60min at RT, washed 3x 10min with PBS-Tx afterwards and stained with the secondary antibody (goat-anti-rabbit IgG (Dako), 1:300 in 0.2% BSA/PBS-Tx) for 60min at RT. For detection slides were first 3x washed for 10min in PBS-Tx and incubated with the detection antibody (streptavidin-AF594, 1:1000 diluted in 0.2% BSA/PBS-Tx). For counterstaining of the nuclei slides were stained with Hoechst-staining (DAPI) for 10min at RT in the dark. After 3x quickly rinsing with PBS-Tx, slides were stored in aq^{dest} until further use. To preserve the fluorescence signal cover slips were removed

from the wells, carefully dried and mounted on a glass slide with Mowiol. Slides were analyzed with a fluorescence microscope after drying for at least 24h at RT.

3.4.10 Chromium-51 (^{51}Cr) release assay

This test determines the cytolytic function of T cells, as already described (32, 56). $0.5x10^6$ target cells were labeled with a radionuclide of the sodium ^{51}chromate salt ($Na_2{}^{51}CrO_4$) for 90min in a humidified atmosphere with 5% CO_2. Effectors were pooled, counted and plated in 100µl RPMI1640 in duplicates in a 96-well round bottom plate. Effectors were plated in different dilutions according to the effector-to-target ratio (E:T) used in the assay (30:1, 10:1, 3:1, 1:1, 0.3:1). After labeling the target cells were washed 3x with 10ml RPMI1640 (470xg, 5min, RT) and resuspended in 10ml RPMI1640. 100µl target cell solution was transferred to the effector cell plate and incubated for 5.5h in a humidified atmosphere at 37°C with 5% CO_2. To determine the cytotoxic capacity of the effector cells maximum and spontaneous releases were included in the assay. Maximum releases were acquired directly by measuring the freshly labeled target cells in the gamma counter. As spontaneous releases control wells with 100µl target cells but no effector cells, which were treated the same way as all other samples, were measured. After incubation the 96-well plates were centrifuged (353xg, 13min, without break) and 100µl supernatant was carefully removed and transferred to gamma counter tubes for quantification. Percent of specific lysis was calculated according to the formula:

$$\frac{\text{experimental chromium release} - \text{spontaneous chromium release}}{\text{maximum chromium release} - \text{spontaneous chromium release}} \text{ x } 100 = \% \text{ specific lysis}$$

3.4.11 Co-culture proliferation/suppression assays

To determine the suppressive capacity of MDSC, T cell proliferation was assessed in the presence of MDSCs. T cells were harvested, counted, washed with PBS and resuspended in 1ml PBS. Meanwhile the 10mM CFSE stock was diluted in PBS to 50µM. Cells were stained for 5min at RT in the dark with the diluted CFSE solution in a final concentration of 5µM. After staining the T cells were washed 3-4x with PBS or MACS buffer and plated in RPMI1640 + 5% TCGF and 2µg/ml Con A in a total volume of 200µl/well together with MDSC in different ratios according to the

experimental layout. The CFSE intensity of the T cells was analyzed at time point zero at the FACS Canto II and after 72-96h in co-culture.

3.4.12 Flow Cytometry

Fluorescence activated cell sorting (FACS) is used to discriminate different cell populations in a tissue homogenate or to analyze the expression pattern of specific molecules.

For FACS staining 0.2-0.5x10^6 cells were transferred in FACS tubes and washed with 1x PBS (600xg, 3min, RT). Cells were resuspended in 50µl MACS buffer containing the fluorochrome-coupled antibodies (Table 3.7) and stained for 20-30min at 4-8°C in the dark. Finally the samples were washed again in 1x PBS and resuspended to 0.1x10^6 cells/100µl MACS buffer or 1% PFA/PBS.

3.4.12.1 Compensation

Acquisition of the samples took place at a FACS Calibur (BD Bioscience) or FACS Canto II (BD Bioscience). To allow detection of single fluorochromes within a sample of different fluorochromes and to avoid false negative signals of emitted spectral overlap, compensation was performed using the automated compensation feature of the Diva Software for the FACS Canto II. Therefore single color stainings were performed with OneComp eBeads (eBioscience). One drop of OneComp eBeads was transferred in a FACS tube. 0.4µl antibody was applied to the sample, mixed and incubated for 15-20min at 4°C in the dark. Samples were resuspended in 2ml PBS and washed by centrifugation. Finally samples were resuspended in 200µl FACS Buffer and analyzed as single staining controls for compensation. Compensation for the FACS Calibur was performed by manual adjustment using single color stainings.

3.4.12.2 Intracellular p53 staining

Intracellular p53 staining was performed using Intraprep (Beckman Coulter) staining kit. 0.2x10^6 cells were transferred in a FACS tube and washed with 1xPBS. Cells were resuspended in 100µl of fixation reagent 1, vortexed vigorously and incubated for 15min at RT. Afterwards cells were washed again in 1x PBS and resuspended in

100µl of permeablisation and washing reagent 2. Importantly, no shaking was allowed. Samples were incubated for 5min at RT. After careful shaking with the hand for 3sec, 5µl of antibody was added to the tube and incubated for 15min at RT in the dark. Lastly samples were washed with 1x PBS and resuspended in FACS Buffer to $0.1x10^6$/100µl.

3.4.12.3 Intracellular FoxP3 staining

For the determination of T regulatory cells in a tissue sample the FoxP3/ Transcription Factor Staining Buffer Set (eBioscience) was used. Samples were washed in MACS buffer and to block unspecific antibody binding FC-block was applied (0.5µg/100µl CD16/CD32 antibody for 15 min, 4°C in the dark). Directly after FC-block antibodies for surface markers (CD4, CD25) and an optional live/ dead marker was applied to the sample for 20-30min at 4°C in the dark. After surface staining samples were washed with MACS buffer and resuspended in 100µl fixation buffer for 30min at 4°C in the dark. Next samples were washed twice in 1x permeabilization buffer and immediately incubated with the FoxP3 antibody for 30min at 4°C in the dark. After staining samples were washed twice with 1x permeabilization buffer and resuspended to $0.1x10^6$ cells/100µl MACS buffer.

3.4.12.4 Sorting

Cell sorting was performed in the FACSlab Mainz/ FACS and Array Core Facility or in the Flow Cytometry Core Facility (FCCF) of the 3rd Medical Department of the University Medicine of the Johannes Gutenberg University Mainz.

Cells were isolated and prepared as sterile samples as mentioned in 1.4.8. Finally cells were resuspended to $10x10^6$ cells/ml MACS Buffer and stored on ice until sorting.

Table 3.7 Overview of reagents used for flow cytometry

Name	Fluorochrome	Clone	Company
CD8	APC	53-6.7	eBioscience
CD8	PE	53-6.7	BD Pharmigen ™
CD4	PerCP-Cy5.5	RM4-5	BD Pharmigen ™
CD4	PE-Cy5	RM4-5	eBioscience
CD4	PE	GK1.5	BD Pharmigen ™
CD3	APC	17A2	eBioscience
CD16/ CD32	None	93	eBioscience
Vβ3	PE	KJ25	BD Pharmigen ™
CD11b	FITC	M1/70	BD Pharmigen ™
CD11b	PE	M1/70	eBioscience
Gr-1	FITC	RB6-8C5	BD Pharmigen ™
Gr-1	PE	RB6-8C5	BD Pharmigen ™
Gr-1	PE	RB6-8C5	eBioscience
Ly6-C	APC	AL-21	BD Pharmigen ™
F4/80	eFluor® 780	BM8	eBioscience
FoxP3 anti-Mouse/Rat FoxP3 Staining Set	APC	FJK-16s	eBioscience
CD279 (PD-1)	APC	J43	eBioscience
Anti-Mouse HLA-A2	PE	BB7.2	BD Pharmigen ™
Mouse IgG2b κ Isotype	PE	no	Life technologies Invitrogen
Rat IgG2b κ Isotype	FITC	no	eBioscience
CFSE	FITC		
Cell Proliferation Dye	eFluor® 670	No	eBioscience
Cell Viability Dye	eFluor® 450	No	eBioscience
Star™ Multimer Reagents	PE	No	AltorBioScience

TCR p53-264-272			
p53 intracellular: p53 (DO-1): sc-126	PE	DO-1	Santa Cruz Biotechnology, Inc.
CD25	PE	PC61	BD Pharmigen ™
CD25	FITC	CL8925F-3	Cedarlane®
CD107a	PE	1D4B	BD Pharmigen ™

3.4.12.5 Analysis

Flow cytometry data were analyzed with FlowJo software.

4. Results

4.1 Analysis of p53TCR gene transfer associated off-target toxicity

Retroviral transduction of TCR α and β chains leads to their integration into the genome of eukaryotic cells. In order to prevent potential assembly of endogenous and introduced TCR chains (mispairing), p53-specific TCR transgenes were codon optimized and an additional disulfide bond was added between the constant α (Cα) and the constant β (Cβ) chain of the TCR. Furthermore TCR α and β chains were cloned in one retroviral vector including a 2A element for equimolar expression of both TCR chain transgenes. Finally, an additional p53-specific TCR format was designed, where the C-terminus of the variable α (Vα) chain was connected to the N-terminus of the variable β (Vβ) chain via a peptide linker, generating a single-chain (sc) TCR (Figure 4.1). Subsequent analysis of the modified double chain (dc) and sc TCR were performed in comparison to the wild-type (wt) TCR, in order to determine the expression capacity and functionality of the modified TCRs.

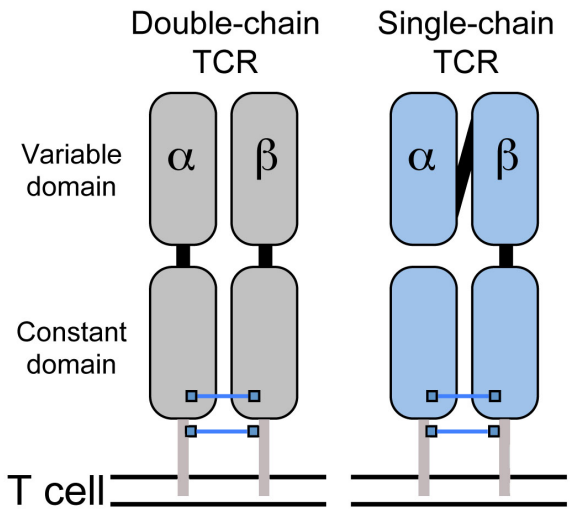

Figure 4.1 Scheme of the dc and sc p53-specific codon optimized TCR.
Amino acid residue replacements via site-directed mutagenesis T84C in Cα and S79C in Cβ introduced an artificial disulfide bridge between the constant domains. The codon optimization (not shown here) was applied to both TCRs. In the sc p53-specific TCR, a 19-residue glycin/serine-rich flexible linker (SL7, glycine-rich motif GlyGlyGlyGlySer) was used to link the C-terminus of the variable TCRα domain to the N-terminus of the variable TCRβ chain.

4.1.1 Expression pattern of wt, dc or sc p53-specific TCRs are similar shortly after retroviral transduction

The efficiency of TCR gene transfer was analyzed 24h after retroviral transduction by flow cytometry. Here, cells were stained for the Vβ3 subfamily TCR chain of the p53TCR (Figure 4.2). The transduction efficiency is expressed as the percentage of Vβ3 positive cells in the CD8 and CD4 compartment in transduced T cells compared to the amount of TCRVβ3 in non-transduced but stimulated control cells. The results reveal minor differences in transduction efficiency between the different p53TCR constructs. Compared to the wt and dc p53TCR (30.9% and 32.3% $V\beta3^+CD8^+$, respectively), the sc p53TCR showed lower Vβ3 surface expression (26.9% $V\beta3^+CD8^+$) in the CD8, as well as in the CD4 compartment (53.2% compared to 63.5% and 70.5% $V\beta3^+CD4^+$, respectively).

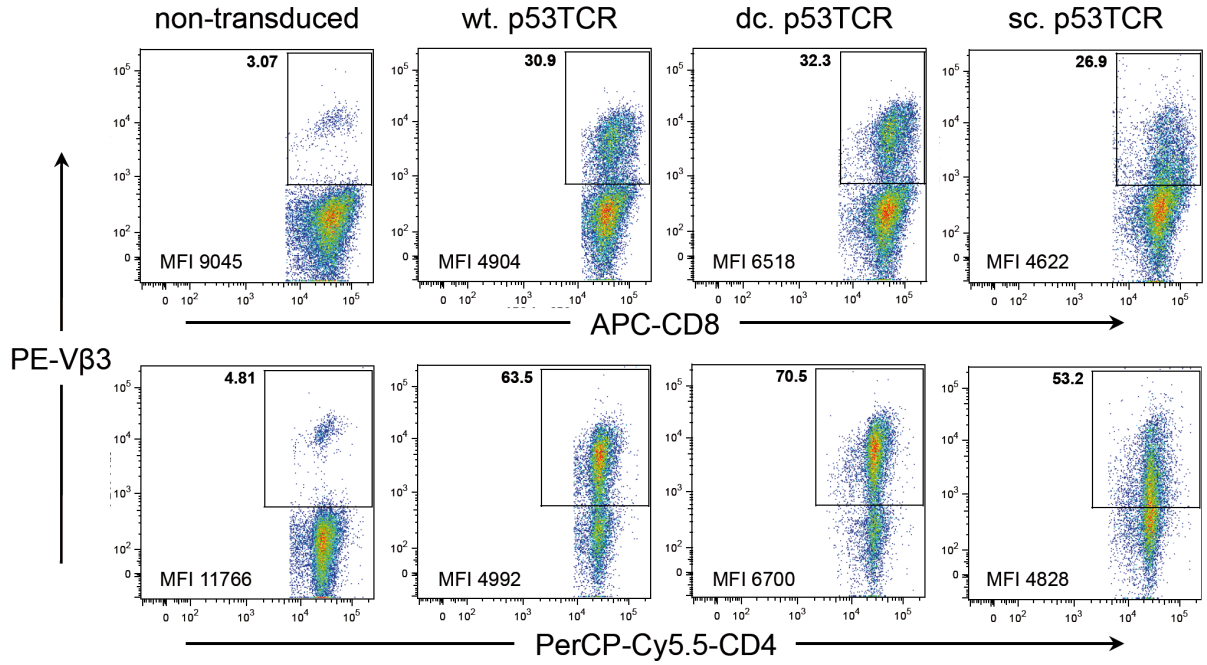

Figure 4.2 Transduction efficiencies show minimal variation between wt p53TCR, dc and sc p53TCR Surface expression of the p53 TCR was analyzed by flow cytometry. Vβ3 expression was quantified one day after retroviral transduction and compared with the endogenous Vβ3 expression of non-transduced T cells. Representative flow cytometry density plots for the Vβ3 expression in transduced cells compared to non-transduced control cells are shown. The level of TCR expression is determined by the mean fluorescence intensity (MFI) values.

For comparison, only low expression levels could be observed for the endogenous Vβ3 compartment of the non-transduced cells (3.07% $V\beta3^+CD8^+$ and 4.31% $V\beta3^+CD4^+$). In contrast, a clear shift was observed in the mean fluorescence intensity (MFI), which reflects the signal strength (here Vβ3 intensity), between the non-transduced cells and cells transduced with wt, dc or sc p53-specific TCR. Non-

transduced cells showed a distinct population of highly Vβ3-positive cells in comparison to a blurred $V\beta3^+$ staining in transduced cells. Importantly, the MFI as well as the total percentage of $V\beta3^+$ cells of sc p53TCR-transduced T cells was lower than compared to the wt and dc p53TCR (MFI_{sc} 4622 versus MFI_{wt} 4904 and MFI_{dc} 6518 $V\beta3^+CD8^+$). The dc p53TCR showed the highest MFI and transduction efficiency of all TCR constructs in both, the CD4 as well as the CD8 compartment.

4.1.2 Engineered sc p53-specific TCR shows specific target recognition

To determine whether optimized TCRs still maintain a tumor-specific function, mouse $CyA2K^b$ T cells transduced with either wt, dc or sc $p53_{(264-272)}$-specific TCR were compared in their capacity to lyse syngeneic tumor cell lines expressing different mutants of p53. Here, the cytotoxic function is expressed as percentage of specific lysis of tumor cells as assessed by the chromium-release assay.

Dc p53TCR-redirected T cells (Figure 4.3 B) showed the strongest recognition of a MEF mut 7 tumor cell line compared to wt (Figure 4.3 A) or sc p53TCR-redirected T cells (Figure 4.3 C). However, there were only minor differences between the different p53TCR constructs in terms of killing at an effector-to-target (E:T) ratio of 7:1. Wt p53TCR and sc p53TCR transduced T cells recognized MEF mut #4 clone 7 to nearly the same level (28% and 26%, respectively). Only the dc p53TCR transduced T cells showed a slightly higher lysis (33%). MEF mut #7 recognition at an E:T of 7:1 was similar for wt and sc p53TCR redirected T cells (30% and 31%), but a major difference was observed when compared to dc p53TCR-specific T cells (56%). It is worth mentioning that sc p53TCR redirected T cells at an E:T of 7:1 showed the lowest level of unspecific lysis (7%) of the control cell line MEF mut #3 clone A6, which is HLA-A2 positive but p53 negative, compared to wt p53TCR (13%) and dc p53TCR (21%). Thus the unspecific killing is decreased in sc compared to dc p53TCR.

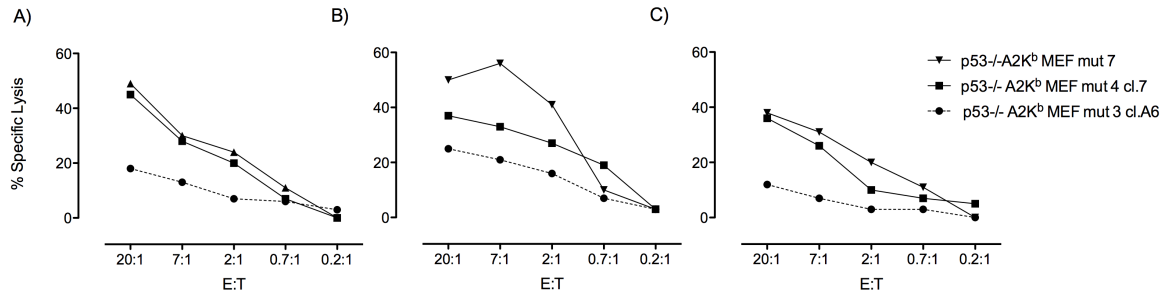

Figure 4.3 The sc p53TCR has similar cytotoxic function, but shows less unspecific killing compared to wt and dc p53TCR.
^{51}Chromium (^{51}Cr) release assay showing the cytolytic function of T cells retrovirally transduced with the wt (A), dc (B) or sc (C) p53 TCR as effectors in different ratios. Effector-to-target ratio (E:T) is calculated as $CD8^+Vb3^+$ effector (E) T cells to target (T) cells. As target cells different MEF tumor cell lines were used harboring specific p53 hotspot mutations. MEF mut3 clone 6 (dashed line) serves as negative control (p53 negative, HLA-A2 positive). All tumor cell lines were treated for 18h with 20ng/ml mouse IFN-γ and were loaded with100µCi ^{51}Cr for 90min. Target cells were incubated in coculture with effector cells for 5.5h. One representative assay (mean of duplicates) is shown.

4.1.3 Introduction of a single α- and β-chain of the p53-specific TCR into mature T cells

In order to proof the hypothesis that introduced TCR chains form heterodimers with endogenous TCR chains the codon-optimized transgenes for the α and β chain of the dc p53-specific TCR were cloned separately as single chains into a pMx-IE-GFP vector. After sequence accordance these retroviral vectors were used to transduce mouse T cells. Already 20h after transduction transduced T cells showed a strong GFP expression, which served as a surrogate marker for integration of the single α and β chain TCR into the genome (Figure 4.4). Surface expression of the β chain p53TCR could be tracked similar to the full-length p53TCR constructs (wt, dc or sc) by staining for Vβ3. Transduction efficiency in the CD4 compartment (57.5%, Figure 4.5 lower panel) was often observed to be higher than in the CD8 compartment (24.6%, Figure 4.5 upper panel). GFP expression in single α and β chain p53TCR-modified T cells in the CD4 (~78% and ~55%) and CD8 (~48% and ~21%) compartment could be used as indirect evidence for the expression of the introduced TCR chains (Figure 4.4).

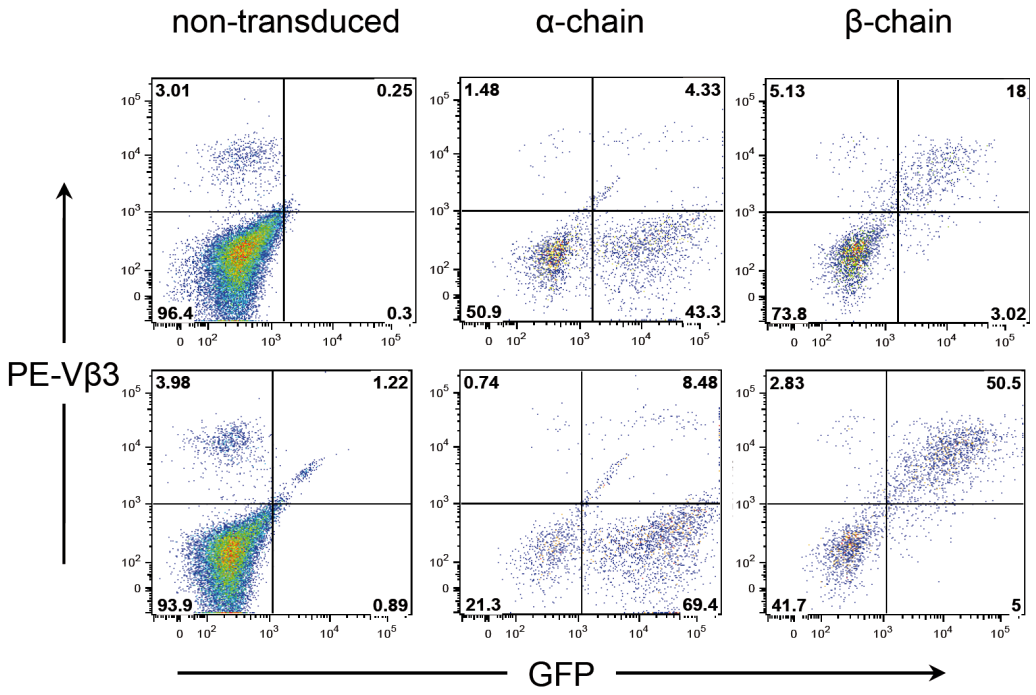

Figure 4.4 High transduction efficiencies observed already 24h after introduction of a single α and β chain p53TCR construct.
Cells transduced with the α or β chain p53TCR were analyzed for Vβ3 expression 24h after retroviral transduction. GFP served as an additional surrogate marker for the expression of the α and β chain p53TCR construct. One representative experiment with B6/J splenocytes gated on the $CD8^+$ (upper panel) or $CD4^+$ T cell subset (lower panel) is shown.

In addition, the Vβ3 surface expression of α and β chain p53TCR transduced cells was increased compared to the endogenous Vβ3 level of non-transduced control cells in both CD8 and CD4 T cells (Figure 4.5). Here, endogenous Vβ3 expression again showed a higher MFI of 9045 and 11766 for the $CD8^+$ and $CD4^+$ compartment compared to p53TCR α and β chain (MFI 5062 and 11252 as well as 6462 and 8985, respectively). Importantly, compared with the β chain construct, α chain transduced cells showed only a slight increase of $Vβ3^+$ cells in both, CD4 and CD8 T cells (Figure 4.5), thus reflecting the limited pool of endogenous available Vβ3 chains.

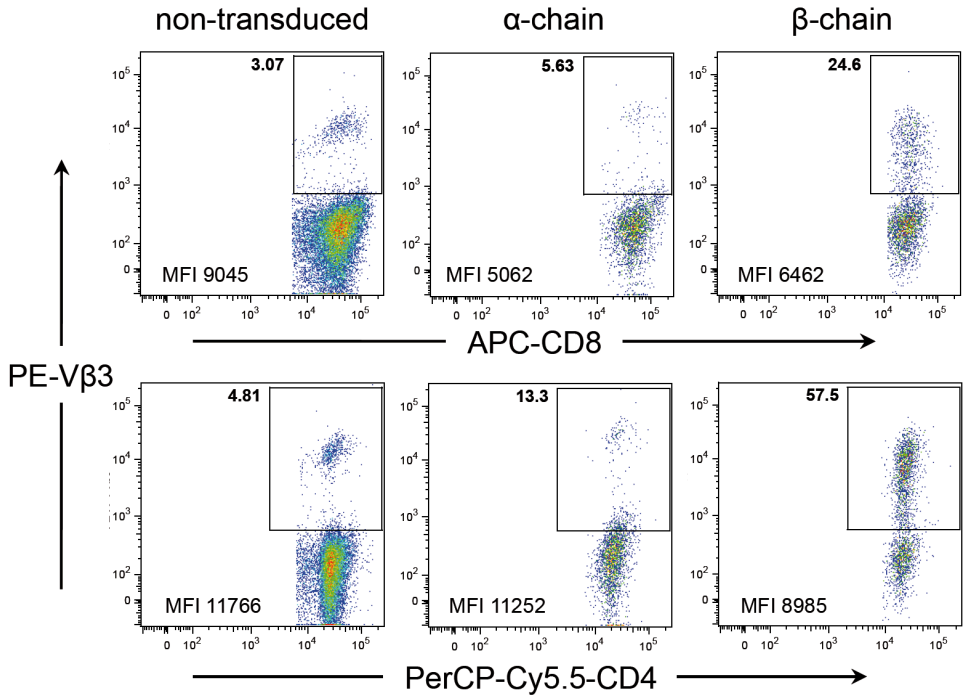

Figure 4.5 Transduction efficiencies of p53TCR α or β chain p53TCR as determined by Vβ3 expression Surface expression of the Vβ3 chain was analyzed by flow cytometry. $CD4^+V\beta3^+$ (lower panel) and $CD8^+V\beta3^+$ (upper panel) levels were quantified one day after retroviral transduction and compared with the endogenous Vβ3 level of non-transduced control T cells. Representative flow cytometry density plots are shown.

Taken together, these *in vitro* experiments provided strong evidence for the formation of heterodimers by pairing of endogenous and introduced TCR chains upon retroviral transduction of single p53TCR α and β chain constructs. This could be nicely demonstrated by strong Vβ3 expression of T cells transduced with the p53TCR β chain only. For α chain transduced cells it was difficult to draw conclusions due to the lack of commercially available antibodies for the Vα chain of the p53TCR. However, considering that most of the GFP^+ cells were also $V\beta3^+$, as shown for the p53TCR β chain (Figure 4.4), it is feasible to assume that GFP^+ cells are also $TCR\alpha^+$ cells.

4.1.4 Mispairing induced autoimmunity is observed in p53-/- $A2K^b$ mice receiving dc, α or β chain p53TCR – but not sc p53TCR-redirected T cells

To analyze whether mispairing events as seen by transduction of splenocytes with the α or β chain p53TCR constructs, leading to high expression of the introduced Vβ3 chain in combination with an endogenous α chain (part 4.1.3), also occur *in vivo*, adoptive cell transfer (ACT) experiments were performed in p53-/-$A2K^b$ mice.

The potential formation of mixed heterodimers resulting from mispairing events can lead to TCRs with an unknown specificity (47). T cells bearing such TCRs could induce autoimmune toxicity, which resembles GvHD reactions. In general the overall

health status of laboratory animals is measured by five criteria. The manifestation of GvHD-associated symptoms can be scored according to these criteria, which are: (i) weight, (ii) posture, (iii) activity, (iv) fur and (v) skin integrity. The mentioned characteristics are scaled as listed in Table 4.1. Mice reaching the highest grade (grade 2) in at least three parameters are sacrificed for ethical reasons.

Table 4.1 GvHD scores.
The following scores were modified from (53). GvHD was manifested as cachexia, anemia, loss of hematopoietic reconstitution, pancreatitis, colitis, and death. Mice were graded according to the criteria listed in the table and sacrificed when reaching grade 2 in three of five parameters.

	Weight loss	Posture	Activity	Fur texture	Skin integrity
Grade 0	< 10%	Normal	Normal	Normal	Normal
Grade 1	> 10% to <25%	Hunching noted only at rest	Mild to moderately decreased	Mild to moderate ruffling	Scaling of paws/ tail
Grade 2	> 25%	Severe hunching impairs movement	Stationary unless stimulated	Severe ruffling/ poor grooming	Obvious areas of denuded skin

Here, mice were preconditioned with sub-lethal total body irradiation (5.5Gy) followed by injection of freshly transduced T cells 24h later. Mice were separated in 5 groups according to the injected T cells: (i) Mock group (T cells transduced with a red fluorescent protein (pMx-Tomato)), (ii) dc p53TCR-, (iii) α chain p53TCR-, (iv) β chain p53TCR- or (v) sc p53TCR-transduced T cells. All mice were injected with $1x10^6$ $CD8^+$ and $CD4^+$ specific cells, since both compartments show the same transduction efficiency. In general, for all *in vivo* experiments transduced and non-transduced $CD4^+$ and $CD8^+$ cells were injected as a bulk culture. The number of injected specific $CD8^+$ and $CD4^+$ cells was based on the transduction efficiency ($V\beta3^+CD8^+$ and $V\beta3^+CD4^+$ cells). The injection scheme is illustrated in Figure 4.6.

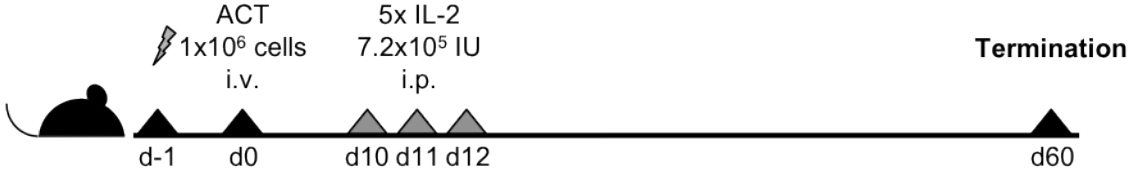

Figure 4.6 Injection scheme for mispairing-induced autoimmunity in p53-/- $A2K^b$ mice.
p53-/- $A2K^b$ mice were irradiated with a sub-lethal dose of 5.5 Gy and 24h later received ACT with $1x10^6$ effective T cells freshly transduced with Mock-plasmid (pMx-Tomato), sc p53TCR, dc p53TCR, α chain or β chain p53TCR. T cell expansion was induced by i.p. injection of high dose IL-2 twice on day 10, 11 with 8h in between injections and once on day 12 after ACT. Mice were scored and sacrificed according to GvHD criteria (Table 4.1). Termination of the experiment was set to 60 days post ACT.

On day 10 to 12 after ACT mice were injected with high dose of IL-2 to maintain T cell expansion of the already pre-activated transduced T cells. Before and after injection and as follow-up, blood was drawn from mice one weekly and T cells frequencies were calculated based on the amount of blood taken. The proliferation of the total $CD4^+$ and $CD8^+$ T cells in blood after IL-2 injection (day 10-12) was increased about 100-fold in all groups (Figure 4.7). In addition, also the number of $V\beta3^+$ cells increased after IL-2 injection (data not shown).

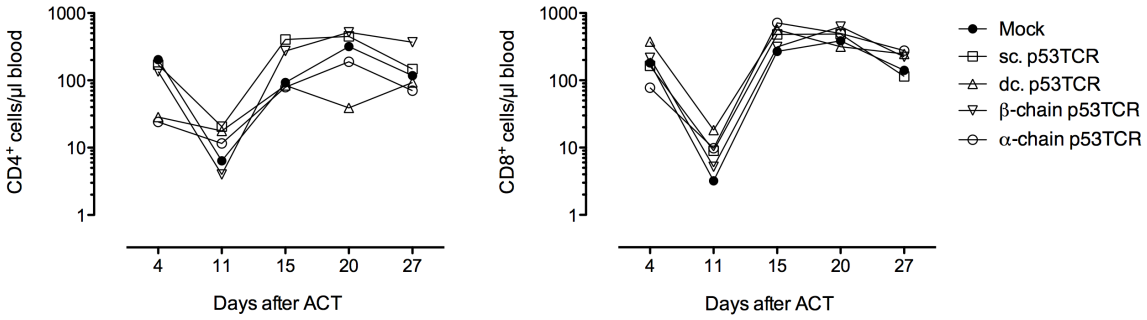

Figure 4.7 T cell proliferation in blood of mice after ACT and treatment with IL-2.
Mice were treated as desribed in Figure 4.6. Blood T cells were analyzed for $CD4^+V\beta3^+$ and $CD8^+V\beta3^+$ by flow cytometry on a weekly basis throughout the experiment as described in 3.4.3.2 and 3.4.7.3. Absolute T cell count was calculated using a defined number of latex beads in each sample as a reference. Mock n=5; sc p53TCR n=5; dc p53TCR n=5, α/β-chain p53TCR n=5. Stopping gate was set to 5,000 gated beads. Mean values for each group are plotted on logarithmic scale.

Already at day 18 after ACT one mouse of the β chain p53TCR group developed severe signs of GvHD as demonstrated by loss of bodyweight and reduced activity. By day 38 after ACT all mice, which received β chain p53TCR were sacrificed due to severe GvHD symptoms (Figure 4.8). The overall surveillance of the mice (Figure 4.8) showed that mice receiving β chain p53TCR transduced T cells developed earlier signs of GvHD than mice receiving dc p53TCR transduced T cells. Interestingly, 60% of the mice receiving α chain and 40% of mice receiving dc p53TCR transduced T cells survived the experiment without any signs of GvHD. Moreover, all mice infused with sc p53TCR or Mock-transduced T cells survived without developing signs of GvHD.

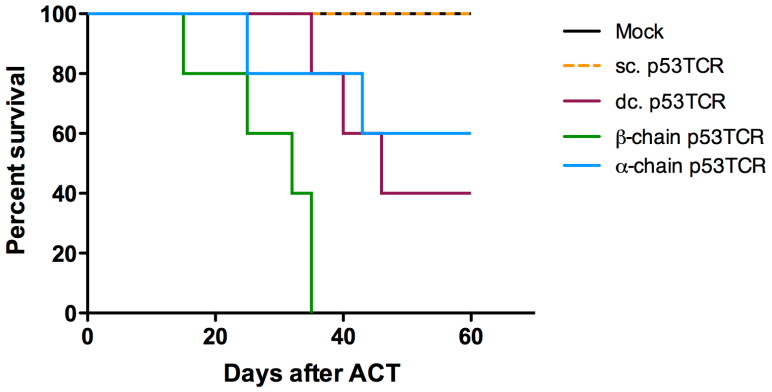

Figure 4.8 GvHD-free survival after ACT reveals that sc p53TCR does not induce TCR-related autoimmunity
Mice were treated as described in Figure 4.6. Survival is expressed as percent of GvHD-free mice, n= 5 per group.

When reaching a total score of 5 according to disease grading as shown in Table 4.1, or at the day of termination (day 60 after ACT) mice were sacrificed and samples were collected for flow cytometric analysis and/or histological analysis. Flow cytometric analysis of bone marrow, liver, lung and spleen was carried out as described in 3.4.12. Flow cytometric analysis of all organs showed massive infiltration of $V\beta3^+CD8^+$ and $V\beta3^+CD4^+$ T cells in samples of mice receiving dc p53TCR or β chain p53TCR T cells. In some animals up to 50% of all infiltrating $CD8^+$ cells were harboring the $V\beta3^+$ TCR, as observed in bone marrow (44.3% and 45.5%) and liver (32.2% and 49%; Figure 4.9). In contrast, less or almost no infiltrating $CD8^+V\beta3^+$ cells were found in the bone marrow and liver of mice receiving either Mock (0% and 4.7%) or sc p53TCR transduced T cells (1.7% and 3.1%), respectively. Similar results were observed in spleen and lung tissues (data not shown). Samples from the α chain p53TCR group were additionally analyzed for the surrogate marker GFP (Figure 4.9), since only slight increases of infiltrating $V\beta3^+$ cells could be observed (compare with Figure 4.5). Given the evident infiltration of cells into the key organs, samples were checked for GFP expression in the CD4 and CD8 compartment. Samples from mice receiving the α chain p53TCR showed infiltration of GFP^+ cells in bone marrow (25.4%) and liver (27.7%). In accordance to these observations, mice infused with dc or β chain p53TCR also showed high numbers of infiltrating $V\beta3^+$ cells in key organs for GvHD (Figure 4.9).

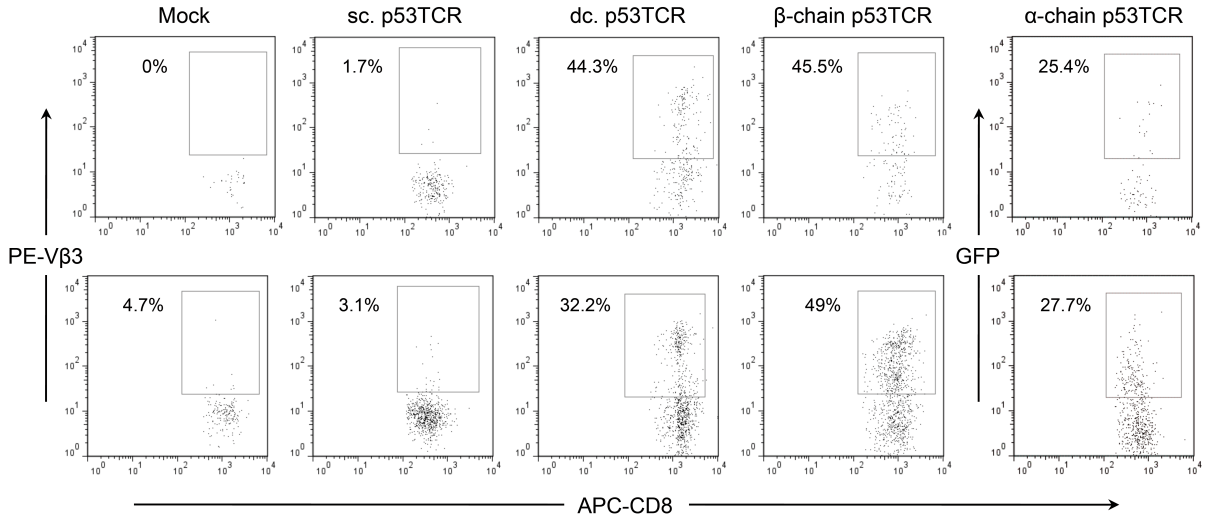

Figure 4.9 High amounts of Vβ3$^+$ infiltrating lymphocytes in key organs for GvHD.
Flow cytometric analysis revealed infiltrating CD8$^+$Vβ3$^+$ lymphocytes in bone marrow (upper panel) and liver (lower panel) of p53-/- A2K^b mice, which were treated as described in Figure 4.6 (Mock n=1; sc p53TCR n=2; dc p53TCR n=5, α/β chain p53TCR n=3). For mice receiving α chain p53TCR transduced T cells (n=3) bone marrow and liver samples were analyzed for GFP expression after pre-gating on CD8$^+$ cells.

To confirm the flow cytometry data, histological sections of spleen and liver were taken. Here, organs were snap-frozen in OCT and sections were prepared for staining of infiltrating CD4$^+$ or CD8$^+$ T cells (3.4.9). As expected and according to the flow cytometry results (Figure 4.9), spleen and liver sections of mice receiving either dc or β chain p53TCR transduced T cells also showed high amounts of infiltrating CD4$^+$ and CD8$^+$ T cells (Figure 4.10 and data not shown). Even more striking was the severly impaired tissue structure, as observed in spleen samples of mice, which were highly infiltrated by T cells harboring the dc, β chain or α chain TCR (Figure 4.10). Spleen morphology was clearly disrupted and structures such as the red and white pulp were not distinguishable any more. As shown in Figure 4.10, spleens from mice treated with dc p53TCR and β chain p53TCR showed high numbers of infiltrating CD8$^+$ cells compared to the sc p53TCR where only few infiltrating cells were detected. Compared to the dc and β chain group the α chain p53TCR showed less numbers of infiltrating T cells in key organs of GvHD (see Figure 4.9), which could be confirmed by histology. Spleens of the α chain p53TCR group showed less infiltration than in the dc and β chain p53TCR and tissue morphology was less damaged. However, compared to the sc p53TCR and Mock group, which showed no tissue destruction at all, tissue damage was observed in all other groups.

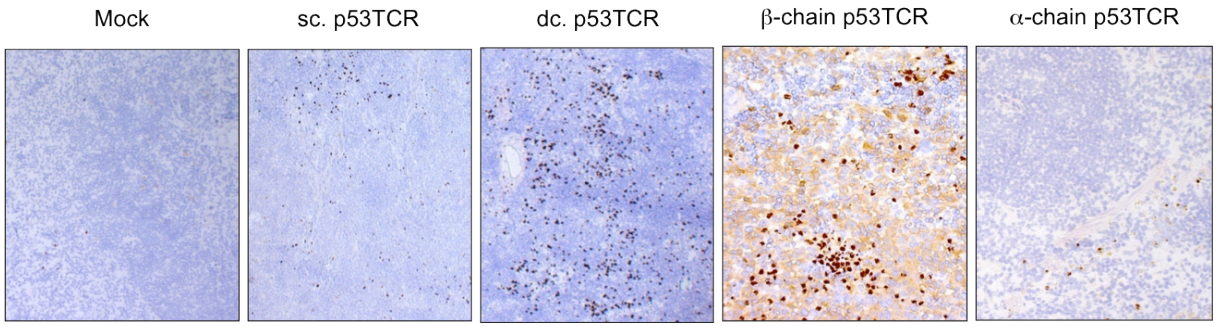

Figure 4.10 Histological analysis of spleens show strong lymphocyte infiltration in mice receiving dc p53TCR or α/β chain p53TCR.
$CD8^+$ lymphocytes (brown staining) in spleens of mice treated as described in Figure 4.6. Representative photomicrographs with 200-fold magnification were taken (Mock n=1; sc p53TCR n=2; dc p53TCR n=5, α/β chain p53TCR n=3 mice). On the day of termination, spleens were harvested and separated in two parts for flow cytometric and histological analysis. Half a spleen was snap-frozen in OCT compound on dry ice. Cryostat sections of 2µm thickness were stained for $CD8^+$ T cells as described in section 3.4.9.

Taken together, after injection of either dc, α chain or β chain p53TCR-redirected T cells, reduced survival, higher GvHD scores and tissue infiltration was observed compared to mice receiving sc p53TCR or Mock transduced T cells.

4.2 Absence of on-target autoimmunity after adoptive T cell transfer of the p53-specific single chain T cell receptor

Since p53 is ubiquitously expressed in both cancer and healthy tissue it is necessary for p53-specific T cells to distinguish between normal cells and p53 over-expressing tumor cells. As we already showed that exclusively the adoptive transfer of sc p53TCR-specific T cells does not induce off-target cytotoxicity (chapter 4.1), proceeding studies were carried out with sc p53TCR transduced T cells. Therefore, we used HupKiCyA2K^b (HupKi) mice to test the sc p53TCR for its potential to induce on-target related autoimmunity. HupKi mice are characterized by a knock in of the human *p53* gene and expression of HLA-A2/K^b molecules, thus representing a relevant experimental model to study p53 on-target related side effects, which might occur by TCRs targeting weakly expressed self-antigens.

4.2.1 p53-expressing normal cells are not recognized by sc p53TCR-redirected T cells

As preliminary *in vitro* tests we performed cytolytic assays using sc p53TCR-transduced Hupki T cells as effector cells. Target cells, which express basal levels of p53 (HupKi MEF), were not recognized (Figure 4.11 A, closed circles) unless they

were loaded with the cognate peptide (closed squares). The specificity of lysis could also be demonstrated by recognition of T2 control cells, which were either loaded with an unspecific (Figure 4.11 A, open circles) or the specific p53 peptide (Figure 4.11 A, open squares), or by using p53-negative cells (Figure 4.11 A + B, closed triangles). Moreover, HupKi T cells specific for the sc p53TCR were also not recognized by themselves when used as target cells after stimulation for 2 days with 10% TCGF and 2µg/ml ConA (Figure 4.11 B, open squares) or when in an activated state (4 days after weekly restimulation; Figure 4.11 B, open circles). In addition, freshly isolated HupKi splenocytes were tested as target cells and were not lysed by sc p53TCR HupKi T cells (data not shown).

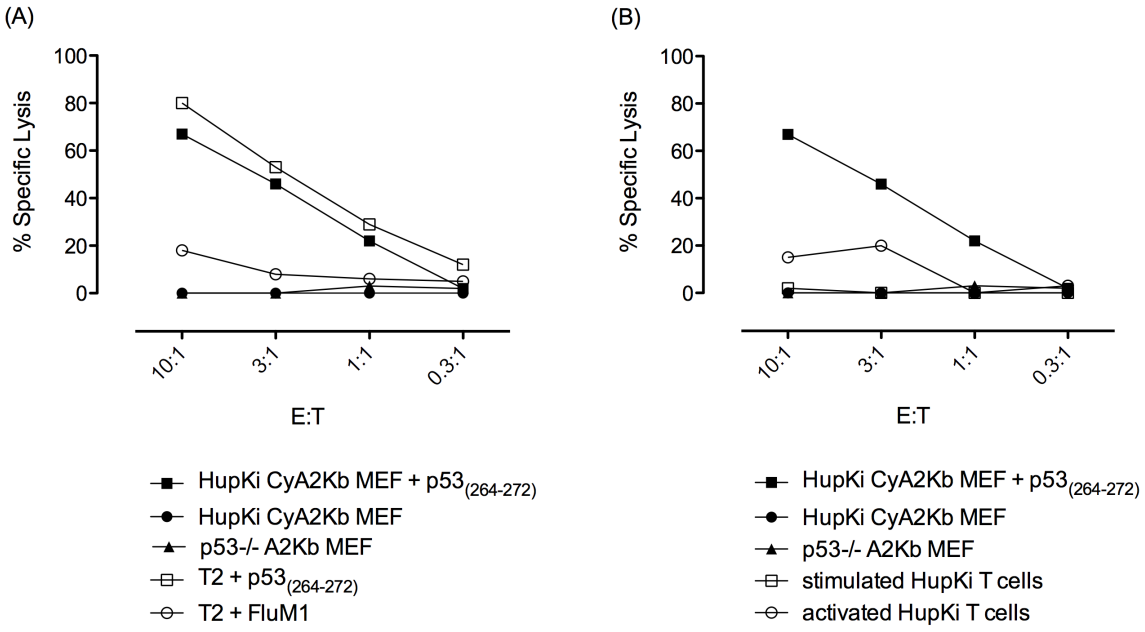

Figure 4.11 Absence of recognition of p53-expressing healthy donor cells.
^{51}Cr-release assay showing the cytolytic function of effector T cells retrovirally transduced with the sc p53TCR. As target cells either (A) the HupKiCyA2K^{b} MEF immortalized cell line, the p53-/-A2K^{b} MEF immortalized cell line, T2 cells, or (B) cultured HupKi T cells transduced with the sc p53TCR were used. As indicated, cells were loaded with 10^{-6}M p53$_{(264-272)}$ peptide. All MEF cell lines were treated for 18h with 20ng/ml mouse IFN-γ and were loaded with100µCi ^{51}Cr for 90 min. ^{51}Cr-labeled target cells (T) were incubated with effector cells (E) for 5.5h at the indicated E:T ratios. One representative assay (mean of duplicates) is shown.

Hence, these *in vitro* results strongly suggest that there is no on-target reaction triggered when using the sc p53TCR-modified T cells.

4.2.2 Absence of on-target toxicity *in vivo* after transfer of high numbers of sc p53TCR-specific T cells and IL-2

To test the safety of sc p53TCR-specific ACT in terms of undesired on-target toxicity, *in vivo* experiments using HupKi mice were performed. In brief, HupKi mice were preconditioned with sub-lethal TBI and one day later received $20x10^6$ sc p53TCR or Mock-transduced T cells i.v. (Figure 4.12). Between days 10 to 12 after the first ACT the injected T cells were stimulated *in vivo* by applying high dose IL-2 i.p. in total of five injections. Body weight as well as the overall health status was scored according to above described GvHD criteria (Table 4.1).

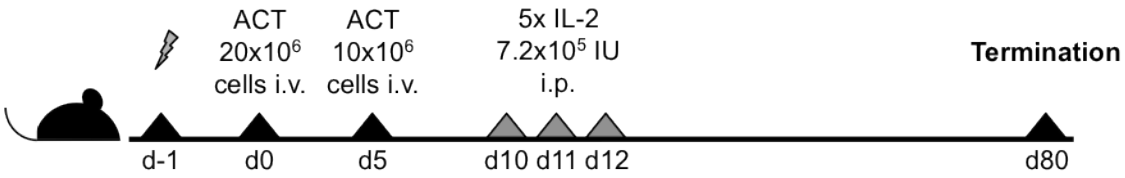

Figure 4.12 Injection scheme for on-target induced toxicity in HupKi mice pretreated with irradiation plus ACT and IL-2.
HupKi mice were irradiated with a sub-lethal dose of 5.5 Gy and 24h later received ACT with $20x10^6$ effective (sc p53TCR) or control (Mock) T cells i.v.. Leftover cells, which were not used for injection, were stimulated for 4 days with Dynabeads® Mouse T-Activator CD3/CD28 and 600IU/ml IL-2. Five days after ACT mice received another $10x10^6$ effective T cells i.v.. *In vivo* expansion of infused T cells was induced by i.p. injection of high dose IL-2 twice on day 10 and 11, with 8h in between injections, and once on day 12 after the first ACT. Mice were scored and sacrificed according to GvHD criteria (Table 4.1). Termination of the experiment was set to 80 days after ACT.

Shortly after the second T cell injection the body weight of mice receiving sc p53TCR dropped massively (Figure 4.13 B) compared to mice injected with Mock transduced T cells (Figure 4.13 A). One mouse of the sc p53TCR group died directly after IL-2 treatment (Figure 4.13 B, open circles). However, mice recovered progressively right after IL-2 treatment and reached their initial body weight at around day 35 (Mock, Figure 4.13 A) and day 59 (sc p53TCR, Figure 4.13 B), respectively. One mouse out of each group (open squares) was not affected from weight loss during the course of the experiment.

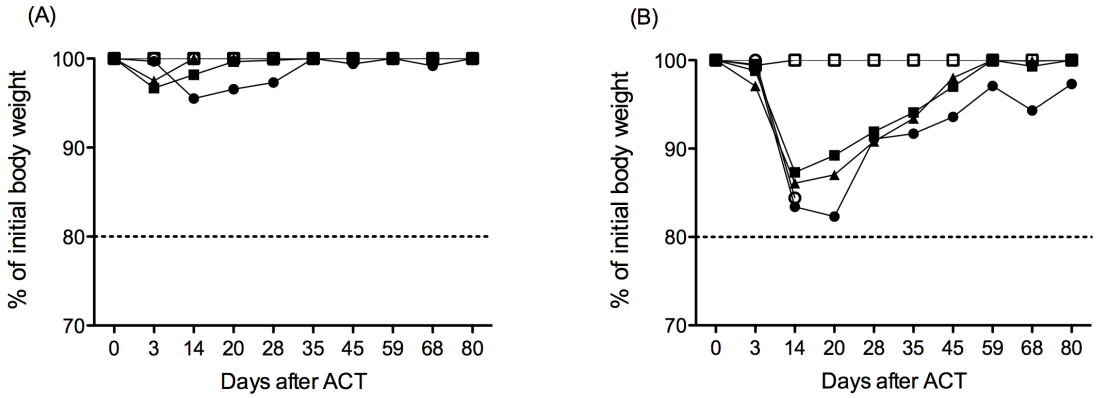

Figure 4.13 Injection of high number of sc p53TCR T cells does not induce GvHD-associated weight loss. Monitoring of body weight of mice receiving Mock (A) or sc p53TCR-transduced T cells (B). Body weight was determined prior to TBI on day -1 and was set to 100%. According to the animal protection law mice had to be sacrificed when loosing ≥20% of body weight (dashed line).

It is important to mention that injected cells included transduced as well as non-transduced $CD4^+$ and $CD8^+$ T cells. The number of effective cells was calculated according to the percentage of transduced $V\beta3^+CD8^+$ and $V\beta3^+CD4^+$ cells as determined by flow cytometry. Hence, the total number of injected cells was higher than the number of injected TCR-specific cells. However, during the course of the experiment no signs of GvHD could be observed in any of the groups. Moreover, after termination of the experiment on day 80 only slightly increased numbers of $V\beta3^+$ cells were detected in target organs (i.e. bone marrow and spleen) in the sc p53TCR group. A distinct variability in the presence of $V\beta3^+$ cells within different organs between and within the groups could be noted (Figure 4.14). No significant difference in infiltrating $V\beta3^+$ cells in the CD4 and CD8 compartment in bone marrow and liver could be observed in both groups (Figure 4.14). In contrast, there was a significant increase in $V\beta3^+CD4^+$ cells in lung and spleen as well as a significant increase in $V\beta3^+CD8^+$ cells in spleen of mice treated with sc p53TCR, even though these mice did not show any signs of GvHD.

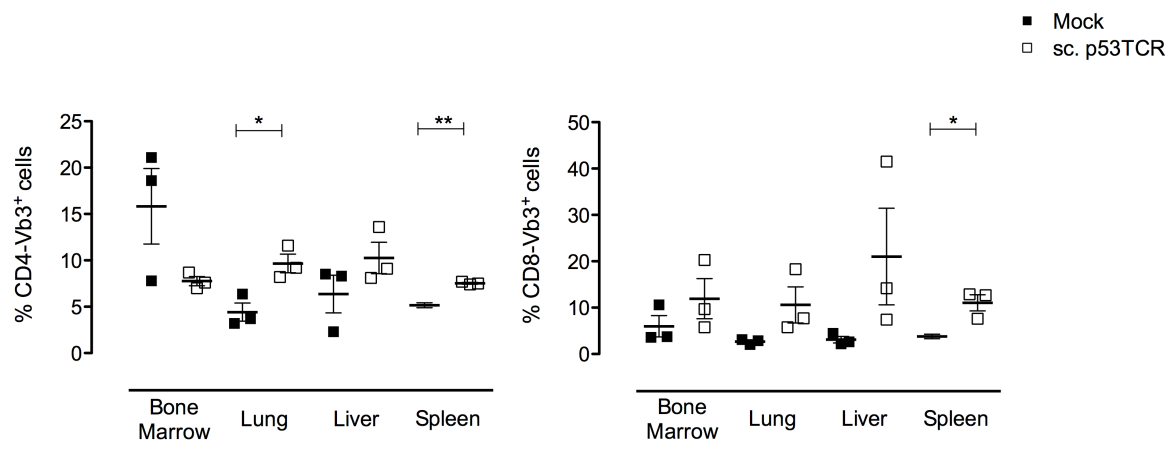

Figure 4.14 Mild rate of infiltration of Vβ3$^+$ T cells in GvHD target organs after ACT.
Infiltration of CD4$^+$ and CD8$^+$ Vβ3$^+$ T cells into target organs of mice receiving sc p53TCR (open squares) or Mock (closed squares) transduced T cells was assessed after termination of the experiment on day 80 after ACT. Tissues were harvested and prepared for flow cytometric analysis as described in section 3.4.12. Vβ3$^+$ cells were pregated on CD4$^+$ and CD8$^+$ cells, respectively. * p<0.05, ** p<0.01, all others not significant, n=3.

Histological analysis confirmed the absence of tissue lesions and revealed very weak infiltration of CD4$^+$ or CD8$^+$ T cells in the spleen of mice injected with sc p53TCR specific T cells (Figure 4.15). Normal tissue morphology was maintained in both groups.

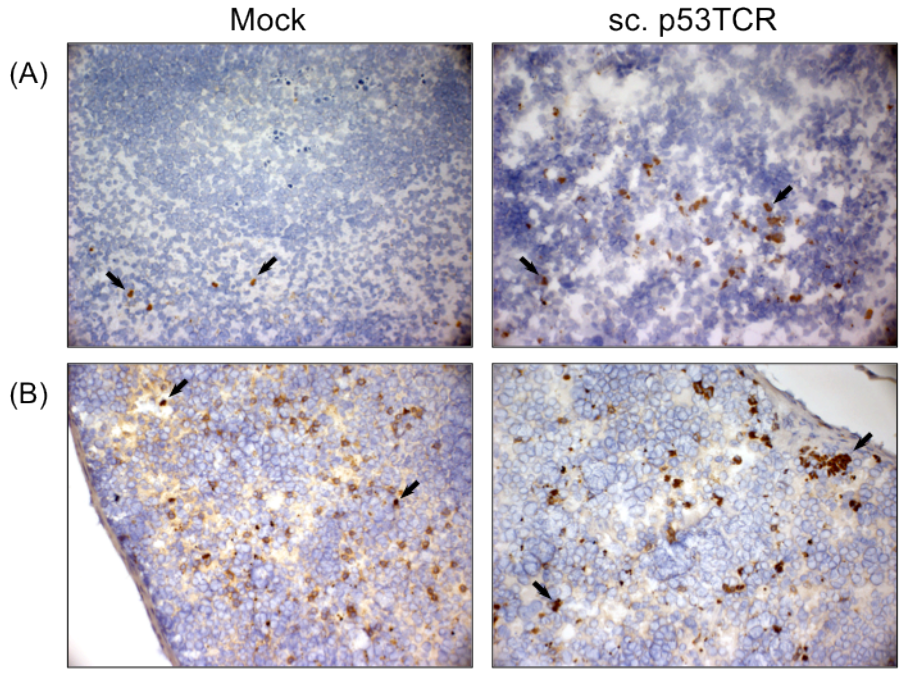

Figure 4.15 Tissue morphology is not altered following ACT.
Cryostat sections of 2µm thickness were prepared and stained as described in section 3.4.9. Frozen sections of spleen tissue were stained for (A) CD4$^+$ and (B) CD8$^+$ T cells in spleen tissue. Examples of positively stained cells are indicated by arrows (dark brown). Magnification x400.

4.2.3 Absence of on-target toxicity in vivo after chemotherapy, transfer of p53TCR-specific T cells and peptide vaccination

A main feature of GvHD is targeting normal host tissue such as skin, gut, liver and spleen, but possibly also the hematopoietic compartment. To further test the safety of the sc p53TCR gene transfer, HupKi mice were pre-conditioned by chemotherapy with 2mg cyclophosphamide for 2 days and 2mg fludarabine for 3 days prior to injection of 2.5x 10^6 sc p53TCR transduced T cells in order to deplete circulating leukocytes. Mice were separated into two groups, one group receiving an i.p. injection of PBS, the other group being vaccinated with $p53_{(257-282)}$ peptide and adjuvants as described in Figure 4.16. Mice were monitored for signs of GvHD and the reconstitution of the hematopoietic compartment was evaluated by weekly analysis of the immune cell composition in peripheral blood.

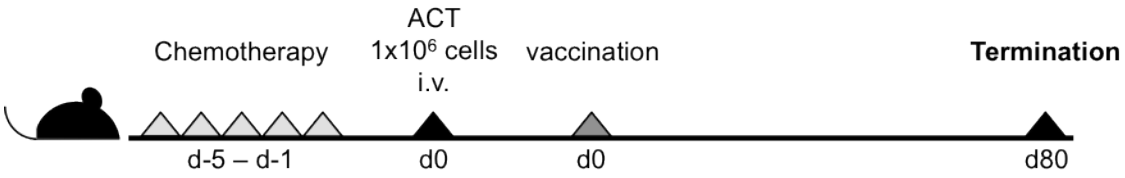

Figure 4.16 Injection scheme on-target induced toxicity in HupKi mice with chemotherapy, ACT and peptide vaccination.
HupKi mice were preconditioned with chemotherapy. On day -5 to day -3 mice received fludarabine (2mg) i.p. and afterwards on day -2 and day -1 cyclophosphamide (2mg) i.p.. After pre-conditioning mice were injected with 1x10^6 cells freshly transduced sc p53TCR T cells i.v. and were subsequently vaccinated with 100µg $p53_{(257-282)}$ peptide, 20µg CpG1668 and 50µg anti-CD40. Mice were scored and sacrificed according to GvHD criteria (Table 4.1). Termination of the experiment was set to 80 days after ACT.

Pre-conditioning with chemotherapy caused depletion of T cells and B cells lasting up to 20 days after ACT (Figure 4.17 A, C). Both cell subsets started to come back at around day 33 after ACT in both groups and showed massive increase at a very late time point of the experiment around day 54 to 74 after ACT. $CD3^+V\beta3^+$ T cells showed a similar kinetic throughout the experiment (Figure 4.17, D) with the highest amount of cells detected in the blood at later time points. The $V\beta3^+$ population was increased in peptide-vaccinated mice mainly due to vaccination. Overall, mice did not show any signs of GvHD. No significant differences in T and B cell numbers were observed between the groups. In addition, macrophages showed an increase in cell number directly after chemotherapy (Figure 4.17, B), but quickly decreased again within the first week after ACT. A significant decrease was observed in the peptide-vaccinated group at day 10 after ACT, which was maintained during the experiment.

Therefore, ACT plus peptide-specific vaccination did not affect the hematopoietic reconstitution in mice that were pre-conditioned by chemotherapy.

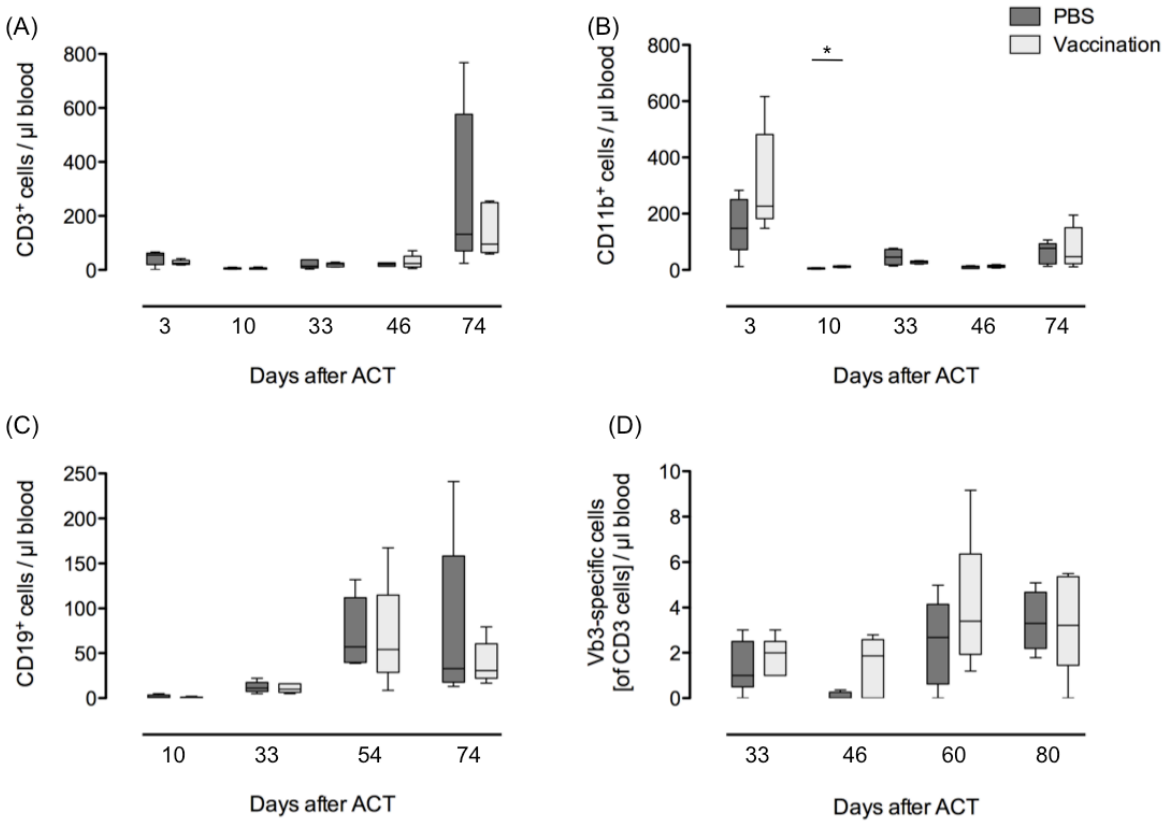

Figure 4.17 Complete restoration of the hematopoietic compartment after adoptive transfer of sc p53TCR transduced T cells.
Blood samples were collected on a weekly basis and analyzed for the presence of $CD3^+$ T cells (A), $CD11b^+$ myeloid cells (B) and $CD19^+$ B cells (C). Additionally, $V\beta3^+CD3^+$ T cells (D) were analyzed to determine the number of p53TCR specific T cells. * $p<0.05$, all others not significant, n=5.

Further analysis of organs for infiltration of $V\beta3^+CD4^+$ and $V\beta3^+CD8^+$ T cells revealed no significant differences between vaccinated and non-vaccinated (PBS) animals (Figure 4.18).

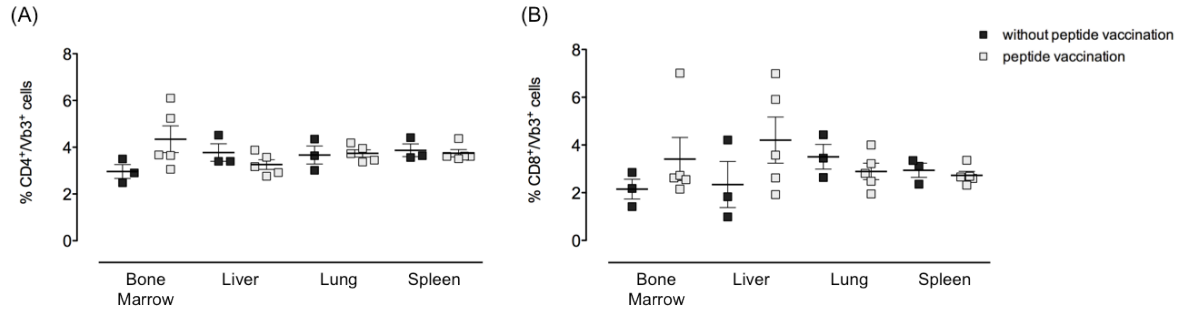

Figure 4.18 Vβ3$^+$CD4$^+$ and Vβ3$^+$CD8$^+$ T cells show similar infiltration pattern in key organs for GvHD regardless of vaccination (previous page).
Vβ3$^+$CD4$^+$ or CD8$^+$ infiltrating T cells in key organs of GvHD of mice receiving peptide vaccination (open squares) or PBS (closed squares) after injection of 1x10^6 sc p53TCR-specific T cells. The experiment was terminated on day 80 after ACT and tissue was harvested for flow cytometric analysis as described in section 3.4.12. Cells were pre-gated on CD4$^+$ or CD8$^+$ cells, respectively. n=3 (closed squares), n=5 (open squares).

Overall, the experiments addressing the potential on-target toxicity of sc p53TCR-redirected T cells showed that neither high number of transferred cells, nor leukodepletion and subsequent peptide vaccination resulted in on-target autoimmunity.

4.3 Adoptive transfer of sc p53TCR-modified T cells triggers partial anti-tumor response *in vivo*

In the previous chapters we addressed the safety concerns regarding off- and on-target toxicity, which can be associated with the use of high-affinity TCRs targeting non-mutated self-antigens. Here, we investigated the therapeutic efficacy of the sc p53TCR in an *in vivo* tumor model. The presence of sufficient amount of antigen on the cell surface is fundamental for for tumor recognition by the sc p53TCR. This was ensured by using p53-/-A2K^b MEF mut#7, a mouse embryonic tumor cell line, which was immortalized and stably transduced with the mouse *wt p53* gene, harboring the human HLA-A2-restricted p53 epitope sequence 264-272 of the DNA binding domain. Furthermore, a point mutation (270 Arg→Cys) was introduced into the mouse *wt p53* gene, mimicking a human hotspot mutation (273 Arg→His) and leading to accumulation of the mutated p53 protein within the cell, which in turn leads to an overexpression on the cell surface (32, 33). First hints on the efficacy of this system were already given by the results of *in vitro* cytolytic assays, demonstrating the specific lysis of tumor cell lines expressing the cognate antigen by sc p53TCR-

redirected T cells (Figure 4.3). To determine whether the sc p53TCR is also efficient in recognizing tumors *in vivo*, the mouse studies described below were performed. Preliminary test to set up the tumor engraftment system showed that injection of $0.2x10^6$ cells of a tumor cell suspension was sufficient to lead to tumor formation within 7-14 days (data not shown).

4.3.1 Delayed tumor growth in a preclinical mouse tumor model after transfer of sc p53TCR-redirected T cells

For all *in vivo* efficacy studies HupKi mice were used as recipient animals as well as for the isolation of donor T cells. Tumor cell suspension was injected into the right flank and resulted in a tumor engraftment rate of 60-70%. Mice were pre-conditioned with sub-lethal total body irradiation (TBI) when they showed palpable tumors and prior to injected of TCR-transduced T cells. Mice received peptide vaccination one day after ACT (Figure 4.19) to stimulate and expand the injected T cells *in vivo*.

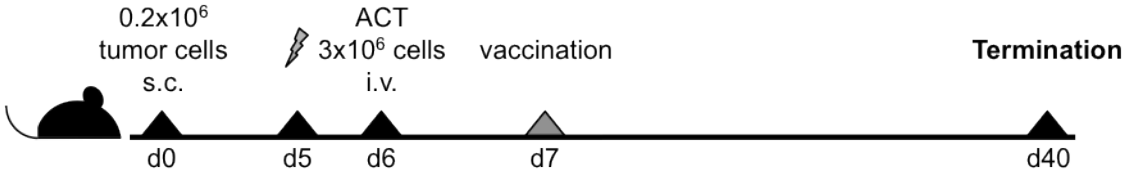

Figure 4.19 Experimental scheme for injection of sc p53TCR redirected T cells leading to delayed tumor growth.
HupKi mice were injected in the right flank with $0.2x10^6$ p53-/-A2K^b MEF mut#7 tumor cells, which were cultivated in exponential phase. 5 days (d5) after tumor cell injection mice were pre-conditioned with 5.5Gy and 24h later were infused i.v. with $3x10^6$ Mock or sc p53TAR-transduced cells. On day 7 (d7) after tumor cell injection and 1 day after ACT mice were anesthetized and received vaccination with 100µg $p53_{(257-282)}$ peptide and 45µg anti-CD40 s.c. as well as 62mg Aldara cream (containing to 3mg imiquimod) on the skin at the tumor site. Mice were sacrificed on day 40 or before, in case the tumor size reached a volume of 1000-1500mm^3.

Already one week after ACT a remarkable difference in tumor size could be observed within the group injected with the sc p53TCR (Figure 4.20). These mice showed smaller tumors compared to the control group. On day 7 after tumor cell injection mice receiving sc p53TCR-transduced T cells showed a mean tumor size of 13mm^3, whereas mice receiving Mock-transduced T cells showed a mean tumor size of 29mm^3 (data not shown). This observation was further confirmed at later time points (day 21 after tumor cell injection), where almost all mice of the Mock group had to be sacrificed compared to mice receiving the sc p53TCR. By day 25 after tumor cell injection all control mice were removed from the experiment due to excessive tumor

growth, whereas 4 out of 7 mice receiving the sc p53TCR showed only small tumors (< 500mm^3).

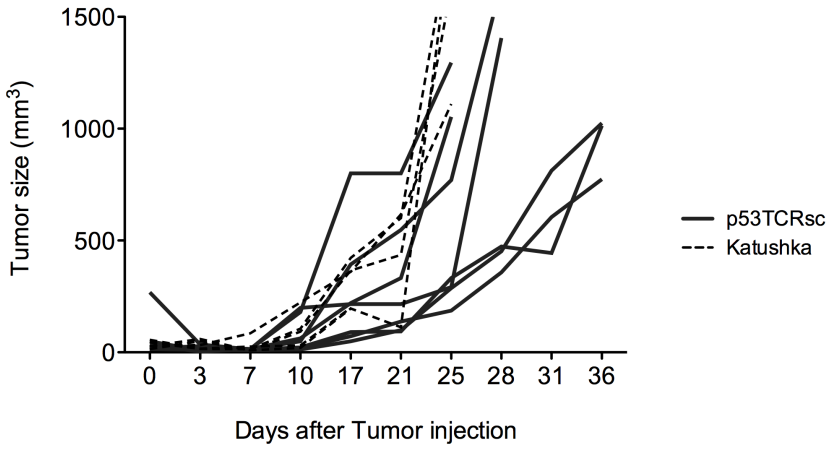

Figure 4.20 Treatment of tumor-bearing mice with sc p53TCR-specific T cells delays tumor growth. Tumor length (L) and width (W) was measured with a caliper twice a week. Tumor size was calculated by the formula LxWxW to get a tumor volume in mm^3, which was plottet against time. Mice were sacrificed when the tumor size reached 1000-1500mm^3. Mice receiving sc p53TCR-transduced T cells in solid lines (n=7), mice receiving Mock (Katushka)-transduced T cells in dashed lines (n=4).

Importantly, about 43% of p53TCR-infused mice were able to control tumor growth for up to 4 weeks after tumor cell injection (3 weeks after ACT), which led us to the conclusion that ACT in tumor-bearing mice provides a time frame in which tumor growth is clearly delayed.

4.3.2 Partial tumor rejection in mice injected with tumor cells and infused with p53TCR-specific T cells at the same time

To improve the already emerging anti-tumor effect of the sc p53TCR another *in vivo* experiment was set up in which tumor cells and T cells were injected at the same time. Thus, mice were pre-conditioned with TBI prior to the injection of T cells (i.v) and tumor cells (s.c). Peptide vaccination was applied one day after T cell/tumor cell injection (Figure 4.21).

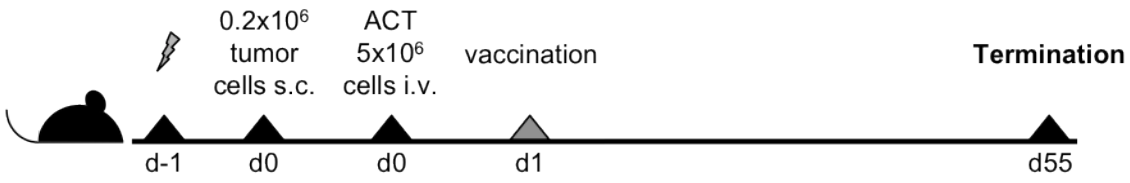

Figure 4.21 Injection scheme for simultaneous injection of tumor cells and T cells. HupKi mice were irradiated with a sub-lethal dose of 5.5Gy on day -1 and were injected s.c. with $0.2x10^6$ p53-/-A2K^b MEF mut#7 tumor cells in the right flank. 24h later, mice were injected i.v. with $5x10^6$ transduced sc p53TCR or Mock transduced T cells. On day 1 after tumor and T cell injection mice were anesthetized and received vaccination with 100µg $p53_{(257-282)}$ peptide and 45µg anti-CD40 s.c. as well as 62mg Aldara cream (containing 3mg imiquimod) on the skin at the tumor site. Mice were sacrificed on day 55 or before in case tumor size reached a volume of 1000-1500mm^3.

Consistent with the previous tumor model, we again observed a control of tumor growth by the transferred T cells. Moreover, in 50% of mice infused with sc p53TCR tumors were controlled until the end of the experiment, whereas in the Mock group all mice had to be sacrificed by day 53 after ACT (Figure 4.22). *Ex vivo* analysis of the controlled tumors revealed that almost no viable tumor cells were detectable and the remaining mass consisted of necrotic and connective tissue (data not shown).

As mentioned before, we could reproduce the above described delayed tumor outgrowth by infusion of sc p53TCR-redirected T cells. In this particular experiment 57% of the mice injected with Mock-transduced T cells had to be removed already on day 32 after T cell and tumor cell injection, in contrast to only 33% of mice from the sc p53TCR group.

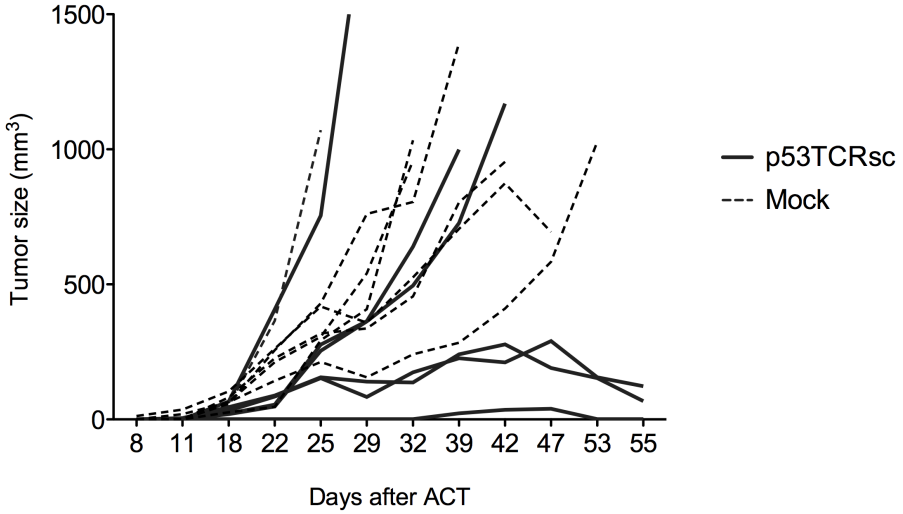

Figure 4.22 Simultaneous injection of tumor cells and sc p53TCR-transduced T cells enhances tumor rejection.
Tumor length (L) and width (W) was measured with a caliper twice a week. Volume was calculated by the formula LxWxW to get a tumor volume in mm^3. Tumor size was plotted against time and mice were sacrificed when tumor size reaches 1000-1500mm^3. Mice receiving sc p53TCR-transduced T cells in solid lines (n=6), mice receiving Mock-transduced T cells in dashed lines (n=7).

Taken together, these results demonstrated the capacity of sc p53TCR-redirected T cells to recognize and eradicate tumor cells when infused early during the course of tumor growth.

4.3.3 Tumor immune escape mechanisms hinder T cells to target the tumor

Tumors have been described to overcome the immune system by using several immune escape mechanisms, such as the loss of immunogenicity (66, 67). So far, our experimental tumor models demonstrated that irrespective of the time of injection of sc p53TCR-transduced T cells, some tumors escaped regulation. Considering already known immune-escape mechanisms, we checked the tumor cells for HLA-A2 expression right after harvesting from sacrificed animals and frequently observed a down-regulation of MHC I molecules (Figure 4.23). Independent of the performed *in vivo* experiment and the specificity of infused cells, tumors showed differently regulated HLA-A2 expression, varying from almost not altered (Figure 4.23, left panel) to a complete shut down (middle panel) or an intermediate expression of HLA-A2 (right panel).

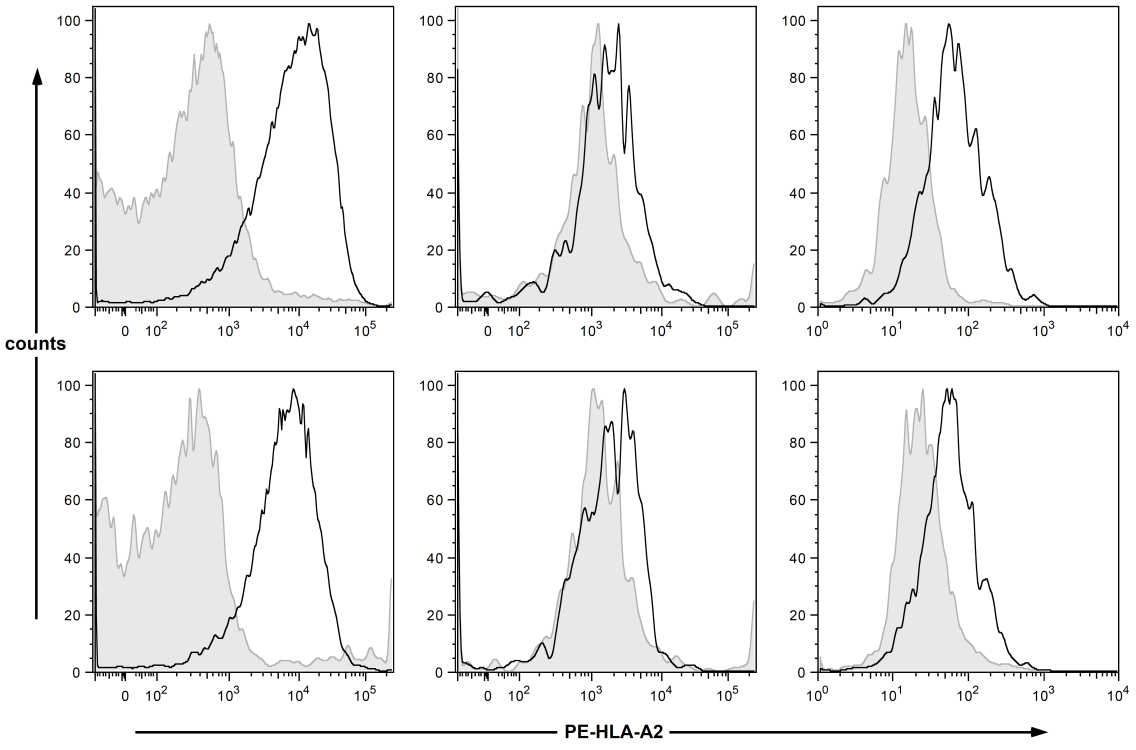

Figure 4.23 Frequently observed down-regulation of HLA-A2 in outgrowing tumors after ACT (previous page).
Extracted tumors were homogenized and cells stained for HLA-A2 (black curve) or with an isotype control antibody (grey filled curves), respectively. Tumor cells of mice infused with sc p53TCR (upper panel) or Mock-transduced T cells (lower panel) were analyzed. Shown here from left to right are representative histograms of 3 different *ex vivo* tumor homogenates from independent *in vivo* experiments (n=4). Cells were pre-gated on GFP^+ live cells.

In order to discriminate whether MHC I expression was lost or just down-regulated *in vivo*, a follow-up flow cytometric analysis was carried out measuring expression on tumor cells before injection in the animals, after harvest and during *ex vivo* culture. The tendency to down-regulate HLA-A2 expression could be observed independently of the performed *in vivo* experiment. At the time of tumor cell injection the frequency of $HLA\text{-}A2^+$ cells varied between 60-80%. When harvesting the tumor cells, this number dropped to 20-50% and sometimes even below 10% of $HLA\text{-}A2^+$ cells (Figure 4.24). Interestingly, HLA-A2 surface expression was restored to initial levels after *in vitro* culture.

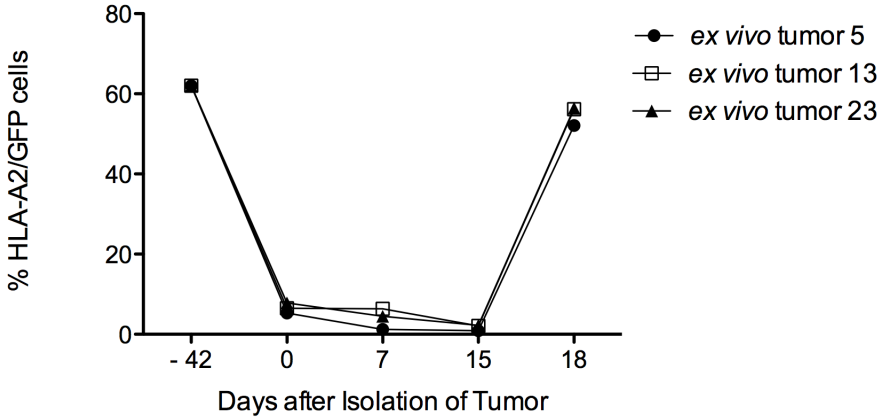

Figure 4.24 Restoration of HLA-A2 expression of *ex vivo* tumors upon *in vitro* culture.
Tumors were harvested, homogenized and cultured as described in section 3.4.3.1. Tumor cells were analyzed by flow cytometry for surface expression of HLA-A2 before injection into mice (day -42), at the day of harvest (day 0) and once weekly during *in vitro* culture (day 7, 15 and 18). Cells were pre-gated on GFP^+ live cells.

Ex vivo tumors were not only analyzed by flow cytometry but also by immunofluorescence staining. MEF tumor cell lines were transduced with a retroviral vector encoding the mouse *wt p53* gene harboring the human epitope 264-272 plus an additional hotspot mutation. The p53-encoding plasmid also included a GFP sequence, which enabled us to track and sort successfully transduced cells. Hence, GFP expression served as a surrogate marker for transduced cells.

Besides the down-regulation of HLA-A2 molecules as shown by flow cytometry also a loss of antigen was observed. In the parental cell line p53-/- $A2K^b$ MEF mut#7 all

cells showed a GFP signal and expressed p53 protein (Figure 4.25 A), whereas some *ex vivo* tumors partially lost the GFP signal as well as p53 expression (Figure 4.25 C). Notably, not all *ex vivo* tumors showed this phenotype switch, as some retained stable antigen expression (Figure 4.25 B). However, since the parental cell line p53-/- A2K^b MEF mut#7 is a bulk cell population, we cannot exclude a possible outgrowth of a subpopulation of non-transduced p53-/- A2K^b MEFs after *in vivo* engraftment.

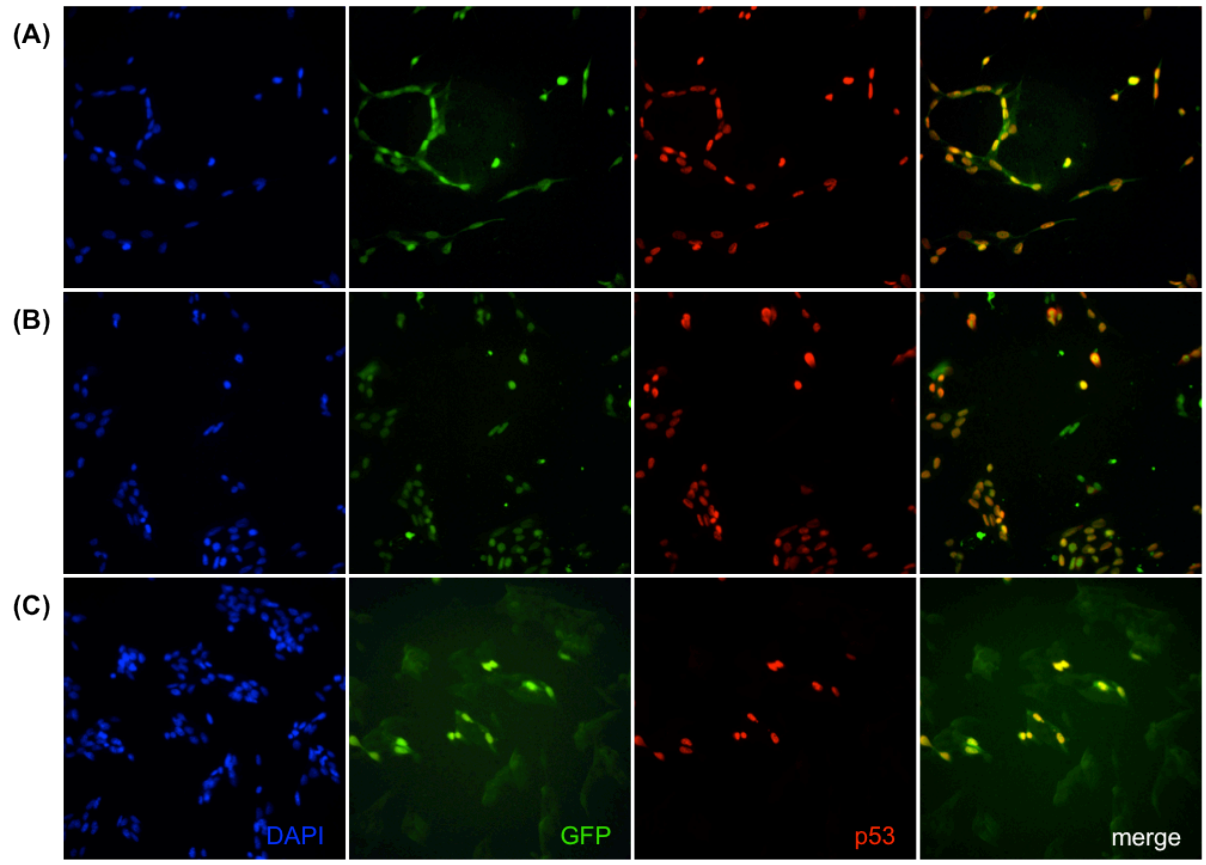

Figure 4.25 Immunofluorescence reveals loss of antigen in *ex vivo* tumors.
Tumor cells were cultured overnight on 8mm cover slips in a 6cm petri dishes. Staining procedure was performed as described in section 3.4.9.3. First column shows counterstaining of nuclei with Dapi, followed by GFP expression of the cells in the second column and staining for mouse p53 in the third column. The right column shows merged pictures of GFP expression and p53 staining. Rows show different tumors. (A) parental tumor cell line p53-/-A2K^b MEF mut#7, (B) *ex vivo* tumor 1, (C) *ex vivo* tumor 4. Shown are representative pictures of 2 independent stainings.

In summary, the first tumor model showed that transfer of sc p53TCR-transduced T cells into tumor-bearing mice led to delayed tumor growth compared to mice which were treated with Mock-transduced T cells (Figure 4.20). In another approach, where we sought to improve anti-tumor response by simultaneous injection of tumor and TCR-transduced T cells, a partial tumor regression was observed (Figure 4.22). Further characterization of outgrowing tumors revealed a down-regulation of HLA-A2

molecules as well as loss of p53 antigen, probably as a consequence of tumor immune escape mechanisms or outgrowth of a p53-negative subpopulation.

4.4 Anti-tumor response is improved by additional targeting of the tumor microenvironment

Previous studies already pointed to tumor immune escape mechanisms such as the loss of immunogenicity via down-regulation of MHC molecules or antigen loss to evade recognition by transferred tumor-specific T cells (see section 4.3.3). Other escape mechanisms are known which are not directly linked to the tumor cells, but rather focus on the surrounding tissue, the tumor microenvironment (TME). There, suppressive immune cells are recruited to the tumor site to establish an immunosuppressive TME. Such suppressive cells in the TME include myeloid-derived suppressor cells (MDSC), macrophages, which have switched from a M1 into a M2 phenotype, or infiltrating regulatory T cells. Together, they mediate immune suppression by direct inhibition of immune effector cells via cell-cell contacts, indirectly by deprivation of essential amino acids (e.g. arginine, tryptophan) in the environment or by secretion of inhibitory factors and cytokines like NO, ROS, TGF-β or IL-10 (90, 96). Taking all this into account it is very likely that ACT alone will probably be a suboptimal therapeutic approach, as long as the immunosuppressive TME is not targeted at the same time, in order to enable the infused redirected T cells to efficiently eradicate tumor cells. Therefore, a potent anti-tumor response may be conducted as a combined therapy.

To test such a combined approach the focus of experimental manipulation was directed to MDSCs. Their impact on sc p53TCR-transduced T cells was tested *in vitro* before trying different strategies to inhibit MDSCs *in vivo* to increase the anti-tumor effect of sc p53TCR-transduced T cells after ACT.

4.4.1 Tumors are infiltrated by different immunosuppressive cells

We performed flow cytometric analysis to determine, whether in our mouse tumor model (chapter 4.3) tumors were infiltrated by immunosuppressive cells. Therefore,

tumors were extracted from tumor-bearing mice, freed from skin tissue, homogenized and stained for different cell subset markers.

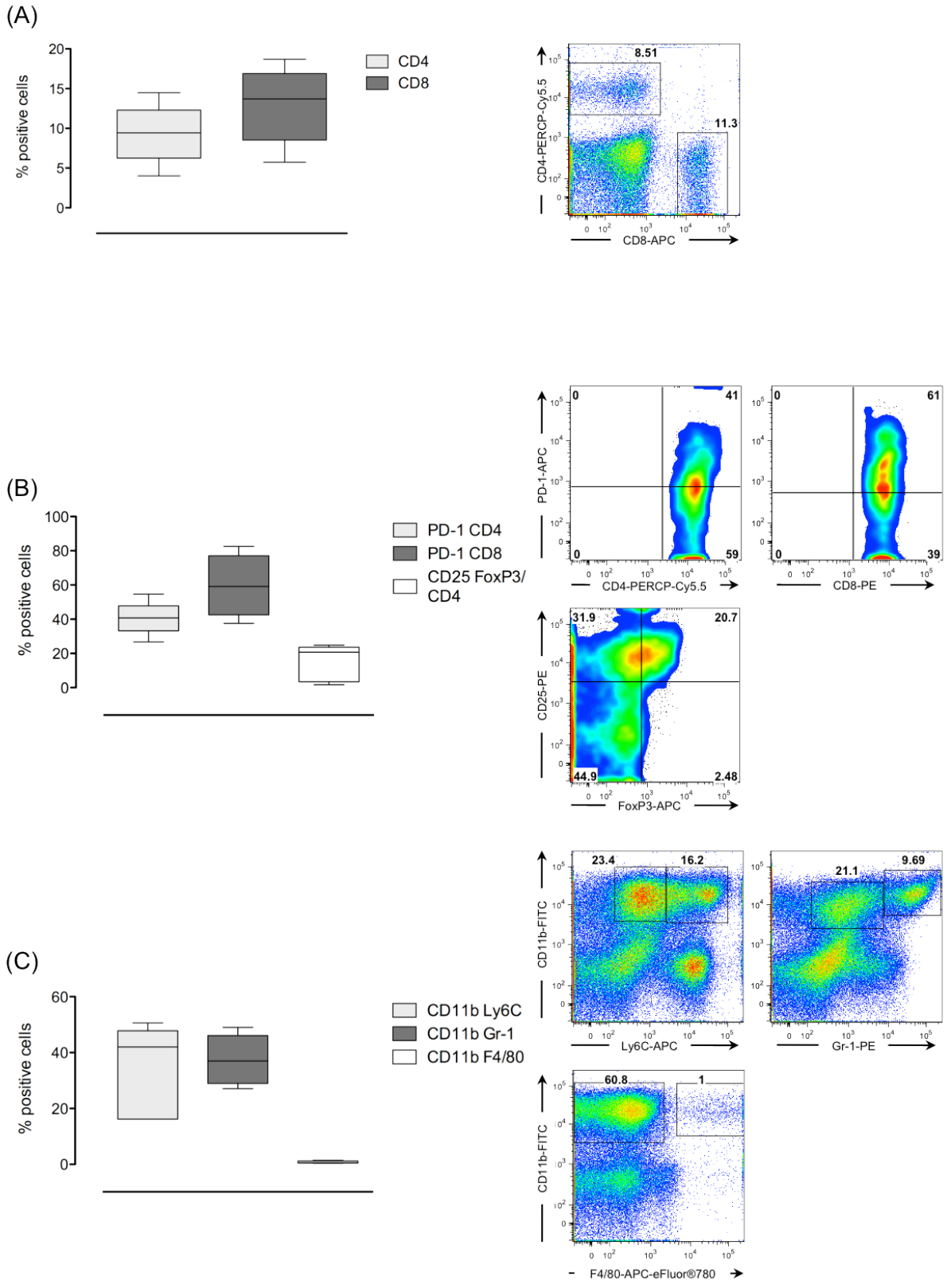

Figure 4.26 Solid tumors are infiltrated mainly by cells of the myeloid lineage (previous page).
Representative flow cytometric analyses of tumor homogenates from tumor-bearing mice (n=5) are shown. (A) Tumor infiltrating $CD4^+$ and $CD8^+$ T cells, (B) expression of PD-1 receptor on $CD4^+$ and $CD8^+$ T cells and frequency of $CD4^+CD25^+FoxP3^+$ T_{reg} cells, (C) tumor infiltrating myeloid cells including monocytes ($CD11b^+Ly6C^+$), granulocytes ($CD11b^+Gr\text{-}1^+$) and macrophages ($CD11b^+F4/80^+$). Cell type-specific analysis was performed after pre-gating on live cells.

All tested tumors showed infiltration by $CD4^+$ and $CD8^+$ T cells, regardless of tumor size or pretreatment conditions. An average of about 10% of all living cells in the tumor tissue were $CD4^+$ and about 15% $CD8^+$ cells (Figure 4.26 A). Further analysis revealed that 40-60% of all infiltrating $CD4^+$ or $CD8^+$ T cells expressed the programmed cell death protein 1 (PD-1) also known as CD279, indicating T cell exhaustion. Moreover, in average more than 20% of all $CD4^+$ cells in the tumor tissue expressed the master transcription factor specific for regulatory T cells ($CD4^+CD25^+FoxP3^+$, Figure 4.26 B). In addition, cells of the myeloid lineage infiltrated the tumors in high numbers (Figure 4.26 C). About 40% of all living cells showed a monocytic phenotype ($CD11b^+Ly6C^+$) and roughly 35% of living cells could be identified as MDSCs ($CD11b^+Gr\text{-}1^+$) (87). In the latter population about 10% of the $Gr\text{-}1^+$ cells showed a $Gr\text{-}1^{high}$ ($Ly6C^-Ly6G^+$) phenotype, identifying cells which were described as granulocytic MDSCs (86, 87). Surprisingly, only very small numbers of $CD11b^+F4/80^+$ macrophages could be detected in the tumor tissue (Figure 4.26 C).

These analyses revealed that the tumor tissue is infiltrated by exhausted T cells, regulatory T cells, as well as high numbers of monocytic and granulocytic myeloid cells, but surprisingly few macrophages.

4.4.2 MDSCs inhibit proliferation of p53TCR-transduced T cells *in vitro*

Since most of the tumor-infiltrating cells could be classified as MDSCs (Figure 4.26), their capacity to suppress effector T cell function was analyzed in *in vitro* assays. In brief, peptide-stimulated sc p53TCR-transduced $CD8^+$ T cells were labeled with CFSE and cultured with 5% TCGF and 2µg/ml Con A in the presence of $CD11b^+Gr\text{-}1^{high}$ spleen- or tumor-derived MDSCs isolated from tumor-bearing mice. Proliferation was determined as a surrogate marker for T cell activation and measured by CFSE dilution. Tumor tissue and spleen of tumor-bearing mice accumulated MDSCs upon tumor formation. While tumor progression correlated with the percentage of tumor-infiltrating MDSCs, no such correlation was observed between tumor size and MDSC frequency in the spleen (data not shown). Interestingly, besides an accumulation of

$CD11b^+Gr\text{-}1^+$ cells in the spleen of tumor-bearing mice upon tumor formation a shift in the $Gr\text{-}1^+$ population ($Gr\text{-}1^{low}/Gr\text{-}1^{intermediate}$ → $Gr\text{-}1^{intermediate}/Gr\text{-}1^{high}$) could be observed, when compared to control animals (data not shown). Moreover, MDSC subsets from spleen and tumor tissue were highly efficient in suppressing T cell proliferation at a 1:1 and 2:1 ratio of MDSCs:T cells (Figure 4.27 A and B, respectively). Even low MDSC:T cell ratios (0.2:1) still affect T cell proliferation.

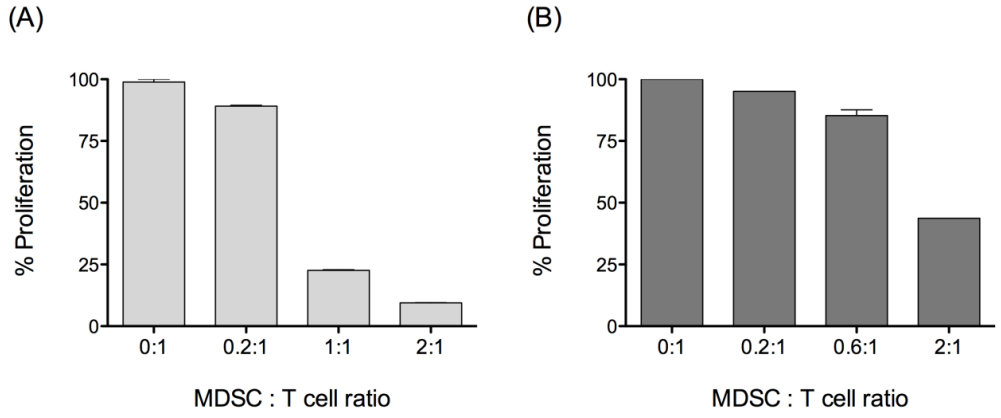

Figure 4.27 T cell proliferation is highly inhibited in the presence of MDSCs.
MDSCs isolated from spleens (A) and tumors (B) from tumor-bearing mice were co-cultured with sc p53TCR transduced T cells. MDSCs were MACS-purified and sorted as described in section 3.4.8 and 3.4.12. CFSE-labeled T cells were co-cultured for 72h with different ratios of MDSCs in presence of 5% TCGF and 2µg/ml Con A. Proliferation at the 0:1 ratio was set to 100%. (A) 1 out of 3 independent experiments with similar results, mean±SEM from duplicates. (B) Experiment with single values except of 0.6:1 ratio, which shows mean±SEM from duplicates.

Preliminary *in vivo* studies indicated, that MDSCs accumulated not only in the tumor, but also in peripheral immune organs during to process of tumor progression. To further confirm these observations, blood of tumor-bearing and tumor-free mice was taken on a weekly basis and analyzed for the frequency of $Gr\text{-}1^+$ cells. We observed a significant increase in the percentage of $Gr\text{-}1^+$ cells in the blood of tumor-bearing mice versus tumor-free animals (Figure 4.28). However, the number of $Gr\text{-}1^+$ cells in the blood did not correlate with tumor size, most likely due to highly variable frequencies of blood MDSCs during tumor progression. Yet, $Gr\text{-}1^+$ cell numbers were increased only in tumor-bearing mice.

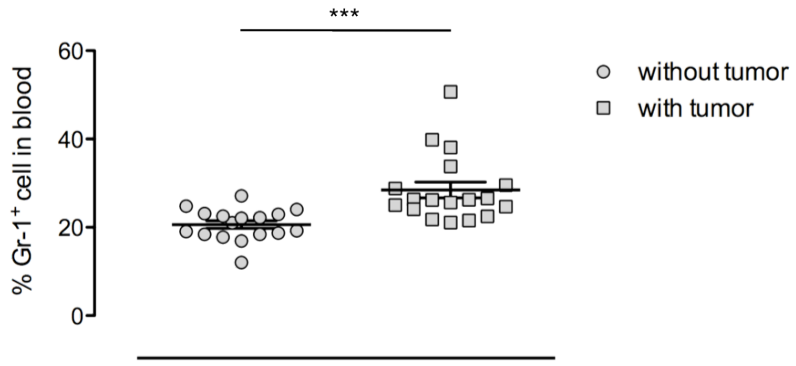

Figure 4.28 The frequency of Gr-1$^+$ cells is significantly increased in tumor-bearing mice.
Blood samples from tumor-bearing (n=18) and tumor-free (n=9) mice were taken on a weekly basis and the frequency of Gr-1$^+$ cells in the blood samples was analyzed by flow cytometry. *** $p<0.001$.

Taken together, these results show that MDSCs play an important role in tumor progression since their accumulation in the blood and spleen correlated with tumor occurrence, but not with tumor size. Moreover, MDSCs from spleen or tumor tissue exhibit a strong suppressive capacity on T cell proliferation.

4.4.3 Depletion of MDSCs *in vivo* increases tumor recognition of sc p53TCR-redirected T cells

In vitro studies indicated that MDSCs play an important role in promoting tumor progression. Since our previous *in vivo* studies already showed that ACT with sc p53TCR-transduced T cells led to delayed tumor growth or partial rejection (chapter 4.3), a combined therapy with depletion of immunosuppressive MDSCs was designed to support the infused T cells in targeting the tumor. Therefore, mice were pre-conditioned with sublethal TBI prior to the s.c. injection of tumor and T cells and peptide vaccination on day 1 after ACT. Additionally, mice were treated with anti-Gr-1 antibodies to deplete granulocytes and monocytes as described below (Figure 4.29). Blood samples were taken on a weekly basis to follow T cell expansion and MDSC depletion. In addition tumor size was measured twice a week.

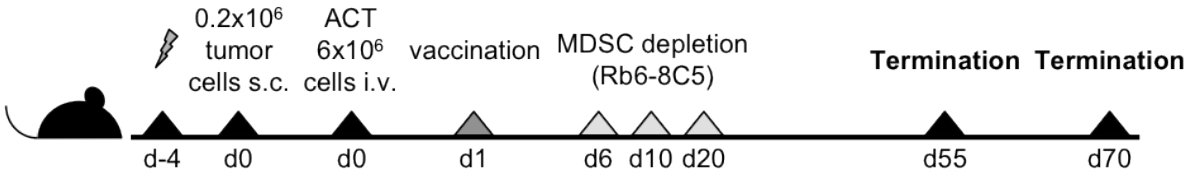

Figure 4.29 Injection scheme for combined therapy of sc p53TCR-transduced T cells and depletion of MDSC, which delayed tumor growth.
HupKi mice were irradiated with a sub-lethal dose of 5.5Gy. Four days later $0.2x10^6$ p53-/-A2K^b MEF mut#7 tumor cells were injected s.c. in the right flank. The same day mice were injected i.v. with $6x10^6$ sc p53TCR or Mock-transduced T cells. On day 1 after tumor and T cell injection mice were anesthetized and received s.c. vaccination with 100µg $p53_{(257-282)}$ peptide and 45µg anti-CD40 plus cutaneous application of 62mg Aldara cream (containing to 3mg imiquimod). All mice received i.p. injections of 150µg anti-Gr-1 antibody (Rb6-8C5) or PBS on days 6, 10 and 20 after tumor and T cell injection. Mice were sacrificed when tumor size reached a volume of 1000-1500mm^3. Termination for PBS-treated control mice was set to day 55, termination for mice receiving anti-Gr-1 treatment was set to day 70 after ACT.

Shortly after application of anti-Gr-1 antibody (day 6 after ACT) the frequency of Gr-1$^+$ cells in the blood decreased massively compared to PBS-treated mice (Figure 4.30).

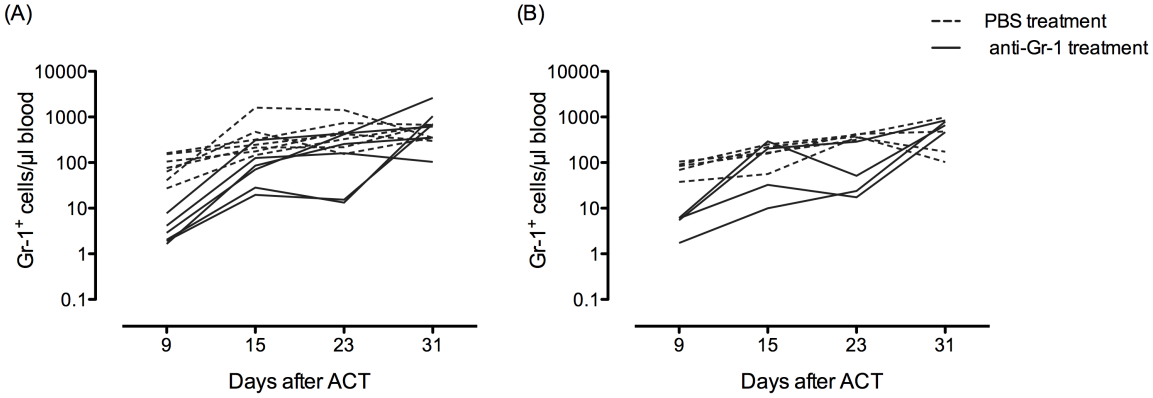

Figure 4.30 Anti-Gr-1 treatment efficiently reduces Gr-1$^+$ cells in peripheral blood.
Mice were treated as described in Figure 4.29. Blood samples were acquired on a weekly basis and analyzed for the frequency of Gr-1$^+$ cells by flow cytometry. Mice were treated with PBS (dashed lines) or anti-Gr-1 antibody (RB6-8C5, solid lines) on days 6, 10 and 20 after ACT. Shown are mice, which received (A) sc p53TCR-transduced T cells (n=13) or (B) Mock-transduced cells (n=9).

Depletion of Gr-1$^+$ cells in the blood lasted for 4 days, thus the second injection of the antibody followed on day 10 after ACT. Accordingly, the level of Gr-1$^+$ cells in the blood was kept at low levels throughout the treatment period (Figure 4.30). Since most mice injected with the antibody experienced severe weight loss after the second injection, the third injection was postponed to day 20 after ACT. By that time some mice already restored their levels of Gr-1$^+$ cells in blood. After the third injection the Gr-1$^+$ levels remained stable or slightly decreased in the blood of treated mice, however, levels were restored to those of PBS-control mice by day 30 after ACT.

In contrast to the previous data, which showed a partial tumor rejection after simultaneous injection of tumor and T cells, no tumor rejection could be observed in the actual experimental setting. Nevertheless, injection of anti-Gr-1 antibody led to a delayed tumor growth in 50% of mice receiving sc p53TCR-transduced T cells (Figure 4.31 A). The reduced kinetic of tumor growth in mice receiving ACT plus anti-Gr-1 treatment allowed an additional delay of outgrowth of up to 20 days. All mice receiving Mock-transduced T cells showed a similar tumor growth kinetic, regardless of the presence or absence of anti-Gr-1 (Figure 4.31 B).

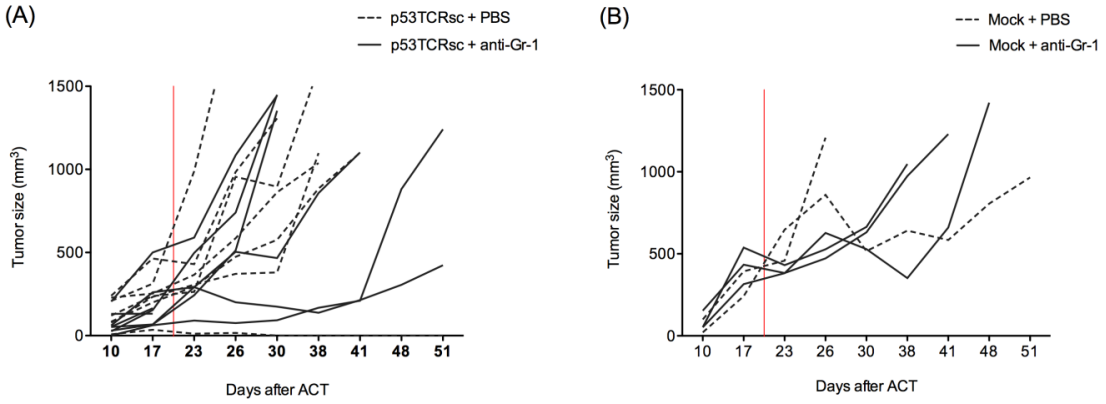

Figure 4.31 Depletion of MDSCs in combination with ACT of the sc p53TCR delays tumor growth.
Tumor length (L) and width (W) was measured with a caliper twice a week. Volume was calculated by the formula LxWxW to get a tumor volume in mm^3. Tumor size was plotted against time and mice were sacrificed when tumor size reaches 1000-1500mm^3. (A) Mice received sc p53TCR-transduced T cells and were treated with anti-Gr-1 antibody (solid lines, n=6) or PBS (dashed lines, n=6). (B) Mice received Mock-transduced T cells and were treated with anti-Gr-1 antibody (solid lines, n=3) or PBS (dashed lines, n=2). The red line indicates the last anti-Gr-1 or PBS treatment (day 20 after ACT).

Ex vivo analysis of growing tumors revealed that all tumors down-regulated HLA-A2 molecules independently of their growth kinetic, therapeutic application of anti-Gr-1 or ACT (Figure 4.32), confirming the data obtained in the previous tumor models (Figure 4.20 and 4.22). Although no tumor rejection could be observed – most likely because of a down-regulation of HLA-A2 – these data suggest that Gr-1 antibody treatment could be useful in combination with transfer of tumor-reactive T cells.

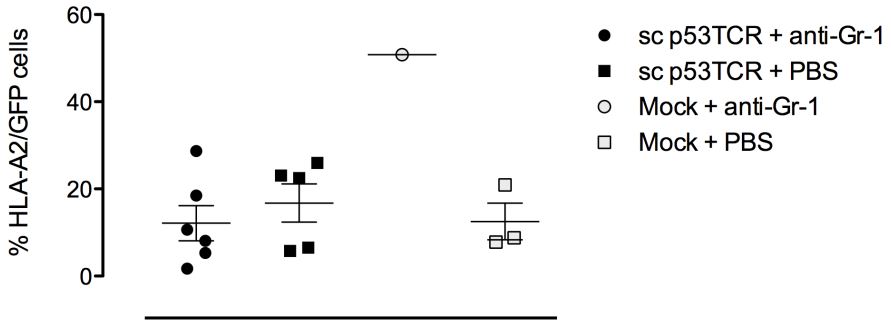

Figure 4.32 Down-regulation of HLA-A2 in tumor cells is independent of the therapeutic approach.
Mice were treated as described in Figure 4.29. Whole tumor homogenates were harvested and subsequently analyzed by flow cytometry for the expression of HLA-A2 on tumor cells. Tumor samples were grouped according to the treatment: ACT with sc p53TCR-transduced T cells plus Gr-1 treatment (solid circles, n=6), ACT with sc p53TCR-transduced T cells plus PBS (solid squares, n=5), ACT with Mock-transduced T cells plus anti-Gr-1 treatment (open circle, n=1) and ACT with Mock-transduced T cells plus PBS (open squares , n=3). Cells were pre-gated on GFP^+ live tumor cells.

To avoid the rough side effects associated with the anti-Gr-1 treatment an alternative approach to deplete MDSCs was tested. As described before, mice were treated with pre-conditioning TBI one day prior to injection of tumor cells and T cells. Mice were vaccinated with p53 peptide, anti-CD40 and Aldara cream one day after ACT. In addition, mice were injected once a week for three weeks with low dose paclitaxel, a chemotherapeutic agent shown to inhibit the function of MDSCs (107).

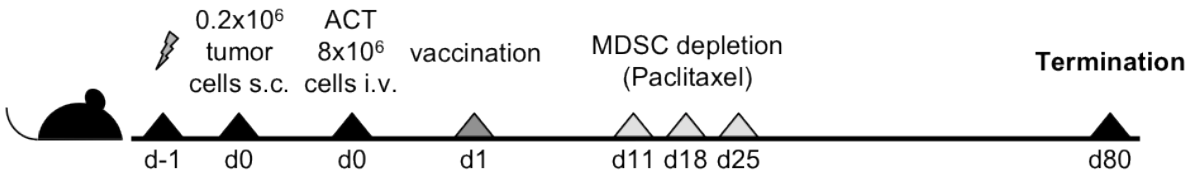

Figure 4.33 Injection scheme of ACT with additional application of low dose paclitaxel to inhibit the function of MDSC.
HupKi mice were irradiated with a sub-lethal dose of 5.5Gy. Four days later $0.2x10^6$ cells of an *ex vivo* tumor (parental cell line: p53-/-$A2K^b$ MEF mut#7) were injected s.c. in the right flank. The same day mice were injected i.v. with $8x10^6$ sc p53TCR or Mock-transduced T cells. On day 1 after tumor and T cell injection mice were anesthetized and received s.c. vaccination with 100µg $p53_{(257-282)}$ peptide and 45µg anti-CD40 plus cutaneous application of 62mg Aldara cream (containing to 3mg imiquimod). All mice received 1mg/kg body weight paclitaxel i.p. on days 11, 18 and 25 after tumor and T cell injection in mice of the sc p53TCR and Mock group. Mice were sacrificed when tumor size reached a volume of 1000-1500mm^3

Mice were examined once a week for weight loss and twice weekly for tumor growth. Paclitaxel treatment did not lead to weight loss as was previously observed with the anti-Gr-1 treatment. Additionally, we and others did not observe a depletion of peripheral $Gr\text{-}1^+$ cells in the blood, since paclitaxel did not deplete MDSCs, but inhibited their function (data not shown and (107)). Unfortunately, further analysis of the injected *ex vivo* tumor cells revealed a contamination with mycoplasma.

Consequently, almost all tumors were rejected as soon as the peripheral immune cells were restored after irradiation, happening around day 20-25 after ACT (see also Figure 4.17), resulting in a dramatically reduced number of tumor-bearing mice that could be analyzed for tumor growth. Nevertheless, paclitaxel treatment showed a clear effect on tumor growth as it delayed growth kinetic (Figure 4.34) compared to previous experiments (Figure 4.20). In this context the injection of sc p53TCR-transduced T cells only showed a minor effect on the growth kinetic in this experiment, since only 1 out of 3 tumors could be controlled. However, due to the above-mentioned experimental drawback, the number of animals was too small to draw a solid conclusion. As expected, all other tumors in both groups grew out during the course of the experiment.

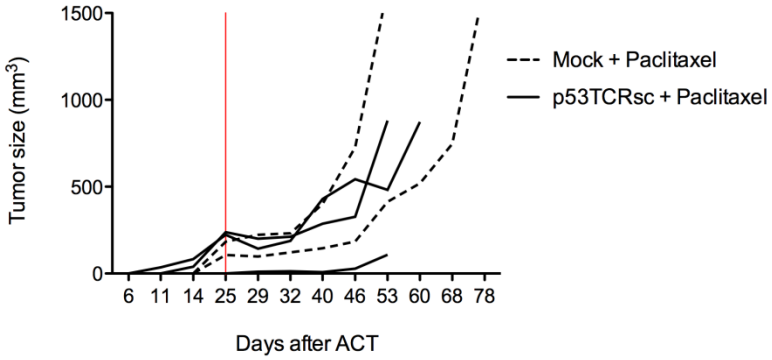

Figure 4.34 Low dose chemotherapy does not show synergistic effects in combination with ACT.
Mice were treated as described in Figure 4.33. Tumor length (L) and width (W) was measured with a caliper twice a week. Volume was calculated by the formula LxWxW to get a tumor volume in mm^3. Tumor size was plotted against time and mice were sacrificed when tumor size reaches 1000-1500mm^3. Mice receiving sc p53TCR-transduced T cells (solid lines, n=3) or Mock-transduced T cells (dashed lines, n=2) and were treated with paclitaxel. Red line indicates last treatment with paclitaxel (day 25 after ACT).

Taken together, this data revealed that tumors were massively infiltrated by cells of the myeloid lineage, which were highly immunosuppressive and inhibited T cell proliferation. Moreover, the performed experiments showed that tumor-infiltrating T cells were either of a suppressive phenotype (regulatory T cells) or expressed proteins (e.g. PD-1), which led to a shutdown of T cell effector function. Therefore, we focused on combined therapeutic approaches, which aimed at improving ACT by targeting suppressive cells in the TME. Both of our approaches of a combined therapy were designed to either deplete or inhibit MDSCs. As such they showed advantages in terms of delayed growth kinetics of the tumors, compared to ACT alone, and can therefore be seen as improvement of existing therapies.

5 Discussion

5.1 Safety of adoptive p53TCR gene transfer

To be able to target a wide range of different tumor entities by adoptive TCR gene therapy, we focused on p53 as universal TAA. Generating a high-affinity TCR targeting a self-peptide also implies the need to overcome self-tolerance, which was achieved by the isolation of a high-affinity p53TCR specific for the human p53 epitope 264-272 from HLA-A*0201 transgenic mice (56). This TCR was modified and further improved to avoid mispairing reactions with endogenous TCR chains. Therefore, to avoid such mispairing reactions, a double chain (dc) p53-specific TCR was generated, which was codon optimized and had an additional disulfide bond between the C domains of the TCR α and β chain. Moreover, a single chain (sc) p53TCR was designed, by connecting the Vα domain of the p53TCR to the TCR β chain via a variable SL7 peptide linker along with codon optimization and the additional disulfide bond between the C domains of α and β chain, similar to the dc p53TCR. However, cells transduced with high-affinity TCRs, such as the p53-specific TCR, which recognize their target antigen presented by an MHC complex in nM range, with a K_d< 1µM, are also thought to lead to loss of function by down-regulation of the TCR, intracellular TCR signaling and the expression of activating tumor necrosis factor receptor (TNFR) superfamiliy members (108). In contrast to the optimized transgenic (tg) TCRs used in this paper, which had sequence substitutions in the CDR2 and/or CDR3 loops to increase TCR-MHC interaction in terms of half-life and affinity, the codon-optimized p53-specific TCRs were altered only on the nucleotide level to enable an improved assembly of amino acids. Besides functionality of the TCRs the question was raised whether p53-specific TCRs are also safe in terms of undesired off-target toxicity. The safety issue was hypothesized by Schumacher and colleagues (47), suggesting that by introducing tg TCRs into T cells, TCR chains of the exogenous (introduced) TCRs might pair with native (endogenous) TCR chains to form mixed TCR heterodimers of unknown specificity. The same group further confirmed this hypothesis by using a mouse model of adoptive TCR gene transfer (103). We analyzed the optimized sc and dc p53-specific TCRs for their potential to generate harmful mixed TCR dimers by pairing endogenous and introduced TCR chains. First *in vitro* functional studies revealed

slightly better frequencies of TCR-positive cells of the dc p53TCR construct following retroviral transduction (Figure 4.2). The surface expression, reflected by the MFI of the different constructs (wt, sc and dc), showed the highest MFI level for the dc p53TCR. Yet, the shift of the MFI from very high values in non-transduced cells to lower values in TCR-transduced cells reflects the varying expression level of the TCR β chain. Moreover, specific cytotoxic activity of transduced cells showed no differences between the various TCR constructs (Figure 4.3). Thus, we could show that the modified TCR constructs were expressed at higher levels on transduced T cells and showed the same functional properties than the wt TCR.

To further address the mispairing potential, we cloned the α and β chain of the optimized dc p53TCR construct each into a separate retroviral GFP-containing vector. Upon transduction of T cells with the p53TCR β chain we could detect high levels of the p53-specific Vβ3 chain and accordingly GFP expression. Since no commercial antibody was available for the Vα chain we could only indirectly conclude the expression of the α chain by the measured GFP signal (Figure 4.4). We observed a more efficient pairing of introduced β chains with endogenous α chains, which could be observed by high surface expression levels of TCR Vβ3 chain after transduction compared to the pairing of introduced α chains and endogenous β chains (GFP expression). In contrast the level of the endogenous Vβ3 TCR chain, which varies depending on the mouse strain between 3-5% of $CD4^+$ and $CD8^+$ T cells, was only slightly increased after retroviral transduction with the p53TCR α chain construct (Figure 4.5). Thus, by introducing a single α or β chain via transduction into the cell, mixed heterodimers can be generated by pairing of introduced and endogenous TCR chains, which is undesirable and can harm the host by leading to GvHD reactions.

As a final proof for the safety of the modified TCRs, we adoptively transferred cells transduced with sc, dc, α chain or β chain constructs into p53-/-$A2K^b$ mice. Prior to T cell transfer mice were lymphodepleted by total body irradiation, since *in vivo* activity and persistence of transferred T cells is enhanced upon depletion of the endogenous T cell pool (109). In this study, de Witte and colleagues showed that non-myeloablative chemotherapy or irradiation promote the outgrowth of infused T cells. By reducing endogenous T cells, cytokines favorable for T cell proliferation are available for the infused T cell populations and in addition endogenous T regulatory cells (T_{regs}) are diminished. Inhibition of T_{reg} function is highly favorable, as they

inhibit the function of (infused) effector T cells and with this dampen the anti-tumoral response.

In our experimental model, mice were treated with high dose of IL-2 after ACT, since data of Shirkant and Bendle showed the feasibility of this therapy to expand and enhance the *in vivo* function of the transferred T cells (103, 110). In our study, mice infused with dc, α or β chain p53TCR developed lethal forms of GvHD, as evidenced by weight loss, decreased mobility and grooming, as well as loss of fur. In contrast, mice infused with sc p53-specific TCR remained GvHD-free. Moreover, we observed a slightly different kinetic and incidence in developing GvHD upon injection of T cells transduced with only the TCR α or β chain, respectively, reflecting the above discussed *in vitro* pairing behavior of the TCR α and β chain. Since severe levels of GvHD and increased mortality were noted in mice injected with the dc p53TCR, α or β chain p53TCR, but not in mice receiving the sc p53TCR, we concluded that GvHD occurred upon formation of mixed TCR dimers *in vivo* and could only be prevented by injection of sc p53TCR-redirected T cells. Indeed, mice developing GvHD showed strong infiltration of $V\beta3^+CD4^+$ and $V\beta3^+CD8^+$ as well as GFP^+CD4^+ and GFP^+CD8^+ T cells in target organs such as spleen, liver, lung and bone marrow. Besides T cell infiltration we could also document destruction of tissue morphology in liver and spleen of GvHD-burdened mice (Figure 4.9 and 4.10).

Similar observations were reported in a study of Bendle and colleagues (103), where C57BL/6J cells transduced with an OT-I-specific TCR induced GvHD as a result of mispaired TCRs, which targeted an unspecific antigen. Moreover, lower doses of IL-2 injection led to a reduced lethality, but mice developed a chronic form of GVHD, which was characterized by colitis, diarrhea and a reduction in lymphocytes in the spleen. Only by modification of the OT-I-specific TCR construct through insertion of an additional disulfide bond between the C domains of the TCR chains and by replacement of the IRES sequence with a 2A element, to connect the TCR α chain with the TCR β chain transgenes in the retroviral construct (similar to the TCR constructs used in our studies), the incidence of lethal GvHD could be significantly reduced from 80% to 14.3%. In concordance with the study of Bendle and colleagues, our results confirmed that TCR mixed dimer formation can lead to GvHD. However, in contrast to the study of Bendle we could show that TCR optimization alone (as for our dc p53TCR) does not prevent GvHD. Therefore, the degree to which genetic modifications of a transgenic TCR are necessary in order to prevent

GvHD is variable and depends on the nature and specificity of each TCR.

Because our mispairing studies showed only the sc p53TCR to be safe in terms of off-target toxicity, all further studies were carried out with this construct. Besides the risk of off-target toxicity, also on-target related toxicity has to be considered when targeting non-mutated TAAs with high-avidity TCRs. On the one hand high-avidity TCRs have been demonstrated in clinical trials to show anti-tumor responses due to increased affinity (favorable on-target effect), but on the other hand bear also the risk for an increased potential to develop on-target/off-tumor toxicity (unfavorable on-target toxicity) (111). In 2011 a clinical trial showed that patients with metastatic melanoma or metastatic synovial cell sarcoma, which were refractory to all standard treatments, could be treated successfully with T cells transduced with a NY-ESO-1-specific TCR, without developing toxicities (112). Only a transient neutropenia and thrombocytopenia could be observed after pretreatment conditions (chemotherapy) and during IL-2 treatment. In contrast to the cancer-testis antigen NY-ESO-1, which is only expressed in cancer cells and adult reproductive tissue, which lacks MHC I expression, p53 is ubiquitously expressed in all tissues. Therefore, the sc p53TCR had to distinguish between healthy and neoplastic cells to efficiently target cancer cells and to avoid destruction of the host tissue. This discrimination between healthy and neoplastic cells is believed to rely on different expression patterns of p53, as it is overexpressed and presented on the cell surface with an extended half-life only in cancer cells but not in healthy tissue (33).

To address the question of on-target toxicity we tested sc p53TCR-transduced T cells in an *in vitro* cytolytic assay for their potential to recognize mouse immortalized embryonic fibroblasts, which express HLA-A2 and human p53 (HupKi MEFs) (Figure 4.11). We did not observe any cytolysis of HupKi MEFs, confirming that no recognition of the cognate antigen (when presented by non-tumor cells) takes place. In addition activated HLA-A2 HupKi T cells transduced with sc p53TCR were not recognized, suggesting that neither highly activated cells with an increased metabolism and therefore an increased expression level of antigens via MHC molecules, nor cells of the same origin, which also express the p53TCR as well as the antigen in the context of HLA-A2 are targeted. These results are strengthened by findings of Leisegang and colleagues (113) describing self-MHC-restricted fratricide of survivin-specific TCRs due to a 10^8-fold increased expression level in activated compared to non-activated PBMCs or enriched $CD8^+$ T cell populations. In contrast

to survivin other TAAs show no (Tyrosinase or NY-ESO-1) or minor increased levels in activated cells in a range roughly around 10 to 100-fold (p53, c-myc or WT-1). This study demonstrated that fratricide might occur when the TAA expression threshold is exceeded, suggesting that on-target reactions directed against p53-associated antigens are unlikely. Encouraged by the lack of on-target toxicity *in vitro*, we set up an experiment similar as the off-target model in HupKi mice. After preconditioning with TBI, injection of sc p53TCR-specific T cells and IL-2 we did not observe any signs of GvHD. Further analysis of target organs revealed no infiltration of $CD4^+V\beta3^+$ or $CD8^+V\beta3^+$T cells. Therefore, we decided to rigorously challenge HupKi mice by injecting high numbers of sc p53TCR-transduced T cells after TBI followed by IL-2 injection (Figure 4.12). There, we observed dramatic body weight loss upon IL-2 injection in concordance with increase of $CD4^+$ and $CD8^+$ cells in the blood (Figure 4.13). Mice receiving Mock-transduced T cells showed stable body weight but also elevated $CD4^+$ and $CD8^+$ blood counts due to the high number of adoptively transferred cells. However, in contrast to the persisting high levels of blood $CD4^+$ and $CD8^+$ cells in mice of the off-target toxicity study (Figure 4.7), HupKi mice of both groups showed a decrease of $CD4^+$ and $CD8^+$ cells in the blood shortly after the IL-2 treatment and normalization of blood cell counts to initial levels already two weeks later (data not shown). The drop in bodyweight in the sc p53TCR group can be explained by the high total number of injected T cells. Moreover, by injecting IL-2 shortly after adoptive transfer, we even expanded the already high T cell numbers. Compared to other mouse studies, the transferred cell density was higher than used elsewhere (103, 114). Overall, we did not observe significant infiltration of $CD4^+V\beta3^+$ and $CD8^+V\beta3^+$ T cells in target organs except for the spleen. Since the spleen is capable to store blood (in case of hemorrhagic shock) as well as lymphocytes, the significant difference in $V\beta3^+$ cells is likely due to the high amount of injected $V\beta3^+$ cells in the sc p53TCR group. Again, in contrast to the tissue destruction and tissue infiltration of $CD4^+$ and $CD8^+$ lymphocytes observed in the off-target study, here we did not detect any signs of GvHD in histology. To finally address on-target toxicity, we adapted an experimental protocol described in the PhD thesis of [redacted] (Leiden University Medical Center, Department for Immunohematology and Blood Transfusion, 2008). In this study, the group generated a high-affinity TCR αβ chain $CD8^+$ CTL clone, which recognized the mouse wt $p53_{(158\text{-}166)}$ epitope in the context of $H\text{-}2K^b$. In this model elimination of the entire hematopoietic system of

p53+/+ mice, resulting in weight loss and mortality, was observed after infusion of splenocytes derived from p53-/- TCR-tg donors combined with peptide vaccination. Expansion of TCR-tg $CD8^+$ T cells after vaccination correlated with the onset of hematopoietic ablation. Moreover, a decline in host B- and T- lymphocytes, erythrocytes, hemoglobin levels and platelets as well as hematopoietic stem cells plus a disturbed anatomy in spleen of host mice was observed. However, no detectable pathology in any of the non-hematopoietic tissues was found, suggesting that toxicity was restricted to the hematopoietic compartment due to higher expression levels of MHC I. Similar to this study, we pre-conditioned mice with chemotherapy (fludarabine and cyclophosphamide), injected sc p53TCR-transduced T cells and subsequently vaccinated the mice with a cocktail of human $p53_{(257\text{-}282)}$ peptide, anti-CD40 and CpG1668. In contrast to the mouse p53 studies of Lauwen, HupKi mice injected with sc p53TCR showed no defect in restoring the hematopoietic compartment after leukodepleting chemotherapy in presence or absence of peptide vaccination (Figure 4.16). Moreover, after ACT plus peptide vaccination, T cells, B cells and cells of the myeloid lineage could be readily detected in peripheral blood. In addition, $V\beta3^+$ cells were detected in the vaccinated as well as non-vaccinated (control) group and showed a similar frequency than the endogenous $V\beta3^+$ cell subset (compare with Figure 4.14, Mock control group). In line with the reconstitution of the hematopoietic compartment HupKi mice showed no elevated levels of infiltrating $CD4^+V\beta3^+$ and $CD8^+V\beta3^+$ cells in target organs, as we observed $V\beta3^+$ cell infiltrations in the range of the endogenous $V\beta3^+$ frequencies (compare with Figure 4.2 Mock plasmid-transduced cells). Importantly, after injection of low numbers ($2.5x10^6$) of sc p53TCR-transduced T cells only low fractions (3-4%) of $V\beta3^+$ infiltrating cells could be detected in the spleen of mice either treated with PBS or peptide vaccination. In contrast, high numbers of injected sc p53TCR-transduced T cells, as demonstrated in the previous 'on-target' experiment, resulted in increased amounts (7-12%) of infiltrating $V\beta3^+$ cells in the spleen (Figure 4.14). Therefore, as discussed, the earlier observed high numbers of infiltrating cells in the spleen most likely reflect the high numbers of initially injected cells. All HupKi mice tested under various *in vivo* conditions remained GvHD-free, demonstrating the absence of on-target toxicity following sc p53TCR-gene transfer.

Targeting of self-antigens with high affinity TCRs can potentially result in on-target toxicity as shown in a study by Bos and colleagues (114). In contrast to our findings

they observed severe on-target toxicity in a carcinoembryonic antigen (CAE)-tg mouse model. CAE is widely known as TAA for colorectal cancers, but is also expressed on healthy tissue. Bos and colleagues observed severe forms of colitis simultaneously to the anti-tumor response in mice after sub-lethal or lethal TBI plus bone marrow transplantation and adoptive T cell transfer. Importantly, severe risks of potential on-target toxicity were also observed in clinical trials. Morgan and colleagues initially isolated an anti-MART-1 TCR from a melanoma patient (38), which showed no on-/ or off-target toxicities, but at the same time only a poor clinical response rate of 16% of tumor patients. In a second approach Morgan and colleagues isolated an anti-MART-1 TCR from fresh melanoma tumors (111), which showed higher avidity and affinity, yet recognizing the same peptide epitope as the first anti-MART-1 TCR. As expected, the second isolated TCR showed a higher response rate of 30%, however, severe on-target reactions such as skin rashes and eye and ear toxicity were observed shortly after ACT. Although skin rashes dropped off during the course of the trial, some patients showed only partial remission of their hearing loss.

Together, our studies confirmed the safety in terms of off- and on-target toxicity of adoptive sc p53-specific TCR gene transfer into HLA-A2-tg mice, since no unspecific or specific tissue destruction was observed after infusing redirected T cells.

5.2 Efficiency of adoptive p53TCR gene transfer

Earlier studies already showed the feasibility and therapeutic benefit of adoptive transfer of T cells in tumor patients. Studies using transfer of *ex vivo* tumor-infiltrating lymphocytes (TILs) in melanoma patients mediated complete or partial cancer regression (115). However, this therapeutic approach is limited by the fact that patients (i) need to have tumor-infiltrating T cells, which can be isolated from tumor tissue and (ii) need to have TILs, which can be expanded *ex vivo* and in addition are highly tumor-reactive. Such limitations are especially restricted to cancers other than melanoma, where it is more difficult to identify and extract TILs. To overcome these limitations, we and others use TCR gene transfer, which aims to transfer immune reactivity towards defined TAA-bearing cancer cells, to which the endogenous T cell repertoire responds only weakly or is even non-responsive. By transferring a defined single specificity to T cells we can spare time-consuming tests of the redirected T

cells for their tumor killing capacity prior to reinfusion. Moreover, by redirecting high numbers of T cells at the same time, we reduce the time necessary for T cell expansion in *ex-vivo* culture, which is an important safety aspect with regard to clonal expansion and/or differentiation during *in vitro* culture. As already known, mutations of p53 can account for the development of cancer, thus peptides encoding for the mutated p53 sequence are favorable tumor-specific antigens. However, p53 mutations are highly divers in cancers and thereby limit their use as universal antigens. Therefore, to be able to target a wide range of different tumor entities harboring a p53 mutation, we used a p53-specific TCR recognizing the human p53 epitope 264-272, which is located in a conserved region of the DNA-binding domain of the p53 protein, where no mutation was described so far.

We could already show that our sc p53TCR-redirected T cells recognize and lyse different MEF tumor cell lines *ex vivo* in cytolytic assays (Figure 4.3 and Figure 4.11). Therefore, we translated this approach into a mouse model by injecting HupKi CyA2K^b mice with mutant p53-expressing MEF tumor cell lines one week prior to sub-lethal TBI followed by ACT with sc p53TCR-transduced T cells and vaccination with $p53_{(257\text{-}282)}$ peptide, Aldara cream and anti-CD40. We injected a bulk population of mainly p53-TCR$^+$ CD4$^+$ and CD8$^+$ naïve T cells into engrafted mice, to minimize the already mentioned drawbacks of T cell *in vitro* culture. Although we injected $3x10^6$ effective T cells, we detected a growing tumor in all mice. Yet, mice injected with sc p53TCR-transduced T cells showed a delayed tumor outgrowth and extended survival as compared to control animals injected with Mock-transduced T cells (Figure 4.19 and 4.20). Moreover, changing the protocol to injection of tumor and T cells at the same time (Figure 4.21), we could show that even 50% of mice receiving sc p53TCR-redirected T cells controlled the tumor (Figure 4.22), demonstrating that transduced T cells are also able to target tumors *in vivo*. Although we observed tumor recognition in 50% of the tested mice, the remaining other 50% of mice receiving sc p53TCR-redirected T cells showed unimpaired tumor growth. We could show that tumors, which escaped the T cell control, showed a dramatic down-regulation of HLA-A2 expression (Figure 4.23 and Figure 4.24, d0 after isolation), which was restored *in vitro* after tumor resection. The down-regulation of MHC molecules is a common tumor-immune escape mechanism and can originate from mutations in the MHC genes, abnormalities in their regulation or defects in MHC-dependent antigen processing. Moreover, there are different forms or phenotypes of

MHC class I down-regulation, which were identified by screening malignant lesions, including (i) total loss or down-regulation, (ii) selective loss of an haplotype, (iii) selective down-regulation of a gene locus, (iv) selective loss or down-regulation of alleles or (v) a complex phenotype combining (i)-(iv). The frequency of HLA down-regulation depends on the tumor type and also on the kind of lesion (primary or metastatic) (116). However, the reason for down-regulation of HLA-A2 in our tumor model is not fully understood. Yet, a possible explanation could be a selection pressure induced by invading immune cells, since we observed restoration of HLA-A2 in *ex vivo* cultures and upon treatment with IFN-γ (data not shown). Most likely the number of infiltrating activated T cells in the tumor tissue was insufficient to lead to a significant amount of released IFN-γ necessary to up-regulate HLA-A2 *in vivo*. Indeed, we could observe less infiltrating T cells in outgrowing tumors exhibiting HLA-A2 down-regulation (data not shown). In addition to HLA-A2 down-regulation we observed a process of antigen loss or outgrowth of antigen-negative subpopulations among the tumor cells, leading to diminished tumor recognition by infused redirected T cells. Initially, the p53-/- MEF cells were immortalized and stably transduced with a retroviral vector containing a GFP gene and the mouse wt p53 containing the human p53 epitope 264-272 and, in addition, a point mutation (270 Arg→Cys) in the mouse p53 gene. Interestingly, we observed antigen loss or an *in vivo* outgrowth of p53-/- MEF subpopulations in some of the isolated *ex vivo* tumors, which showed a reduced GFP and intracellular p53 expression in immunofluorescence analysis after extraction (Figure 4.25). Thus, tumor samples derived from outgrowing tumors were initially under immune-selective pressure of the injected p53-specific T cells. It has been shown that antigen loss or decrease in antigen expression is a primary sign for tumor immune escape. Jensen and colleagues observed in their ACT mouse model, that recurrent melanomas showed depigmentation, which was a clear sign for decreased expression of gp100, a protein, which is important for melanosome biogenesis, and which is often used as TAA (117). The recurrent depigmented tumors were able to grow out since the injected pmel-specific T cells targeted gp100-positive tumor cells but could not kill antigen loss variants. As a final proof for the phenomenon of antigen loss, those depigmented and outgrowing tumors were tested negative for gp100.

To further analyze tumor tissue, including the TME, for escape mechanisms other than down-regulation of HLA-A2 and antigen loss, which is directly mediated by the

tumor cells, we performed flow cytometric analysis of whole tumor samples (Figure 26). As already described, tumors are able to generate an immunosuppressive microenvironment by attracting macrophages, myeloid-derived suppressor cells (MDSCs) and stromal cells. Our main focus was directed towards infiltrating T cells and MDSCs. Although we could detect p53 TCR^+ cells in the blood and within the tumor tissue of mice shortly after adoptive transfer, tumor growth was not impaired. T cell subset analysis revealed a frequency of infiltrating $CD4^+$ and $CD8^+$ T cells of roughly 10% of all living cells in the tumor homogenate. However, within those 10% of $CD4^+$ cells around 20% had a T_{reg} phenotype ($CD4^+CD25^{hi}FoxP3^+$) and another 40% expressed the T cell exhaustion marker PD-1. In addition, the infiltrating $CD8^+$ population showed even higher percentages of PD-1^+ cells. Moreover, even though the initial bulk T cell population contained 20-30% TCR^+CD4^+ and TCR^+CD8^+ T cells at the time of adoptive transfer, we could hardly detect such levels of TCR expression in the TILs. During the course of the experiment, especially at the time of reconstitution, the number of TCRV$\beta3^+$ T cells in the blood of mice injected with sc p53TCR adapted to the endogenous level of TCRV$\beta3^+$ and, therefore, were similar to Mock-control mice. Thus, discrimination between endogenous TCRV$\beta3^+$ expressing cells and infused TCRV$\beta3^+$ cells was difficult at a late time point. However, we observed about 6-10% $V\beta3^+CD4^+$ and $V\beta3^+CD8^+$ TILs in tumor tissue, which retained their HLA-A2 expression and were injected with sc p53TCR T cells, compared to 3-5% $V\beta3^+CD4^+$ and $V\beta3^+CD8^+$ TILs in tumors of control animals. In contrast, tumors with a down-regulated HLA-A2 expression were hardly infiltrated by TILs and in addition, those TILs showed a highly reduced TCRVβ3 expression of 1-2% only. These results indicated that in either case the p53TCR is down-regulated in TILs and even stronger, when the tumors showed additional escape mechanisms.

It has been shown that the process of T cell activation induces expression of co-inhibitory receptors, i.e. activated T cells express PD-1. However, a high and lasting level of PD-1 expression on T cells (induced by cytokines like IFN-γ and IL-4) leads to a feedback loop that down-modulates effector responses of the T cells to prevent further (uncontrolled) immune-mediated tissue damage. Upon binding of the ligand PD-L1 or PD-L2, expressed on APCs or in this case on tumor cells, the PD-1 molecule on T cells will be phosphorylated, leading to de-phosphorylation of TCR-proximal signaling molecules including ZAP70, PKCθ and CD3ζ, resulting in the shut down of TCR function (118). These facts are in concordance with our observation of

increased levels of PD-1 expression on TILs and along with a diminished TCR expression, which together clearly points to a shut-down of T cell function in the TME, although one more necessary proof by staining PD-L1 or PD-L2 on tumor cells is still missing. This in turn might explain the poor anti-tumor response even though we could detect T cells in the tumor homogenates. It has been shown that PD-1 is expressed at higher levels in $CD4^+$ and $CD8^+$ T cells in patients with chronic lymphocytic leukemia. Leukemic lymphocytes also expressed high amounts of PD-L1 and it could be shown that PD-1 blockage with soluble PD-L1 could restore T cell functions in the chronic lymphocytic leukemia microenvironment *in vitro* (119). Successful targeting of PD-L1-expressing tumor cells in combination with ACT has also been shown in a mouse melanoma model (120). In addition to the expression of inhibitory molecules like PD-1 we could also show that a prominent population of T_{reg} cells can be found among the $CD4^+$ tumor-infiltrating T cells. Already more than 10 years ago Peng and colleagues could show that ACT can fail, when suppressive cells such as tumor-induced T_{reg} cells are co-transferred into tumor bearing mice (121). In addition, Curtis and colleagues showed similar results for a glioblastoma model (122). Moreover, it could also be demonstrated that T_{reg} cells infiltrate predominantly at the tumor site to carry out their suppressive capacity and that local depletion of $CD4^+$ cells in the tumor to diminish T_{reg} cells led to tumor eradication also at later stages (123).

We found a massive level of $CD11b^+$ myeloid cells in the TME (Figure 4.26 C). Most of the detected $CD11b^+$ cells were also positive for Ly6C or Gr-1, the latter being a combination of Ly6C and Ly6G epitopes. Both populations ($CD11b^+Ly6C^+$ and $CD11b^+Gr\text{-}1^{high}$) are described as MDSCs, whereas there is a strict separation between $CD11b^+Ly6C^+$ ($CD11b^+Gr\text{-}1^{low}$) monocytic MDSCs and $CD11b^+Gr\text{-}1^{high}$ ($CD11b^+Ly6C^-Ly6G^+$) granulocytic MDSCs. We found slightly higher numbers of monocytic MDSCs compared to granulocytic MDSC at the tumor site in our mouse model. MDSC are defined according to their co-expression of myeloid cell markers CD11b and Gr-1 associated with the functional ability to inhibit T cell activation. Yet, it is still not clear which of the two MDSC sub-populations is the more suppressive and therefore indispensible for the immunosuppressive character of MDSCs as a whole (87). In addition to the massive infiltration of MDSC in the tumor we could also observe a shift in the $Gr\text{-}1^+$ population in the spleen of tumor bearing mice (data not shown). We detected a shift from $Gr\text{-}1^{low/intermediate}$ towards $Gr\text{-}1^{intermediate/high}$ as soon

as the tumor was palpable, suggesting that these cells are pre-conditioned already before migrating to the tumor site. Accumulation of increased numbers of MDSCs in spleen and lymph nodes under pathological conditions was also described for other tumor models (124). Finally, we also checked for the co-expression of the myeloid marker F4/80 in $CD11b^+(Gr\text{-}1^-)$ populations to determine the amount of macrophages or MDSCs, which arise from $CD11b^+Gr\text{-}1^+$ cells but retain their suppressive character, respectively (125). In contrast to our assumption to find also high amounts of tumor-associated macrophages (TAM) in the TME, we could hardly detect any $CD11b^+F4/80^+$ population. The appearance of macrophages in the TME can vary, depending on the type of cancer. In an orthotopic syngeneic mouse model of colon cancer Kruse and colleagues could show that macrophages play an important role in tumor growth and metastasis formation (126). In their study, they observed massive infiltration of $F4/80^+$ macrophages in tumor tissue, with the highest density in the center and in the invasive front of the tumor. They could show that depletion of macrophages not only decreased tumor growth and metastasis, but also decreased vascular density within the tumor tissue. TAMs are also playing a role in human cancer patients. Pantano and colleagues could show that 50% of the tumor-resected gastric cancer patients with a M1/M2 ratio – ratio of M1 macrophages to M2 macrophages – above the median showed prolonged median overall survival compared to patients below the median (127). However, since we observed only a minor fraction of a $CD11b^+F4/80^+$ population, we further focused on the role of MDSCs in our tumor model. To finally proof that MDSCs in spleen and tumor of tumor-bearing mice show an inhibitory phenotype, we sorted the $CD11b^+Gr\text{-}1^{intermediate/high}$ population out of spleen and tumor tissue and analyzed their immunosuppressive capacity in co-culture with p53-specific T cells stimulated with ConA. We did not distinguish between monocytic and granulocytic MDSCs, since both subsets are in principle highly capable to inhibit T cell activation (87). We could show that MDSCs sorted from spleens or tumors of tumor-bearing mice can efficiently suppress proliferation of p53-specific $CD8^+$ T cells (Figure 4.27). Moreover, by analyzing the blood of tumor-bearing mice and comparing the frequency of $Gr\text{-}1^+$ cells with that found in tumor-free mice, we saw a highly significant increase of $Gr\text{-}1^+$ cells in the blood of tumor-bearing mice (Figure 4.28). Similar results of increased MDSC levels in blood were found in other mouse tumor models (128) as well as in

cancer patients (summarized in (129)). Therefore, Gr-1$^+$ cell levels in blood could be used as predictive marker for a developing tumor.

Taken together, our findings reveal various and per se very potent immune escape mechanisms to efficiently prevent an anti-tumor immune response by our p53-specific T cells. Besides outgrowth of a p53-negative sub-population in a fraction of tumor cells and down-regulation of HLA-A2, we could detect high numbers of tumor-infiltrating immunosuppressive MDSCs, T_{regs} and an up-regulation of inhibitory molecules such as PD-1 on tumor-infiltrating T cells, which altogether limits an effective anti-tumor response.

Although we could detect high numbers of T_{reg} cells in the TME, we decided to focus on MDSCs for a combined therapeutic approach, to effectively target tumor cells, since targeting T_{regs} is more unspecific than targeting MDSCs. Depletion of T_{reg} cells is usually achieved by using anti-CD25 antibodies. However, depletion has been shown to be a sensitive process, which only leads to tumor regression when performed in a short time window after tumor emergence (121, 122). Moreover, since we perform ACT experiments and infuse activated transduced T cells, we would also target infused T cells because of their elevated expression of CD25.

By additional targeting of MDSCs we planned to increase the anti-tumor effect of p53TCR-redirected T cells. Therefore, as a combined therapeutic approach, we depleted monocytic and granulocytic MDSCs systemically using an anti-Gr-1 antibody (clone RB6-8C5). The antibody was efficiently reducing Gr-1$^+$ cells in the blood of treated animals up to 30-fold decreased levels (Figure 4.30 A), however, we noticed only a weak anti-tumor response, since only 1/3 of mice treated with p53TCR-transduced T cells plus anti-Gr-1 treatment showed transient tumor control (Figure 4.31 A). In contrast, mice receiving Mock-transduced T cells did not show any improvement in terms of tumor control when receiving anti-Gr-1 antibody (Figure 4.31 B). These data suggest that the combined therapy principally worked, as shown by a partially delayed outgrowth of tumors. However, we could show that all tumors down-regulated HLA-A2, therefore, the injected sc p53-transduced T cells were only partially able to target the tumors. Assuming a scenario where the tumors would keep a sufficient HLA-A2 expression on their surface, the combination of specific T cells and anti-Gr-1 treatment likely would lead to tumor rejection instead of just a delayed outgrowth. Importantly, we did not observe an effect of the antibody in Mock-treated animals. Therefore, we can conclude that an anti-tumor effect can only be achieved

by combining both therapeutic approaches (antibody and specific T cells). Indeed, the efficiency of the anti-Gr-1 antibody in a mouse tumor model has been reported before. Srivastava and colleagues observed complete tumor control or even tumor rejection after applying anti-Gr-1 antibody without additional ACT (130). However, they treated the mice with 200µg anti-Gr-1 antibody every other day during the experiment until termination. This approach is not very likely to be translated into the clinic, since costs, patient handling and application would hardly be manageable. Moreover, our approach of treating the mice in a very early stage of tumor growth for three to four times, to open a time window for the injected T cells to reach and eliminate the tumor, is much more feasible in terms of costs and application. So far, there is no antibody available to deplete MDSCs in humans, since human MDSCs have different subset markers other than the Gr-1 (Ly6C/Ly6G) in mice. Therefore, other strategies were developed such as (i) to promote differentiation of MDSCs into mature, non-suppressive cells (all-trans retinoic acid, vitamin D), (ii) to reduce MDSC levels in the periphery (sunitinib, gemcitabine, 5-FU, CDDO-Me) and (iii) to inhibit the function of MDSCs (PDE-5 inhibitors, cyclooxygenase 2 inhibitors). The different therapeutic strategies are summarized in Table 5.1.

Table 5.1 Targeting regulatory immune cells to improve immunotherapy
Data adapted from James H Finke, PhD, Cleveland Clinic, as presented at the 25th Anniversary Meeting of the Society for Immunotherapy of Cancer, 2010

Agents	Mode of Action
Triterpenoids (CDD0-Me)	Antioxidant, reduced ROS
Phosphodiesterase-5 (Sildanefil)	Reduces arginase 1 & NOS-2 expression
All-Trans retinoic Acid	MDSC differentiation (increased glutathione synthetase and reduced ROS)
Vitamin D3 (Bioactive metabolite)	Promotes differentiation
Gemcitabine & Cyclophosphamide	Chemotherapeutic drug
Sunitinib	TKI (blocks proliferation of monocytic MDSC and causes apoptosis of neutrophilic MDSCs)

To apply a therapeutic approach, which is more close to a clinical application, we also used low dose chemotherapeutic agents to inhibit the function of MDSCs in a combined therapy with ACT. Just recently such an approach has been published by Sevko and colleagues (107). In this study the authors used the ret tg mouse model,

which spontaneously develops skin melanoma with metastases in lymph nodes, bone marrow, liver and lung. They could show that ultralow non-cytotoxic doses of paclitaxel breaks down p38 MAPK activation in MDSCs resulting in reduced MDSC frequency in tumor lesions, without altering the MDSC levels in the blood, lymph nodes and bone marrow. On top they could show a reduced NO production, leading to restored T cell function and prolonged cell survival. We adapted the protocol of this study and combined the ultralow-dose paclitaxel treatment with our ACT approach. Therefore, we irradiated mice prior to tumor cell injection and transferred sc p53TCR-transduced T cells. One day after injection we used a vaccination protocol to boost infused T cells and initiated paclitaxel treatment when mice developed palpable tumors (Figure 4.33).

We could show that paclitaxel treatment delayed tumor outgrowth, however, *ex vivo* analysis showed evidence that the injected tumor cells were contaminated with mycoplasma. We could observe that almost all engrafted tumors were rejected by the restored host innate immune system due to recognition of mycoplasma-contaminated tumors. Thus, a final conclusion about the efficacy of our therapeutic approach cannot be drawn, since the number of remaining tumor-engrafted animals was too small. In addition, we did not observe any differences between mice injected with Mock-transduced or sc p53TCR-transduced T cells, respectively (Figure 4.34). Ultimately, we can only refer to our observation of a prolonged time of tumor control with the help of paclitaxel and ACT compared to earlier experiments.

Altogether, we could demonstrate that tumors use different escape strategies to circumvent an antitumor response mediated by adoptively transferred TCR-redirected T cells. In our studies especially MDSCs in the TME accounted for failure of tumor eradication through their potent immunosuppressive properties. Depletion or inhibition of MDSCs has been shown to be a promising approach when combined with ACT.

5.3 Conclusion

Adoptive TCR gene transfer is a feasible approach to target solid tumors. However, the safety issue of TCR gene transfer came to the center of attention within the last decade. Preventing off- and on-target toxicity, which can lead to GvHD or death of the host, is therefore indispensible when performing ACT experiments with TCR-redirected T cells targeting TAAs.

In this study we could show that off-target toxicity does not occur when using a codon optimized high-affinity p53-specific sc TCR with an additional disulfide bond between the TCR chain C domains. Importantly, we could also demonstrate the absence of on-target toxicity by using a relevant pre-clinical mouse model of TCR-gene transfer.

Nevertheless, adoptive TCR gene transfer alone turned out to be not sufficient to overcome tumor burden, but led only to a delayed tumor growth instead of the favorable tumor eradication. To improve the tumor reactivity *in vivo* we used pre-conditioning regimens like sub-lethal TBI or chemotherapy, followed by specific peptide vaccination or IL-2 administration, and could observe that this was undoubtedly necessary to pave the way for expansion of functional redirected T cells. In addition, we could demonstrate that highly suppressive cells, predominantly cells of the myeloid lineage, determine the TME, leading to an inhibition of the anti-tumor response by infused redirected T cells. Therefore, using combined therapeutic approaches such as adoptive TCR gene transfer together with depletion or inhibition of suppressive cell subsets in the TME, demonstrated to be a feasible approach in terms of applicability and therapeutic outcome – not only in our but also in other studies performed so far. Conclusively, using multiple therapeutic approaches to target tumors and their environment on a tumor-specific level will lead to a more effective strategy to cure cancer patients.

6 Bibliography

1. Coley WB. 1891. II. Contribution to the Knowledge of Sarcoma. *Annals of surgery* 14: 199-220
2. Sylvester RJ. 2011. Bacillus Calmette-Guerin treatment of non-muscle invasive bladder cancer. *International journal of urology : official journal of the Japanese Urological Association* 18: 113-20
3. Herr HW, Schwalb DM, Zhang ZF, Sogani PC, Fair WR, Whitmore WF, Jr., Oettgen HF. 1995. Intravesical bacillus Calmette-Guerin therapy prevents tumor progression and death from superficial bladder cancer: ten-year follow-up of a prospective randomized trial. *Journal of clinical oncology : official journal of the American Society of Clinical Oncology* 13: 1404-8
4. Thomas ED, Lochte HL, Jr., Lu WC, Ferrebee JW. 1957. Intravenous infusion of bone marrow in patients receiving radiation and chemotherapy. *The New England journal of medicine* 257: 491-6
5. Nahta R, Esteva FJ. 2006. Herceptin: mechanisms of action and resistance. *Cancer letters* 232: 123-38
6. Aggarwal S, Pittenger MF. 2005. Human mesenchymal stem cells modulate allogeneic immune cell responses. *Blood* 105: 1815-22
7. June CH. 2007. Principles of adoptive T cell cancer therapy. *The Journal of clinical investigation* 117: 1204-12
8. Kantoff PW, Higano CS, Shore ND, Berger ER, Small EJ, Penson DF, Redfern CH, Ferrari AC, Dreicer R, Sims RB, Xu Y, Frohlich MW, Schellhammer PF. 2010. Sipuleucel-T immunotherapy for castration-resistant prostate cancer. *The New England journal of medicine* 363: 411-22
9. Kenter GG, Welters MJ, Valentijn AR, Lowik MJ, Berends-van der Meer DM, Vloon AP, Essahsah F, Fathers LM, Offringa R, Drijfhout JW, Wafelman AR, Oostendorp J, Fleuren GJ, van der Burg SH, Melief CJ. 2009. Vaccination against HPV-16 oncoproteins for vulvar intraepithelial neoplasia. *The New England journal of medicine* 361: 1838-47
10. Voo KS, Bover L, Harline ML, Vien LT, Facchinetti V, Arima K, Kwak LW, Liu YJ. 2013. Antibodies targeting human OX40 expand effector T cells and block inducible and natural regulatory T cell function. *Journal of immunology* 191: 3641-50
11. Schwartzentruber DJ, Lawson DH, Richards JM, Conry RM, Miller DM, Treisman J, Gailani F, Riley L, Conlon K, Pockaj B, Kendra KL, White RL, Gonzalez R, Kuzel TM, Curti B, Leming PD, Whitman ED, Balkissoon J, Reintgen DS, Kaufman H, Marincola FM, Merino MJ, Rosenberg SA, Choyke

P, Vena D, Hwu P. 2011. gp100 peptide vaccine and interleukin-2 in patients with advanced melanoma. *The New England journal of medicine* 364: 2119-27

12. Rosenberg SA, Packard BS, Aebersold PM, Solomon D, Topalian SL, Toy ST, Simon P, Lotze MT, Yang JC, Seipp CA, et al. 1988. Use of tumor-infiltrating lymphocytes and interleukin-2 in the immunotherapy of patients with metastatic melanoma. A preliminary report. *The New England journal of medicine* 319: 1676-80
13. Rosenberg SA, Yang JC, Sherry RM, Kammula US, Hughes MS, Phan GQ, Citrin DE, Restifo NP, Robbins PF, Wunderlich JR, Morton KE, Laurencot CM, Steinberg SM, White DE, Dudley ME. 2011. Durable complete responses in heavily pretreated patients with metastatic melanoma using T-cell transfer immunotherapy. *Clinical cancer research : an official journal of the American Association for Cancer Research* 17: 4550-7
14. Murphy MM TP, Walport M. 2008. *Janeway's Immunobiology*: Taylor & Francis; 7th Revised edition (REV)
15. Su D, Shen M, Li X, Sun L. 2013. Roles of gammadelta T cells in the pathogenesis of autoimmune diseases. *Clinical & developmental immunology* 2013: 985753
16. Kufe DW PR, Weichselbaum RR, et al., editors. 2003. *Holland-Frei Cancer Medicine, 6th edition*. Hamilton (ON): BC Decker
17. Karan D, Johansson SL, Lin MF, Batra SK. 2001. Expression of tumor-associated glycoprotein-72 (TAG-72) antigen in human prostatic adenocarcinomas. *Oncology reports* 8: 1123-6
18. Li F, Song D, Lu Y, Zhu H, Chen Z, He X. 2013. Delayed-type hypersensitivity (DTH) immune response related with EBV-DNA in nasopharyngeal carcinoma treated with autologous dendritic cell vaccination after radiotherapy. *Journal of immunotherapy* 36: 208-14
19. Breitburd F, Coursaget P. 1999. Human papillomavirus vaccines. *Seminars in cancer biology* 9: 431-44
20. Gjerstorff MF, Pohl M, Olsen KE, Ditzel HJ. 2013. Analysis of GAGE, NY-ESO-1 and SP17 cancer/testis antigen expression in early stage non-small cell lung carcinoma. *BMC cancer* 13: 466
21. Coulie PG, Brichard V, Van Pel A, Wolfel T, Schneider J, Traversari C, Mattei S, De Plaen E, Lurquin C, Szikora JP, Renauld JC, Boon T. 1994. A new gene coding for a differentiation antigen recognized by autologous cytolytic T lymphocytes on HLA-A2 melanomas. *The Journal of experimental medicine* 180: 35-42
22. Brichard V, Van Pel A, Wolfel T, Wolfel C, De Plaen E, Lethe B, Coulie P, Boon T. 1993. The tyrosinase gene codes for an antigen recognized by

autologous cytolytic T lymphocytes on HLA-A2 melanomas. *The Journal of experimental medicine* 178: 489-95

23. Ghosh SK, Pantazopoulos P, Medarova Z, Moore A. 2013. Expression of underglycosylated MUC1 antigen in cancerous and adjacent normal breast tissues. *Clinical breast cancer* 13: 109-18
24. Reddy SA, Okada C, Wong C, Bahler D, Levy R. 2001. T cell antigen receptor vaccines for active therapy of T cell malignancies. *Annals of the New York Academy of Sciences* 941: 97-105
25. DeLeo AB. 1998. p53-based immunotherapy of cancer. *Critical reviews in immunology* 18: 29-35
26. Nikiforova MN, Lynch RA, Biddinger PW, Alexander EK, Dorn GW, 2nd, Tallini G, Kroll TG, Nikiforov YE. 2003. RAS point mutations and PAX8-PPAR gamma rearrangement in thyroid tumors: evidence for distinct molecular pathways in thyroid follicular carcinoma. *The Journal of clinical endocrinology and metabolism* 88: 2318-26
27. Aqui NA, Vonderheide RH. 2008. Survivin as a universal tumor antigen for novel cancer immunotherapy: functions of a killer clone. *Cancer biology & therapy* 7: 1888-9
28. Mayr C, Bund D, Schlee M, Bamberger M, Kofler DM, Hallek M, Wendtner CM. 2006. MDM2 is recognized as a tumor-associated antigen in chronic lymphocytic leukemia by CD8+ autologous T lymphocytes. *Experimental hematology* 34: 44-53
29. Alarcon-Vargas D, Ronai Z. 2002. p53-Mdm2--the affair that never ends. *Carcinogenesis* 23: 541-7
30. Levine AJ. 1997. p53, the cellular gatekeeper for growth and division. *Cell* 88: 323-31
31. Wu L, Levine AJ. 1997. Differential regulation of the p21/WAF-1 and mdm2 genes after high-dose UV irradiation: p53-dependent and p53-independent regulation of the mdm2 gene. *Molecular medicine* 3: 441-51
32. Theobald M, Ruppert T, Kuckelkorn U, Hernandez J, Haussler A, Ferreira EA, Liewer U, Biggs J, Levine AJ, Huber C, Koszinowski UH, Kloetzel PM, Sherman LA. 1998. The sequence alteration associated with a mutational hotspot in p53 protects cells from lysis by cytotoxic T lymphocytes specific for a flanking peptide epitope. *The Journal of experimental medicine* 188: 1017-28
33. Wiech M, Olszewski MB, Tracz-Gaszewska Z, Wawrzynow B, Zylicz M, Zylicz A. 2012. Molecular mechanism of mutant p53 stabilization: the role of HSP70 and MDM2. *PLoS One* 7: e51426

34. Dembic Z, Haas W, Weiss S, McCubrey J, Kiefer H, von Boehmer H, Steinmetz M. 1986. Transfer of specificity by murine alpha and beta T-cell receptor genes. *Nature* 320: 232-8
35. Clay TM, Custer MC, Sachs J, Hwu P, Rosenberg SA, Nishimura MI. 1999. Efficient transfer of a tumor antigen-reactive TCR to human peripheral blood lymphocytes confers anti-tumor reactivity. *Journal of immunology* 163: 507-13
36. Cooper LJ, Kalos M, Lewinsohn DA, Riddell SR, Greenberg PD. 2000. Transfer of specificity for human immunodeficiency virus type 1 into primary human T lymphocytes by introduction of T-cell receptor genes. *Journal of virology* 74: 8207-12
37. Kessels HW, Wolkers MC, van den Boom MD, van der Valk MA, Schumacher TN. 2001. Immunotherapy through TCR gene transfer. *Nature immunology* 2: 957-61
38. Morgan RA, Dudley ME, Wunderlich JR, Hughes MS, Yang JC, Sherry RM, Royal RE, Topalian SL, Kammula US, Restifo NP, Zheng Z, Nahvi A, de Vries CR, Rogers-Freezer LJ, Mavroukakis SA, Rosenberg SA. 2006. Cancer regression in patients after transfer of genetically engineered lymphocytes. *Science* 314: 126-9
39. de Witte MA, Coccoris M, Wolkers MC, van den Boom MD, Mesman EM, Song JY, van der Valk M, Haanen JB, Schumacher TN. 2006. Targeting self-antigens through allogeneic TCR gene transfer. *Blood* 108: 870-7
40. Biasco L, Baricordi C, Aiuti A. 2012. Retroviral integrations in gene therapy trials. *Molecular therapy : the journal of the American Society of Gene Therapy* 20: 709-16
41. Zajac AJ, Blattman JN, Murali-Krishna K, Sourdive DJ, Suresh M, Altman JD, Ahmed R. 1998. Viral immune evasion due to persistence of activated T cells without effector function. *The Journal of experimental medicine* 188: 2205-13
42. Hung K, Hayashi R, Lafond-Walker A, Lowenstein C, Pardoll D, Levitsky H. 1998. The central role of CD4(+) T cells in the antitumor immune response. *The Journal of experimental medicine* 188: 2357-68
43. Challita PM, Kohn DB. 1994. Lack of expression from a retroviral vector after transduction of murine hematopoietic stem cells is associated with methylation in vivo. *Proceedings of the National Academy of Sciences of the United States of America* 91: 2567-71
44. Fernandez-Miguel G, Alarcon B, Iglesias A, Bluethmann H, Alvarez-Mon M, Sanz E, de la Hera A. 1999. Multivalent structure of an alphabetaT cell receptor. *Proceedings of the National Academy of Sciences of the United States of America* 96: 1547-52

45. Sommermeyer D, Uckert W. 2010. Minimal amino acid exchange in human TCR constant regions fosters improved function of TCR gene-modified T cells. *Journal of immunology* 184: 6223-31
46. Kolb HJ, Schmid C, Barrett AJ, Schendel DJ. 2004. Graft-versus-leukemia reactions in allogeneic chimeras. *Blood* 103: 767-76
47. Schumacher TN. 2002. T-cell-receptor gene therapy. *Nature reviews. Immunology* 2: 512-9
48. Lutzko C, Kruth S, Abrams-Ogg AC, Lau K, Li L, Clark BR, Ruedy C, Nanji S, Foster R, Kohn D, Shull R, Dube ID. 1999. Genetically corrected autologous stem cells engraft, but host immune responses limit their utility in canine alpha-L-iduronidase deficiency. *Blood* 93: 1895-905
49. Morgan RA, Yang JC, Kitano M, Dudley ME, Laurencot CM, Rosenberg SA. 2010. Case report of a serious adverse event following the administration of T cells transduced with a chimeric antigen receptor recognizing ERBB2. *Molecular therapy : the journal of the American Society of Gene Therapy* 18: 843-51
50. Ly LV, Sluijter M, Versluis M, Luyten GP, van Stipdonk MJ, van der Burg SH, Melief CJ, Jager MJ, van Hall T. 2010. Peptide vaccination after T-cell transfer causes massive clonal expansion, tumor eradication, and manageable cytokine storm. *Cancer research* 70: 8339-46
51. Linette GP, Stadtmauer EA, Maus MV, Rapoport AP, Levine BL, Emery L, Litzky L, Bagg A, Carreno BM, Cimino PJ, Binder-Scholl GK, Smethurst DP, Gerry AB, Pumphrey NJ, Bennett AD, Brewer JE, Dukes J, Harper J, Tayton-Martin HK, Jakobsen BK, Hassan NJ, Kalos M, June CH. 2013. Cardiovascular toxicity and titin cross-reactivity of affinity-enhanced T cells in myeloma and melanoma. *Blood* 122: 863-71
52. Morgan RA, Chinnasamy N, Abate-Daga D, Gros A, Robbins PF, Zheng Z, Dudley ME, Feldman SA, Yang JC, Sherry RM, Phan GQ, Hughes MS, Kammula US, Miller AD, Hessman CJ, Stewart AA, Restifo NP, Quezado MM, Alimchandani M, Rosenberg AZ, Nath A, Wang T, Bielekova B, Wuest SC, Akula N, McMahon FJ, Wilde S, Mosetter B, Schendel DJ, Laurencot CM, Rosenberg SA. 2013. Cancer regression and neurological toxicity following anti-MAGE-A3 TCR gene therapy. *Journal of immunotherapy* 36: 133-51
53. Cooke KR, Kobzik L, Martin TR, Brewer J, Delmonte J, Jr., Crawford JM, Ferrara JL. 1996. An experimental model of idiopathic pneumonia syndrome after bone marrow transplantation: I. The roles of minor H antigens and endotoxin. *Blood* 88: 3230-9
54. Abad JD, Wrzensinski C, Overwijk W, De Witte MA, Jorritsma A, Hsu C, Gattinoni L, Cohen CJ, Paulos CM, Palmer DC, Haanen JB, Schumacher TN, Rosenberg SA, Restifo NP, Morgan RA. 2008. T-cell receptor gene therapy of

established tumors in a murine melanoma model. *Journal of immunotherapy* 31: 1-6

55. de Witte MA, Bendle GM, van den Boom MD, Coccoris M, Schell TD, Tevethia SS, van Tinteren H, Mesman EM, Song JY, Schumacher TN. 2008. TCR gene therapy of spontaneous prostate carcinoma requires in vivo T cell activation. *Journal of immunology* 181: 2563-71
56. Theobald M, Biggs J, Dittmer D, Levine AJ, Sherman LA. 1995. Targeting p53 as a general tumor antigen. *Proceedings of the National Academy of Sciences of the United States of America* 92: 11993-7
57. Pircher H, Rohrer UH, Moskophidis D, Zinkernagel RM, Hengartner H. 1991. Lower receptor avidity required for thymic clonal deletion than for effector T-cell function. *Nature* 351: 482-5
58. Sherman LA, Hesse SV, Irwin MJ, La Face D, Peterson P. 1992. Selecting T cell receptors with high affinity for self-MHC by decreasing the contribution of CD8. *Science* 258: 815-8
59. Voss RH, Kuball J, Engel R, Guillaume P, Romero P, Huber C, Theobald M. 2006. Redirection of T cells by delivering a transgenic mouse-derived MDM2 tumor antigen-specific TCR and its humanized derivative is governed by the CD8 coreceptor and affects natural human TCR expression. *Immunologic research* 34: 67-87
60. Cohen CJ, Zhao Y, Zheng Z, Rosenberg SA, Morgan RA. 2006. Enhanced antitumor activity of murine-human hybrid T-cell receptor (TCR) in human lymphocytes is associated with improved pairing and TCR/CD3 stability. *Cancer research* 66: 8878-86
61. Kuball J, Hauptrock B, Malina V, Antunes E, Voss RH, Wolfl M, Strong R, Theobald M, Greenberg PD. 2009. Increasing functional avidity of TCR-redirected T cells by removing defined N-glycosylation sites in the TCR constant domain. *The Journal of experimental medicine* 206: 463-75
62. Kuball J, Dossett ML, Wolfl M, Ho WY, Voss RH, Fowler C, Greenberg PD. 2007. Facilitating matched pairing and expression of TCR chains introduced into human T cells. *Blood* 109: 2331-8
63. Szymczak AL, Workman CJ, Wang Y, Vignali KM, Dilioglou S, Vanin EF, Vignali DA. 2004. Correction of multi-gene deficiency in vivo using a single 'self-cleaving' 2A peptide-based retroviral vector. *Nature biotechnology* 22: 589-94
64. Voss RH, Thomas S, Pfirschke C, Hauptrock B, Klobuch S, Kuball J, Grabowski M, Engel R, Guillaume P, Romero P, Huber C, Beckhove P, Theobald M. 2010. Coexpression of the T-cell receptor constant alpha domain triggers tumor reactivity of single-chain TCR-transduced human T cells. *Blood* 115: 5154-63

65. Hanahan D, Weinberg RA. 2000. The hallmarks of cancer. *Cell* 100: 57-70
66. Hanahan D, Weinberg RA. 2011. Hallmarks of cancer: the next generation. *Cell* 144: 646-74
67. Schreiber RD, Old LJ, Smyth MJ. 2011. Cancer immunoediting: integrating immunity's roles in cancer suppression and promotion. *Science* 331: 1565-70
68. Reinis M. 2010. Immunotherapy of MHC class I-deficient tumors. *Future oncology* 6: 1577-89
69. Lin WW, Hsieh SL. 2011. Decoy receptor 3: a pleiotropic immunomodulator and biomarker for inflammatory diseases, autoimmune diseases and cancer. *Biochemical pharmacology* 81: 838-47
70. Blank C, Mackensen A. 2007. Contribution of the PD-L1/PD-1 pathway to T-cell exhaustion: an update on implications for chronic infections and tumor evasion. *Cancer immunology, immunotherapy : CII* 56: 739-45
71. Coussens LM, Werb Z. 2002. Inflammation and cancer. *Nature* 420: 860-7
72. Koperek O, Akin E, Asari R, Niederle B, Neuhold N. 2013. Expression of hypoxia-inducible factor 1 alpha in papillary thyroid carcinoma is associated with desmoplastic stromal reaction and lymph node metastasis. *Virchows Archiv : an international journal of pathology*
73. Ahmadzadeh M, Felipe-Silva A, Heemskerk B, Powell DJ, Jr., Wunderlich JR, Merino MJ, Rosenberg SA. 2008. FOXP3 expression accurately defines the population of intratumoral regulatory T cells that selectively accumulate in metastatic melanoma lesions. *Blood* 112: 4953-60
74. Woo EY, Chu CS, Goletz TJ, Schlienger K, Yeh H, Coukos G, Rubin SC, Kaiser LR, June CH. 2001. Regulatory CD4(+)CD25(+) T cells in tumors from patients with early-stage non-small cell lung cancer and late-stage ovarian cancer. *Cancer research* 61: 4766-72
75. Shin JY, Yoon IH, Kim JS, Kim B, Park CG. 2009. Vascular endothelial growth factor-induced chemotaxis and IL-10 from T cells. *Cellular immunology* 256: 72-8
76. Calcinotto A, Filipazzi P, Grioni M, Iero M, De Milito A, Ricupito A, Cova A, Canese R, Jachetti E, Rossetti M, Huber V, Parmiani G, Generoso L, Santinami M, Borghi M, Fais S, Bellone M, Rivoltini L. 2012. Modulation of microenvironment acidity reverses anergy in human and murine tumor-infiltrating T lymphocytes. *Cancer research* 72: 2746-56
77. Perrot I, Blanchard D, Freymond N, Isaac S, Guibert B, Pacheco Y, Lebecque S. 2007. Dendritic cells infiltrating human non-small cell lung cancer are blocked at immature stage. *Journal of immunology* 178: 2763-9
78. Lin EY, Li JF, Gnatovskiy L, Deng Y, Zhu L, Grzesik DA, Qian H, Xue XN, Pollard JW. 2006. Macrophages regulate the angiogenic switch in a mouse model of breast cancer. *Cancer research* 66: 11238-46

79. Qian B, Deng Y, Im JH, Muschel RJ, Zou Y, Li J, Lang RA, Pollard JW. 2009. A distinct macrophage population mediates metastatic breast cancer cell extravasation, establishment and growth. *PLoS One* 4: e6562
80. Zheng Y, Cai Z, Wang S, Zhang X, Qian J, Hong S, Li H, Wang M, Yang J, Yi Q. 2009. Macrophages are an abundant component of myeloma microenvironment and protect myeloma cells from chemotherapy drug-induced apoptosis. *Blood* 114: 3625-8
81. Miotto D, Boschetto P, Bononi I, Milani G, Legorini C, Cavallesco G, Lo Cascio N, Zeni E, Fabbri LM, Mapp CE. 2007. CC ligand 2 levels are increased in LPS-stimulated peripheral monocytes of patients with non-small cell lung cancer. *Respiratory medicine* 101: 1738-43
82. Allavena P, Sica A, Solinas G, Porta C, Mantovani A. 2008. The inflammatory micro-environment in tumor progression: the role of tumor-associated macrophages. *Critical reviews in oncology/hematology* 66: 1-9
83. Li YW, Qiu SJ, Fan J, Zhou J, Gao Q, Xiao YS, Xu YF. 2011. Intratumoral neutrophils: a poor prognostic factor for hepatocellular carcinoma following resection. *Journal of hepatology* 54: 497-505
84. Fridlender ZG, Sun J, Kim S, Kapoor V, Cheng G, Ling L, Worthen GS, Albelda SM. 2009. Polarization of tumor-associated neutrophil phenotype by TGF-beta: "N1" versus "N2" TAN. *Cancer cell* 16: 183-94
85. Corzo CA, Condamine T, Lu L, Cotter MJ, Youn JI, Cheng P, Cho HI, Celis E, Quiceno DG, Padhya T, McCaffrey TV, McCaffrey JC, Gabrilovich DI. 2010. HIF-1alpha regulates function and differentiation of myeloid-derived suppressor cells in the tumor microenvironment. *The Journal of experimental medicine* 207: 2439-53
86. Youn JI, Collazo M, Shalova IN, Biswas SK, Gabrilovich DI. 2012. Characterization of the nature of granulocytic myeloid-derived suppressor cells in tumor-bearing mice. *Journal of leukocyte biology* 91: 167-81
87. Movahedi K, Guilliams M, Van den Bossche J, Van den Bergh R, Gysemans C, Beschin A, De Baetselier P, Van Ginderachter JA. 2008. Identification of discrete tumor-induced myeloid-derived suppressor cell subpopulations with distinct T cell-suppressive activity. *Blood* 111: 4233-44
88. Choi BS, Martinez-Falero IC, Corset C, Munder M, Modolell M, Muller I, Kropf P. 2009. Differential impact of L-arginine deprivation on the activation and effector functions of T cells and macrophages. *Journal of leukocyte biology* 85: 268-77
89. Srivastava MK, Sinha P, Clements VK, Rodriguez P, Ostrand-Rosenberg S. 2010. Myeloid-derived suppressor cells inhibit T-cell activation by depleting cystine and cysteine. *Cancer research* 70: 68-77

90. Rodriguez PC, Quiceno DG, Zabaleta J, Ortiz B, Zea AH, Piazuelo MB, Delgado A, Correa P, Brayer J, Sotomayor EM, Antonia S, Ochoa JB, Ochoa AC. 2004. Arginase I production in the tumor microenvironment by mature myeloid cells inhibits T-cell receptor expression and antigen-specific T-cell responses. *Cancer research* 64: 5839-49
91. Schmielau J, Finn OJ. 2001. Activated granulocytes and granulocyte-derived hydrogen peroxide are the underlying mechanism of suppression of t-cell function in advanced cancer patients. *Cancer research* 61: 4756-60
92. Mazzoni A, Bronte V, Visintin A, Spitzer JH, Apolloni E, Serafini P, Zanovello P, Segal DM. 2002. Myeloid suppressor lines inhibit T cell responses by an NO-dependent mechanism. *Journal of immunology* 168: 689-95
93. Hanson EM, Clements VK, Sinha P, Ilkovitch D, Ostrand-Rosenberg S. 2009. Myeloid-derived suppressor cells down-regulate L-selectin expression on CD4+ and CD8+ T cells. *Journal of immunology* 183: 937-44
94. Molon B, Ugel S, Del Pozzo F, Soldani C, Zilio S, Avella D, De Palma A, Mauri P, Monegal A, Rescigno M, Savino B, Colombo P, Jonjic N, Pecanic S, Lazzarato L, Fruttero R, Gasco A, Bronte V, Viola A. 2011. Chemokine nitration prevents intratumoral infiltration of antigen-specific T cells. *The Journal of experimental medicine* 208: 1949-62
95. Pan PY, Ma G, Weber KJ, Ozao-Choy J, Wang G, Yin B, Divino CM, Chen SH. 2010. Immune stimulatory receptor CD40 is required for T-cell suppression and T regulatory cell activation mediated by myeloid-derived suppressor cells in cancer. *Cancer research* 70: 99-108
96. Huang B, Pan PY, Li Q, Sato AI, Levy DE, Bromberg J, Divino CM, Chen SH. 2006. Gr-1+CD115+ immature myeloid suppressor cells mediate the development of tumor-induced T regulatory cells and T-cell anergy in tumor-bearing host. *Cancer research* 66: 1123-31
97. Filipazzi P, Valenti R, Huber V, Pilla L, Canese P, Iero M, Castelli C, Mariani L, Parmiani G, Rivoltini L. 2007. Identification of a new subset of myeloid suppressor cells in peripheral blood of melanoma patients with modulation by a granulocyte-macrophage colony-stimulation factor-based antitumor vaccine. *Journal of clinical oncology : official journal of the American Society of Clinical Oncology* 25: 2546-53
98. Poulikakos PI, Persaud Y, Janakiraman M, Kong X, Ng C, Moriceau G, Shi H, Atefi M, Titz B, Gabay MT, Salton M, Dahlman KB, Tadi M, Wargo JA, Flaherty KT, Kelley MC, Misteli T, Chapman PB, Sosman JA, Graeber TG, Ribas A, Lo RS, Rosen N, Solit DB. 2011. RAF inhibitor resistance is mediated by dimerization of aberrantly spliced BRAF(V600E). *Nature* 480: 387-90

99. Necchi A, Nicolai N, Mariani L, Lo Vullo S, Giannatempo P, Raggi D, Fare E, Piva L, Biasoni D, Catanzaro M, Torelli T, Stagni S, Milani A, Gianni AM, Salvioni R. 2013. Combination of Paclitaxel, Cisplatin, and Gemcitabine (TPG) for Multiple Relapses or Platinum-Resistant Germ Cell Tumors: Long-Term Outcomes. *Clinical genitourinary cancer*
100. Kohrt HE, Houot R, Weiskopf K, Goldstein MJ, Scheeren F, Czerwinski D, Colevas AD, Weng WK, Clarke MF, Carlson RW, Stockdale FE, Mollick JA, Chen L, Levy R. 2012. Stimulation of natural killer cells with a CD137-specific antibody enhances trastuzumab efficacy in xenotransplant models of breast cancer. *The Journal of clinical investigation* 122: 1066-75
101. Wolchok JD, Kluger H, Callahan MK, Postow MA, Rizvi NA, Lesokhin AM, Segal NH, Ariyan CE, Gordon RA, Reed K, Burke MM, Caldwell A, Kronenberg SA, Agunwamba BU, Zhang X, Lowy I, Inzunza HD, Feely W, Horak CE, Hong Q, Korman AJ, Wigginton JM, Gupta A, Sznol M. 2013. Nivolumab plus ipilimumab in advanced melanoma. *The New England journal of medicine* 369: 122-33
102. John LB, Devaud C, Duong CP, Yong CS, Beavis PA, Haynes NM, Chow MT, Smyth MJ, Kershaw MH, Darcy PK. 2013. Anti-PD-1 Antibody Therapy Potently Enhances the Eradication of Established Tumors By Gene-Modified T Cells. *Clinical cancer research : an official journal of the American Association for Cancer Research* 19: 5636-46
103. Bendle GM, Linnemann C, Hooijkaas AI, Bies L, de Witte MA, Jorritsma A, Kaiser AD, Pouw N, Debets R, Kieback E, Uckert W, Song JY, Haanen JB, Schumacher TN. 2010. Lethal graft-versus-host disease in mouse models of T cell receptor gene therapy. *Nature medicine* 16: 565-70, 1p following 70
104. Dittmer D, Pati S, Zambetti G, Chu S, Teresky AK, Moore M, Finlay C, Levine AJ. 1993. Gain of function mutations in p53. *Nature genetics* 4: 42-6
105. Huber C, Bobek N, Kuball J, Thaler S, Hoffarth S, Theobald M, Schuler M. 2005. Inhibitors of apoptosis confer resistance to tumour suppression by adoptively transplanted cytotoxic T-lymphocytes in vitro and in vivo. *Cell death and differentiation* 12: 317-25
106. Perruche S, Kleinclauss F, Lienard A, Robinet E, Tiberghien P, Saas P. 2004. A single-platform approach using flow cytometry and microbeads to evaluate immune reconstitution in mice after bone marrow transplantation. *Journal of immunological methods* 294: 53-66
107. Sevko A, Michels T, Vrohlings M, Umansky L, Beckhove P, Kato M, Shurin GV, Shurin MR, Umansky V. 2013. Antitumor effect of paclitaxel is mediated by inhibition of myeloid-derived suppressor cells and chronic inflammation in the spontaneous melanoma model. *Journal of immunology* 190: 2464-71

108. Hebeisen M, Baitsch L, Presotto D, Baumgaertner P, Romero P, Michielin O, Speiser DE, Rufer N. 2013. SHP-1 phosphatase activity counteracts increased T cell receptor affinity. *The Journal of clinical investigation* 123: 1044-56
109. de Witte MA, Jorritsma A, Kaiser A, van den Boom MD, Dokter M, Bendle GM, Haanen JB, Schumacher TN. 2008. Requirements for effective antitumor responses of TCR transduced T cells. *Journal of immunology* 181: 5128-36
110. Shrikant P, Mescher MF. 2002. Opposing effects of IL-2 in tumor immunotherapy: promoting CD8 T cell growth and inducing apoptosis. *Journal of immunology* 169: 1753-9
111. Johnson LA, Morgan RA, Dudley ME, Cassard L, Yang JC, Hughes MS, Kammula US, Royal RE, Sherry RM, Wunderlich JR, Lee CC, Restifo NP, Schwarz SL, Cogdill AP, Bishop RJ, Kim H, Brewer CC, Rudy SF, VanWaes C, Davis JL, Mathur A, Ripley RT, Nathan DA, Laurencot CM, Rosenberg SA. 2009. Gene therapy with human and mouse T-cell receptors mediates cancer regression and targets normal tissues expressing cognate antigen. *Blood* 114: 535-46
112. Robbins PF, Morgan RA, Feldman SA, Yang JC, Sherry RM, Dudley ME, Wunderlich JR, Nahvi AV, Helman LJ, Mackall CL, Kammula US, Hughes MS, Restifo NP, Raffeld M, Lee CC, Levy CL, Li YF, El-Gamil M, Schwarz SL, Laurencot C, Rosenberg SA. 2011. Tumor regression in patients with metastatic synovial cell sarcoma and melanoma using genetically engineered lymphocytes reactive with NY-ESO-1. *Journal of clinical oncology : official journal of the American Society of Clinical Oncology* 29: 917-24
113. Leisegang M, Wilde S, Spranger S, Milosevic S, Frankenberger B, Uckert W, Schendel DJ. 2010. MHC-restricted fratricide of human lymphocytes expressing survivin-specific transgenic T cell receptors. *The Journal of clinical investigation* 120: 3869-77
114. Bos R, van Duikeren S, Morreau H, Franken K, Schumacher TN, Haanen JB, van der Burg SH, Melief CJ, Offringa R. 2008. Balancing between antitumor efficacy and autoimmune pathology in T-cell-mediated targeting of carcinoembryonic antigen. *Cancer research* 68: 8446-55
115. Dudley ME, Wunderlich JR, Yang JC, Sherry RM, Topalian SL, Restifo NP, Royal RE, Kammula U, White DE, Mavroukakis SA, Rogers LJ, Gracia GJ, Jones SA, Mangiameli DP, Pelletier MM, Gea-Banacloche J, Robinson MR, Berman DM, Filie AC, Abati A, Rosenberg SA. 2005. Adoptive cell transfer therapy following non-myeloablative but lymphodepleting chemotherapy for the treatment of patients with refractory metastatic melanoma. *Journal of clinical oncology : official journal of the American Society of Clinical Oncology* 23: 2346-57

116. Hicklin DJ, Marincola FM, Ferrone S. 1999. HLA class I antigen downregulation in human cancers: T-cell immunotherapy revives an old story. *Molecular medicine today* 5: 178-86
117. Jensen SM, Twitty CG, Maston LD, Antony PA, Lim M, Hu HM, Petrausch U, Restifo NP, Fox BA. 2012. Increased frequency of suppressive regulatory T cells and T cell-mediated antigen loss results in murine melanoma recurrence. *Journal of immunology* 189: 767-76
118. Freeman GJ. 2008. Structures of PD-1 with its ligands: sideways and dancing cheek to cheek. *Proceedings of the National Academy of Sciences of the United States of America* 105: 10275-6
119. Brusa D, Serra S, Coscia M, Rossi D, D'Arena G, Laurenti L, Jaksic O, Fedele G, Inghirami G, Gaidano G, Malavasi F, Deaglio S. 2013. The PD-1/PD-L1 axis contributes to T-cell dysfunction in chronic lymphocytic leukemia. *Haematologica* 98: 953-63
120. Pilon-Thomas S, Mackay A, Vohra N, Mule JJ. 2010. Blockade of programmed death ligand 1 enhances the therapeutic efficacy of combination immunotherapy against melanoma. *Journal of immunology* 184: 3442-9
121. Peng L, Kjaergaard J, Plautz GE, Awad M, Drazba JA, Shu S, Cohen PA. 2002. Tumor-induced L-selectinhigh suppressor T cells mediate potent effector T cell blockade and cause failure of otherwise curative adoptive immunotherapy. *Journal of immunology* 169: 4811-21
122. Curtin JF, Candolfi M, Fakhouri TM, Liu C, Alden A, Edwards M, Lowenstein PR, Castro MG. 2008. Treg depletion inhibits efficacy of cancer immunotherapy: implications for clinical trials. *PLoS One* 3: e1983
123. Yu P, Lee Y, Liu W, Krausz T, Chong A, Schreiber H, Fu YX. 2005. Intratumor depletion of CD4+ cells unmasks tumor immunogenicity leading to the rejection of late-stage tumors. *The Journal of experimental medicine* 201: 779-91
124. Kusmartsev S, Nagaraj S, Gabrilovich DI. 2005. Tumor-associated CD8+ T cell tolerance induced by bone marrow-derived immature myeloid cells. *Journal of immunology* 175: 4583-92
125. Kusmartsev S, Gabrilovich DI. 2005. STAT1 signaling regulates tumor-associated macrophage-mediated T cell deletion. *Journal of immunology* 174: 4880-91
126. Kruse J, von Bernstorff W, Evert K, Albers N, Hadlich S, Hagemann S, Gunther C, van Rooijen N, Heidecke CD, Partecke LI. 2013. Macrophages promote tumour growth and liver metastasis in an orthotopic syngeneic mouse model of colon cancer. *International journal of colorectal disease* 28: 1337-49
127. Pantano F, Berti P, Guida FM, Perrone G, Vincenzi B, Amato MM, Righi D, Dell'aquila E, Graziano F, Catalano V, Caricato M, Rizzo S, Muda AO, Russo

A, Tonini G, Santini D. 2013. The role of macrophages polarization in predicting prognosis of radically resected gastric cancer patients. *Journal of cellular and molecular medicine* 17: 1415-21

128. Zhao F, Obermann S, von Wasielewski R, Haile L, Manns MP, Korangy F, Greten TF. 2009. Increase in frequency of myeloid-derived suppressor cells in mice with spontaneous pancreatic carcinoma. *Immunology* 128: 141-9
129. Ohki S, Shibata M, Gonda K, Machida T, Shimura T, Nakamura I, Ohtake T, Koyama Y, Suzuki S, Ohto H, Takenoshita S. 2012. Circulating myeloid-derived suppressor cells are increased and correlate to immune suppression, inflammation and hypoproteinemia in patients with cancer. *Oncology reports* 28: 453-8
130. Srivastava MK, Zhu L, Harris-White M, Kar UK, Huang M, Johnson MF, Lee JM, Elashoff D, Strieter R, Dubinett S, Sharma S. 2012. Myeloid suppressor cell depletion augments antitumor activity in lung cancer. *PLoS One* 7: e40677
131. Shaner NC, Campbell RE, Steinbach PA, Giepmans BN, Palmer AE, Tsien RY. 2004. Improved monomeric red, orange and yellow fluorescent proteins derived from Discosoma sp. red fluorescent protein. *Nature biotechnology* 22: 1567-72
132. Shcherbo D, Merzlyak EM, Chepurnykh TV, Fradkov AF, Ermakova GV, Solovieva EA, Lukyanov KA, Bogdanova EA, Zaraisky AG, Lukyanov S, Chudakov DM. 2007. Bright far-red fluorescent protein for whole-body imaging. *Nature methods* 4: 741-6
133. Naviaux RK, Costanzi E, Haas M, Verma IM. 1996. The pCL vector system: rapid production of helper-free, high-titer, recombinant retroviruses. *Journal of virology* 70: 5701-5

7 Annex

7.1 Vector maps

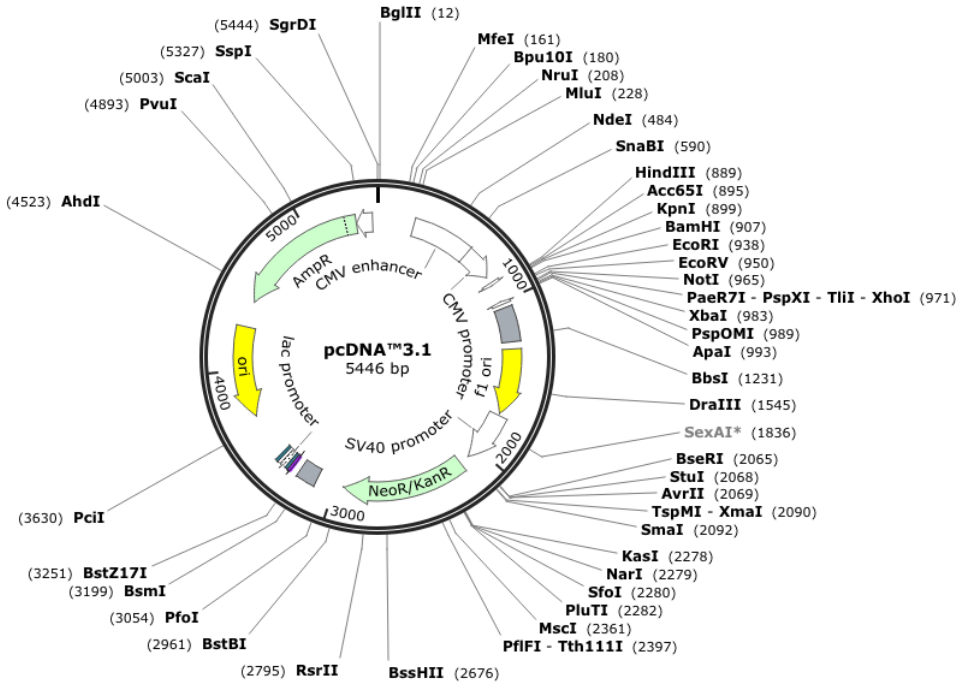

Figure 7.1 Vector map of pcDNA^{TM}3.1 (Invitrogen) used for subcloning of the α- and β-chain p53TCR.

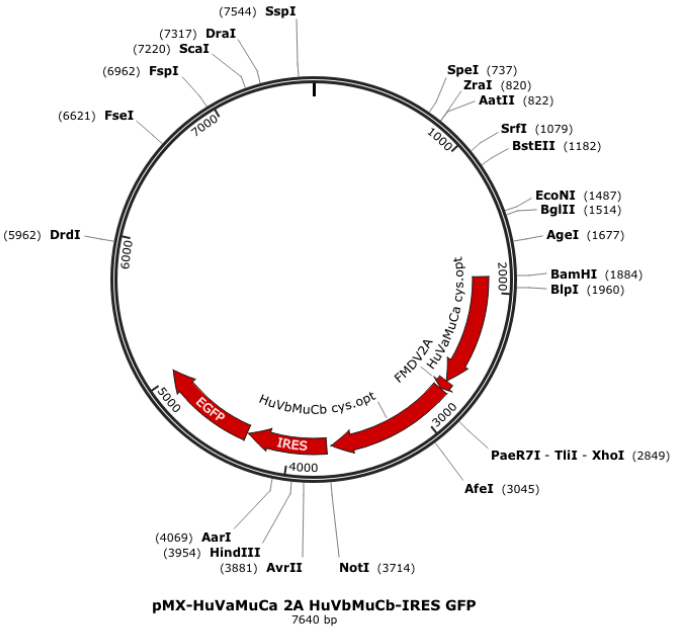

Figure 7.2 Vector map of the (original) pMx-IE-GFP.
The pMX-IRES-Enhanced (IE)-GFP vector originally bearing another TCR, was used as a plasmid-backbone for Katushka, tdTomato, α- and β-chain p53TCR. The pMx vector was linearized (BamHI/NotI) for all cloning steps.

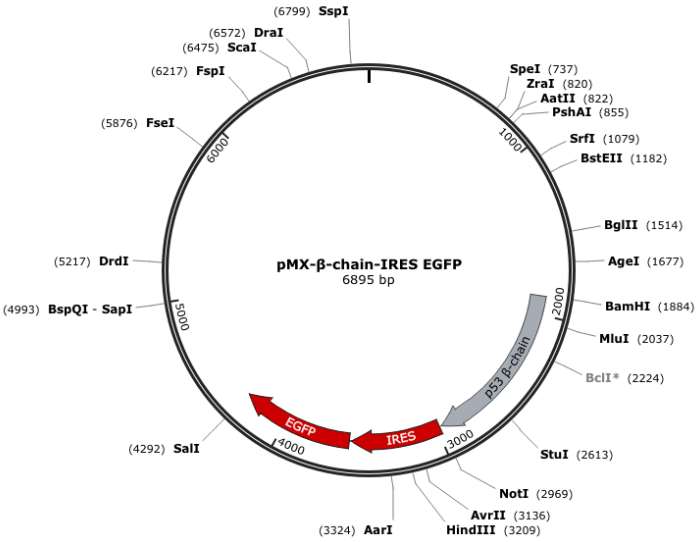

Figure 7.3 Vector map of the p53-specific β-chain TCR.
Suggested vector map. After subcloning of the β-chain p53TCR into pcDNA^{TM}3.1 (BamHI/SwaI) the β-chain p53TCR was finally cloned into pMx-IE-GFP (BamHI/NotI).

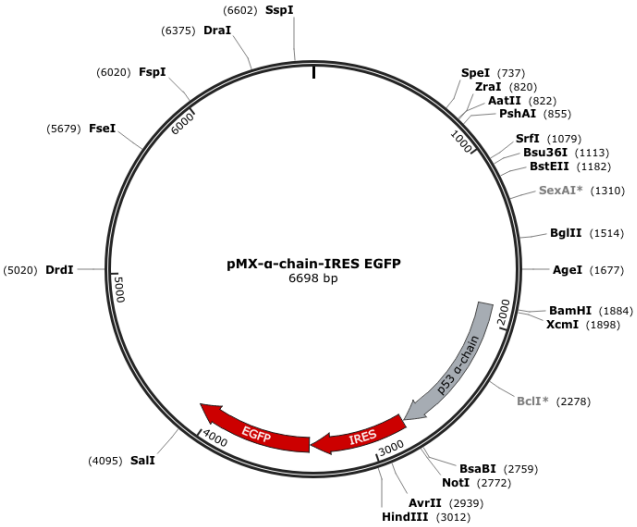

Figure 7.4 Vector map of the p53-specific α-chain TCR.
Suggested vector map. After subcloning of the α-chain p53TCR into pcDNA^{TM}3.1(BamHI/EcoRV) the α-chain p53TCR was finally cloned into pMx-IE-GFP (BamHI/NotI).

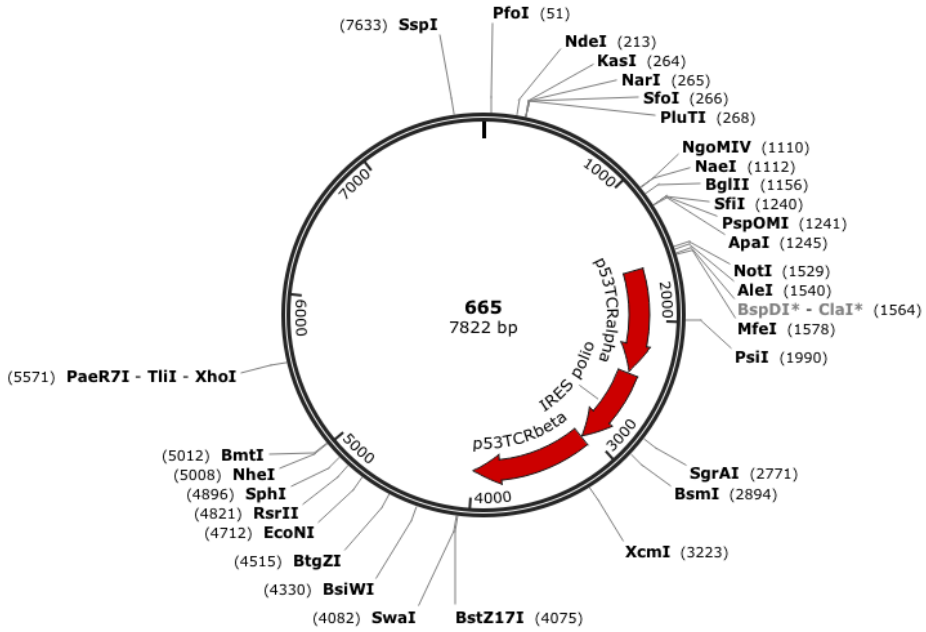

Figure 7.5 Vector map of the wt p53TCR.
The wt p53TCR was cloned into pGMP vector by Genterprise GmbH, Mainz, Germany.

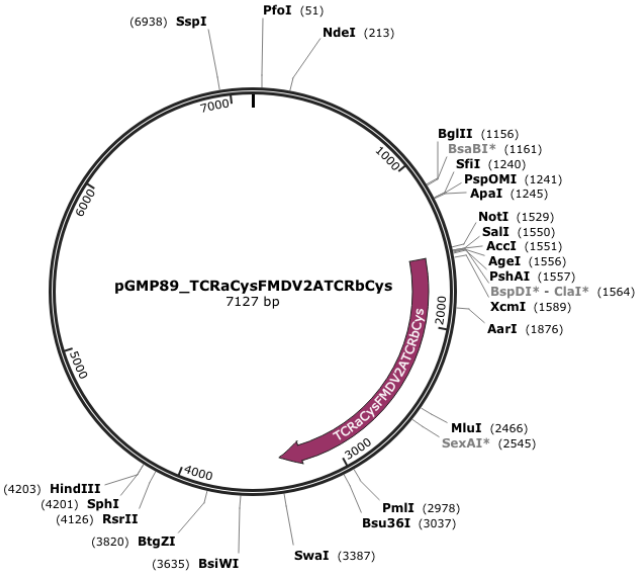

Figure 7.6 Vector map of the dc p53TCR.
The dc p53TCR was optimized and cloned into pGMP vector by GENEART AG, Regensburg, Germany.

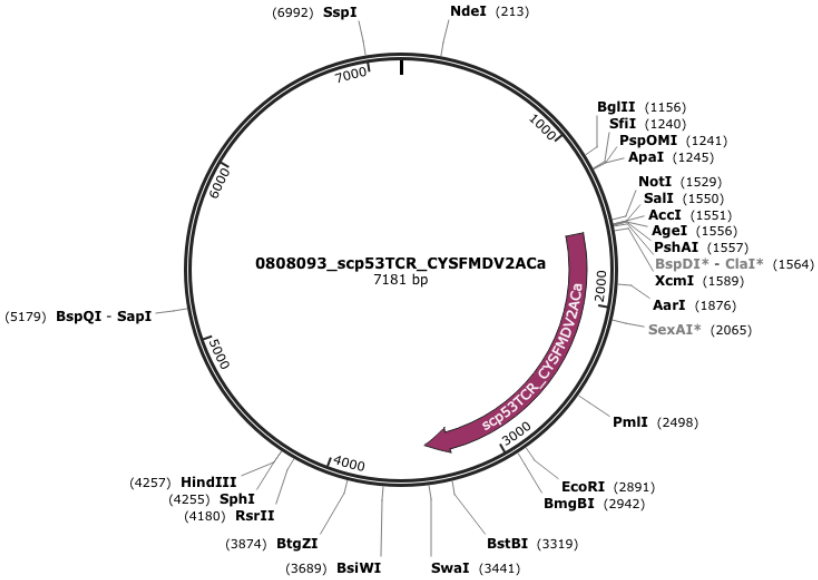

Figure 7.7 Vector map of the sc p53TCR.
The sc p53TCR was optimized and cloned into pGMP vector by GENEART AG, Regensburg, Germany.

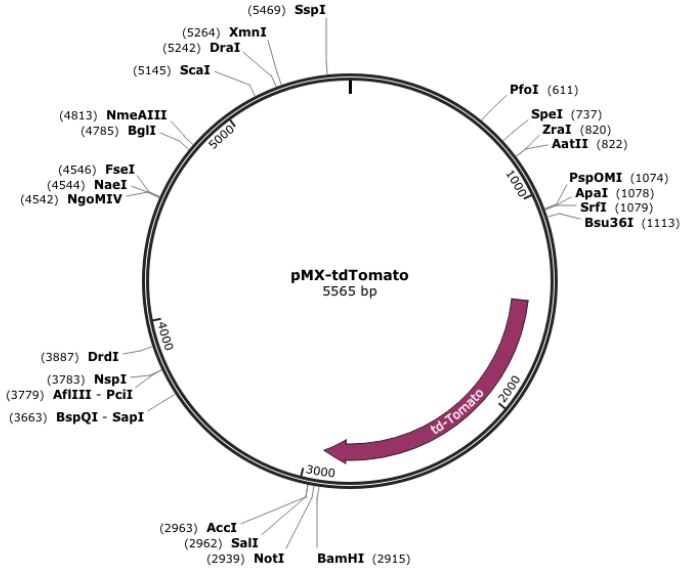

Figure 7.8 Vector map of the pMx-tdTomato.
tdTomato (131) was cloned into the pMx vector (Figure 7.2) (BamHI/NotI) after excision of the TCR and the IE-GFP sequence. The pMx-Katushka cDNA was obtained from Dr. Anton Martens (Department of Cell Biology, UMC Utrecht, The Netherlands) and cloned into pMx vector (BamHI/EcoRI) after excision of the TCR and the IE-GFP sequence (132).

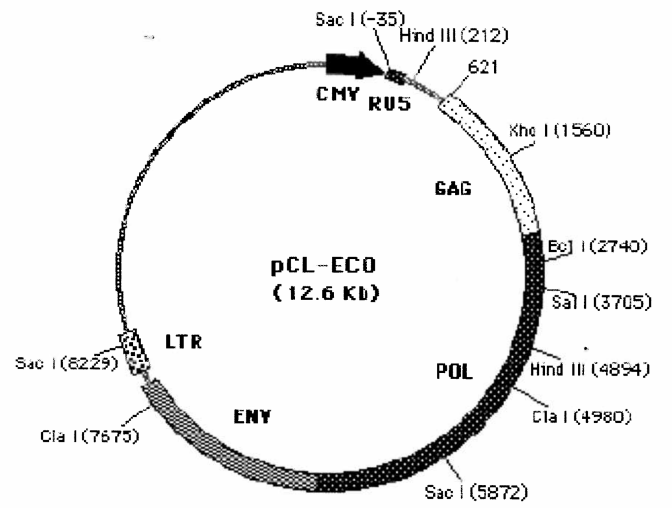

Figure 7.9 Vector map of pCL-Eco helper plasmid.
pCL-Eco, used as helper plasmid for retroviral transductions (133).

7.2 Primer

Table 7.1 Primer used for cloning of the single α- and β-chain.

Primer Name	Primer sequence
α-chain (forward) TCRa89 Fw16	5'-CGA CAC CGG TCA TCG ATC TC-3' (20mer)
α-chain (reverse) TCRa89 Rv909	5'-GGG ATA TCA CTC CAC GTC TCC GGC CAA C-3' (28mer)
β-chain (forward) p53TCR Fw2322	5'-TTG GAT CCG CCA TGG GCC TGA GAA TCC TG-3' (29mer)
β-chain (reverse) p53TCRb Rv3467	5'-GTG GCA ATA CAC CTG AAC-3' (18mer)
Sequencing primer (SE-206)	5'-TTA CAC AGT CCT GCT GAC CAC C-3' (22mer)

Acknowledgment

Curriculum Vitae